Proceeding for International Conference

on

Emerging Trends

In

Engineering and Technology

Trivandrum

22nd November'15

Institute for Engineering Research and Publication

(A Unit of VVERT)

4A, Girija Apartment, MMDA,

Arumbakkam, Chennai-600106, India

www.iferp.in

Publisher: IFERP Explore

Editorial:

We cordially invite you to attend the International Conference on Emerging Trends in Engineering and Technology (ICET-15), which will be held in Hotel Aiswarya, Trivandrum on November 22, 2015. The main objective of ICET-15 is to provide a platform for researchers, engineers, academicians as well as industrial professionals from all over the world to present their research results and development activities in Electronics, Mechanical, Electrical, Computer Science and Information Technology. This conference provides opportunities for the delegates to exchange new ideas and experience face to face, to establish business or research relations and to find global partners for future collaboration.

These proceedings collect the up-to-date, comprehensive and worldwide state-of-art knowledge on software engineering, computational sciences and computational science application. All accepted papers were subjected to strict peer-reviewing by 2-4 expert referees. The papers have been selected for these proceedings because of their quality and the relevance to the conference. We hope these proceedings will not only provide the readers a broad overview of the latest research results on Electrical, Electronics, Mechanical, Computer Science and Information Technology but also provide the readers a valuable summary and reference in these fields.

The conference is supported by many universities and research institutes. Many professors plaid an important role in the successful holding of the conference, so we would like to take this opportunity to express our sincere gratitude and highest respects to them. They have worked very hard in reviewing papers and making valuable suggestions for the authors to improve their work. We also would like to express our gratitude to the external reviewers, for providing extra help in the review process, and to the authors for contributing their research result to the conference.

Since April 2015, the Organizing Committees have received more than 120 manuscript papers, and the papers cover all the aspects in Electronics, Computer Science and Information Technology. Finally, after review, about 10 papers were included to the proceedings of ICET-2015.

We would like to extend our appreciation to all participants in the conference for their great contribution to the success of International Conference 2015. We would like to thank the keynote and individual speakers and all participating authors for their hard work and time. We also sincerely appreciate the work by the technical program committee and all reviewers, whose contributions make this conference possible. We would like to extend our thanks to all the referees for their constructive comments on all papers; especially, we would like to thank to organizing committee for their hard work.

Editor-In-Chief
Dr. Nalini Chidambaram
Professor
Bharth University

Acknowledgement

IFERP is hosting the International Conference on Emerging Trends in Engineering and Technology this year in month of November. Technical advantage is the backbone of development and nanoelectronics has become the platform behind all the sustainable growth International Conference on Emerging Trends in Engineering and Technology will provide a forum for students, professional engineers, academician, scientist engaged in research and development to convene and present their latest scholarly work and application in the industry. The primary goal of the conference is to promote research and developmental activities in Electronics, Mechanical, Electrical Computer Science and Information Technology and to promote scientific information interchange between researchers, developers, engineers, students, and practitioners working in and around the world. The aim of the Conference is to provide a platform to the researchers and practitioners from both academia as well as industry to meet the share cutting-edge development in the field.

I express my hearty gratitude to all my Colleagues, staffs, Professors, reviewers and members of organizing committee for their hearty and dedicated support to make this conference successful. I am also thankful to all our delegates for their pain staking effort to travel such a long distance to attain this conference.

Er. R. B. Satpathy
Secretary
Institute for Engineering Research and Publication (IFERP)

CONTENTS

S.NO	TITLES AND AUTHORS	PAGE NO
1.	Watermarking Algorithm to Protect Electronic Patient Record ➢ *Praveenamol K. P,Kavitha N Nair*	1-6
2.	Development of Algorithms for Contrast Enhancement of Remote Sensing Images ➢ *Ramkumar.M.U, Kavitha.N.Nair*	7-14
3.	ROI Coding of Remote Sensing 2-D Images using Shape Adaptive Eversible Integer Lapped Transform ➢ *Vaisakhan.B,Kavitha N Nair*	15-21
4.	Contrast Enhancement based on Gaussian Mixture Modeling with Noise Adaptive Fuzzy Switching Median Filter ➢ *Jayasilpa S,Kavitha N Nair*	22-28
5.	Efficient Compression and Encryption Method for Secure Transmission of Images Fuzzy Switching Median Filter ➢ *Meera Mohan,Kavitha N Nair*	29-34
6.	Implementation of High Precision Fixed Width Multiplier for DSP Applications ➢ *G.Niharika,B.Santosh Kumar*	35-39
7.	The Effect of Supply Chain management Practices and Competitive Advantage in the Performance of Kerala PSU's: A Structural Equation Modeling Approach ➢ *Arun A,Asok kumar N*	40-44
8.	Multi-Source Piezoelectric Energy Harvester ➢ *Vinitha K J,[1]Nisthul G*	45-53
9.	Dynamics of Pipe Conveying Fluids ➢ *Shibin Pinto, AjuZacharia Mani*	54-57
10.	Development of Finite Element Code for 3D Four Noded Isoparametric Membrane Shell Elements ➢ *Prasanth P Nair,George T. S*	58-64

ORGANIZATION COMMITTEE

MANAGING DIRECTOR
Dr. P. C. Srikanth
Head of the Department
Department of ECE
Malnad College of Engineering

PRESIDENT
Dr. P A Vijaya
Professor, Department of ECE
BNM Institute of Technology

ORGANIZING SECRETARY
Asst. Prof. Bonia Mohan
Department of CSE
Dayananda sagar College of Engineering
Bangalore,

PUBLICATIONS COMMITTEE
Dr. Shankar Narayanan
Dr.S. Sangeetha

PROGRAM CHAIR
Dr. Nalini Chidambaram
Professor
Bharth University

WATERMARKING ALGORITHM TO PROTECT ELECTRONIC PATIENT RECORD

[1]Praveenamol K. P, [2]Kavitha N Nair
[1]PG Scholar, Department of ECE, University College of Engineering, Muttom, Kerala – 685587
[2]Lecturer, Department of ECE, University College of Engineering, Muttom, Kerala - 685587
[1] praveenaajish89@gmail.com

***Abstract*— With the rapid increase in the medical field it is important to keep the details of the patients and using them for the further analysis of the diseases. For keeping the medical data secure hospitals in all over the world is using EPR and EHR. So in order to give an alternative for that hiding the related data of patients by using the digital image watermarking. There are different ways for doing it, but selecting DCT and trying to compare the performance analysis between DCT with using Fuzzy Logic and DCT by block processing. We need to send the data regarding the patients from one place to another by means of internet or any other transfer medium for making some critical judgment. There is a possibility of affecting noise. So trying to analyze the effect of noise in different methods and finding which one is robust against noise.**

***Keywords*— DCT, EPR, FIS, PSNR & MSE, HVS**

I. INTRODUCTION

Medical images require special safety and confidentiality because critical judgment is done on the information provided by medical images. It is important that the integrity and confidentiality of medical data is a serious topic for ethical and legal reasons. Watermarking is a budding technology that is capable of assisting this aim. Encoding an identifying code into digitized music, video, picture, or other file is known as a digital watermark. Watermarking [2] is the process of embedding a message data (watermark) such as a secret image, audio or video into another data (Cover object) which is visible to the public. In case of Blind Watermarking technique [4] the secret message image is invisible. Digital watermarking can be classified into image watermarking, video watermarking and audio watermarking according to the range of application. The current digital watermarking schemes mainly focus on image copyright protection [2]. Due to the transferring of the images and data there is a possibility of affecting noises in the images [5]. So the images we getting may face some distortions or the clarity problem and also the missing data in the watermark is crucial.

Due to all these we are not able to analyze properly and the decisions we are making may become false. So we need a better technique for doing the digital image watermarking.This watermarking algorithms can use any applications where the privacy of the data is of main concern. It can be used in any system which uses confidential data to be passed between the users. As in case of medical applications (EPR) [3] and also for keeping the details of the persons in any organization we can use this method.

Remaining part of the paper is organized as follows. The state of art is discussed in chapter 2 where a closer look to the existing methods can be done. Chapter 3 explains the system development that can be followed to implement the noise analysis and robustness measures. Chapter 4 gives a description about the results obtained. Chapter 5 explains the conclusion of the study and its related future work suggestions.

II. REVIEW OF RELATED LITERATURES

A). Digital Watermarking Techniques

A watermarking algorithm embeds watermark in different kind of data like, text, audio, video etc.. The embedding process is done by use of a private key which decided the locations within the multimedia object (image) where the watermark would be embedded. Once the watermark is embedded it can happens several attacks because the online object can be digitally processed. The attacks can be unintentional Hence the watermark has to be very robust against all attacks which is possible [5]. When the owner wants to check the watermarks in the attacked and damage multimedia object, she/he depends on the private key that was used to embed the watermark. Using the secrete key, the embedded watermark can be detected. This

detected watermark may or may not combine the original watermark because the image might have been attacked. Hence to validate the presence of watermark, the original data is used to compare and extract the watermark signal (non -blind watermarking) or a correlation method is used to detect the strength of the watermark signal from the extracted watermark (Blind watermarking). In the correlation, detected watermark from the original data is compared with the extracted watermark

B). *Discrete Cosine Transform*

Transformation of an image is needed to get more information about the image and to reduce the computational complexity. DCT [1] is a transformation technique for converting a signal into elementary frequency components. In DCT [1], most of the information (dc-coefficient) is present in the first pixel. DCT like a Fourier Transform, it represents data in terms of frequency space rather than an amplitude space. This is useful because that corresponds more to the way humans perceive light, so that the part that are not perceived can be identified and thrown away. DCT based watermarking techniques are robust compared to spatial domain techniques. Such algorithms are robust against simple image processing operations like low pass filtering, brightness and contrast adjustment, blurring etc. However, they are difficult to implement and are computationally more expensive. At the same time they are weak against geometric attacks like rotation, scaling, cropping etc. DCT [1] domain watermarking can be classified into Global DCT watermarking and Block based DCT watermarking. Embedding in the perceptually significant portion of the image has its own advantages because most compression schemes remove the perceptually insignificant portion of the image.[1]

C). Electronic Patient Record

An **electronic patient record (EPR)** [3] is a systematic collection of electronic health information about an individual patient or population. It is a record in digital format that is theoretically capable of being shared across different health care settings. In some cases this sharing can occur by way of network-connected, enterprise-wide information systems and other information networks or exchanges. EPRs[3] may include a range of data, including medical history, medication and allergies, immunization status, laboratory test results, radiology images, personal statistics like age and weight, and billing information. It allows for an entire patient history to be viewed without the need to track down the patient's previous medical record volume and assists in ensuring data is accurate, appropriate and legible.

D). *Human Visual System*

Here dealing HVS [3], human visual system in watermarking. The watermark's invisibility issue is tackled by the embedding depth. Uniform areas of the image are very sensitive to watermark addition so they only support extremely small embedding depth. Whereas edge areas, for instance, support deeper watermark addition. Contrast as a measure of relative variation of luminance for periodic pattern. Contrast as a measure of relative Variation of luminance for periodic pattern. Contrast is the difference in luminance and/or color that makes an object (or its representation in an image or display) distinguishable. In visual of the real world, contrast is determined by the difference in the color and brightness of the object and other objects within the same field of view. Because the human visual system is more sensitive to contrast than absolute luminance, we can perceive the world similarly regardless of the huge changes in illumination over the day or from place to place. The maximum *contrast* of an image is the contrast ratio or dynamic range.[3]

E). Fuzzy Interference System

Mamandi Fuzzy Interference systems are computing frameworks based on the concept of fuzzy set theory. Its success is mainly due to their closeness to human perception and reasoning and simplicity. These are the important factors for acceptance and usability of system. This GUI tool allows editing the highest level features of the fuzzy inference system, such as the number of input and output variables, the defuzzification method used, and so on. FIS systems have three main blocks: Input, Rule base and Output. The core of the FIS is its rule base (knowledge base), which is expressed in terms of fuzzy rules and allows for approximate reasoning. In this method the FIS and the HVS combined are used to adjust the watermarking strength. [6]

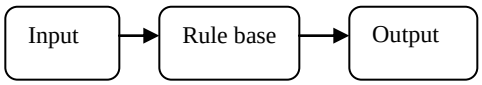

Fig 1. Scheme of Fuzzy Interference System

F). Psnr & Mse

The Mean Square Error (MSE) [5] [8] and the Peak Signal to Noise Ratio (PSNR) [5][8] are the two error metrics used to compare image compression quality. The MSE means the cumulative squared error between the compressed and the original image, whereas PSNR denotes a measure of the peak error. To compute the PSNR, the block first calculates the mean-squared error. This ratio is used as a quality measurement benchmark between the original and a compressed image. The MSE [5] represents the cumulative squared error between the compressed and the original image, whereas PSNR represents a measure of the peak error. The lower the value of MSE, the lower will be the error.

III. SYSTEM DEVELOPMENT

Proposed research is doing in MATLAB. There are different ways to perform watermarking using DCT operation, for applying digital watermarking such as block processing. Selected method is block processing for doing ordinary DCT transform and for watermarking with the help of FIS [6] system. After embedding and retrieving back the watermark for checking the robustness of the method doing some common noise analysis steps. Noise analysis is done by subjecting the watermarked image to cropping of different size, rotating to different angles and applying compression of different levels. Then trying to extract the watermark from that and by analysing the performance we decide which one is the better method. And as the final process making them easy to handle for the users by using GUI tool.

A). Watermark Embedding Using Block Processing Dct

For embedding and extraction of watermark make the cover image into 8×8 block and performing DCT [1] using block processing. For embedding the watermark by using ordinary DCT, after resizing the image insert the corresponding binary equivalent of text value to the block. We are choosing key as the position of watermark embedding pixel. For ordinary DCT [1]choosing the 'α' value a constant all the time, commonly taking as the mean value of the pixels. In watermarking using ordinary DCT [1] chose α value as a constant ranging from 0 to 1. Commonly taking α as the mean value. And according to the rules shown in the flowchart we are doing watermark embedding. In this approach we are not considering about the features of image in corresponding block. Another type of block processing embedding is done with the usage of LSB algorithm. In that embedding the watermark in to the least significant bit. One more approach is also available that is embedding in the mean value of the pixel [2]. We are adopted that technique, here we are taking embedding strength as a mean value. If we are selecting a low value then watermark will become more visible. If we take a high value such as edges values then attacks such as compression and resizing is affecting more in this parts. That is why we are selected mean value as the embedding strength and the embedding is done at the middle value of the 8×8 block. So in this approach we are using two keys for the embedding. One as the position number of the pixels, and another as the no of symbols we are embedding.

B). *Watermark Embedding With Fis*

We perform DCT with the help of FIS for improving the quality of the watermarked image. So instead of taking 'α' a constant value, calculating the value of 'α' according to the character of each block of the image. We are choosing the properties of the images such as 'entropy, correlation, homogeneity, contrast and energy'. Formulating some rules with the help of FIS with the suitability of HVS [3]system. In DCT time to frequency transformation is done. Now the watermarked image we get by converting it to time domain. For extraction process just does the reverse operation of the above for both types. Noise analysis is done by subjecting the watermarked image to cropping of different size, rotating to different angles and applying compression of different levels. Then trying to extract the watermark from that and by analysing the performance we decide which one is the better method. And as the final process making them easy to handle for the users by using GUI tool.

For the case of watermarking with the help of FIS choose α value according to the nature of the particular image block. This value varying with the difference in the property of the image block. Choosing of this doing with the help of FIS [6] toolbox. Here created some rule for finding out the embedding strength of different image blocks by providing input as 'entropy, correlation, energy, homogeneity and contrast'. We are defining some rules in the rule base according to the HVS [3]. FIS toolbox [6] itself finding out the different values of embedding strength according to the rules we created.

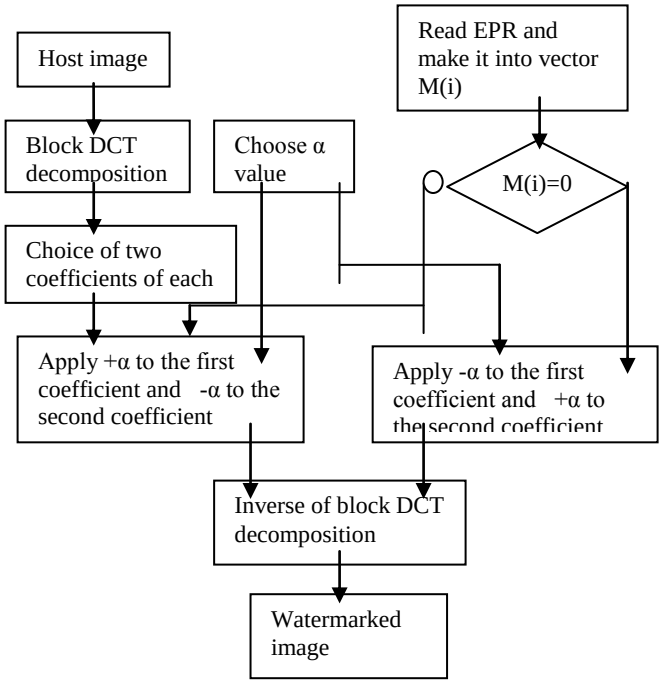

Fig 2. Watermark embedding process

C). *Rules For The Fis Rule Base*

Angular second moment, a measure of homogeneity of an image. The higher the value of this

indicates that the intensity varies less in an image. So we need to make embedding strength as low. Contrast is the measure of local variation in an image. A high value of contrast indicates a high degree of local variation. So a high value of embedding strength can use. Correlation is a measure of linear dependency of intensity values in an image. An image with large area of similar intensity correlation is high. So for a higher value of correlation we need to make embedding strength low. Energy or variance indicates the variation of image intensity values. For an image with identical intensity the energy would be negligible. So for higher value of energy a high value of embedding strength is desirable. Entropy is an indication of the complexity within an image. A complex image produces a high entropy value. For higher entropy value a lower embedding strength is suitable. All these conditions are accordance with the HVS [3]system also. Based on all these condition we made some rules for the FIS [6] system and by trial and error method we defined some range of values as the minimum values average values and maximum values so on. Also we defined the output as embedding strength and defined a set of values as high, low and medium. So for every cover image according to these criteria's the FIS system will itself decide the embedding strength.

TABLE 1. RULES FOR FIS RULE BASE

H	***E***	***V***	***CR***	***CT***	***ES***	***OP***
high			high		low	OR
	high	high		high	high	”
high					low	”
					low	”
					high	”
			low		high	”
high			low		medium	AND
low			high		medium	”
	high	low		low	medium	”
	low	high		low	medium	”
	low	low		high	medium	”

(H= Homogeneity, E= Entropy, V= Variance, CR= Correlation, CT= Contrast, ES= Embedding Strength, OP= Operation)

D). *Watermark Detection*

We use the same technique for detection of both methods. In this we are using semi blind watermarking for the retrieval, i.e., we are retrieving only the embedded message, here the details of the patient. We are not using the cover image for the further process. Using the same key for detection also that is the position no of the pixels where we added the message and the no of characters we are embedded. Here the key for both embedding and extraction is known to both end users. Following flowchart explains the concept behind the detection process. [7]

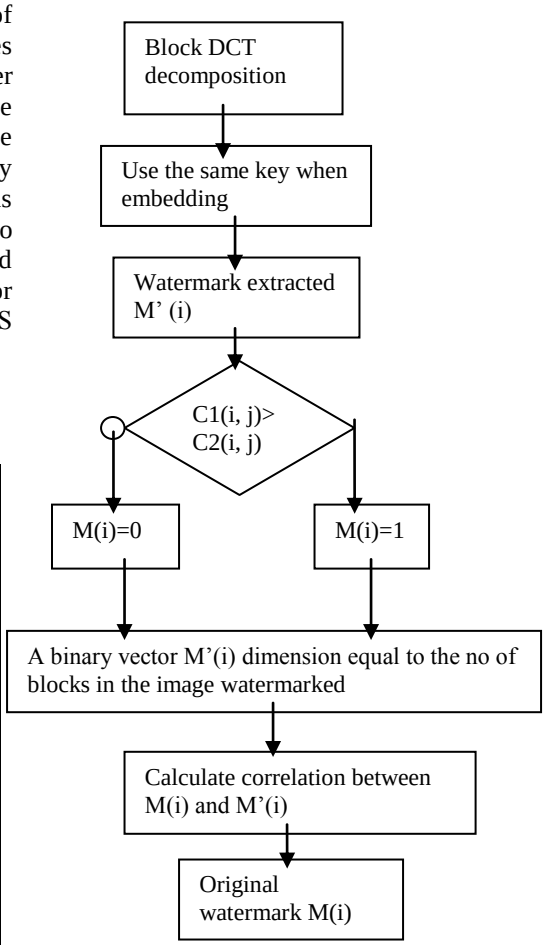

Fig 4. Watermark detection process

E). *Robustness Measure*

1. *PSNR Measure*

The most popular distortion measures in the image field are the Signal-to-Noise Ratio (SNR*)* and the Peak Signal-to-Noise Ratio (PSNR*)*. They are usually measured in decibels, i.e., "dB": The higher value of PSNR indicates noise content is lesser r the signal amount is higher. When comparing the two methods watermarking with FIS [7] offers a higher PSNR value than the other. So it is clear that the technique using FIS is more robust against noise. [5] [8]

2). *Compression measure*

Another attack is the JPEG compression attack. If the watermarked image is not already in JPEG format, the attacker can simply convert the watermarked image into a JPEG, varying the "quality factor" of JPEG compression to as low as he can before the features he needs on the image deteriorates. Even if the watermarked image is already a JPEG, the attacker can resave as a JPEG using a lower quality factor. This attack is a simple one without the need for complicated image processing software and many image viewers is able to save JPEG files using different quality factors. Because of how common and easy the JPEG attack is, resistance to JPEG compression is treated as the most important criteria in this assessment of robustness. In the medical field, the compression rate is constantly a discussion subject because of the importance of the medical information. In order to perform this experiment, the watermarked image was compressed using different quality factors 90%, 70%, 50%, 30% and 10%.[5] [8]

IV. RESULTS AND DISCUSSIONS

The proposed project aims to implement detailed study of watermarking techniques using DCT and the DCT with the help of FIS [6] ,and the performance analysis of them including noise analysis. Watermarking and retrieving of EPR [3] in the form of text is done with ordinary DCT [1] block processing and also with the help of FIS system. Calculated the PSNR [5] [8] value of both the output for the comparison. Made it easy to show the result with the help of GUI. For finding the robustness of the method analysed the performance of both techniques with the normal attacks such as compression.

Figure 4. Shows the first GUI and we can select the cover image from the file by clicking the pushbutton. And there is a column for entering the details of the patient. In Figure 5 shows the output after doing the retrieval also. From the above fig it is clear that the watermarking with the aid of FIS [6] system is offering more quality than the other technique. Figure 6 shows the performance evaluation of both techniques. A comparison is made between the two watermarked images according to the performance of both with different quality factor. The analysis is done based on the compression attack. If one image is sending through some medium such as internet there is a possibility of changing the nature of the file by addition of some noise such as compression and rotation. In this scheme we are conscious abut the position of the pixels so we used a simple Gaussian filter for not losing the content

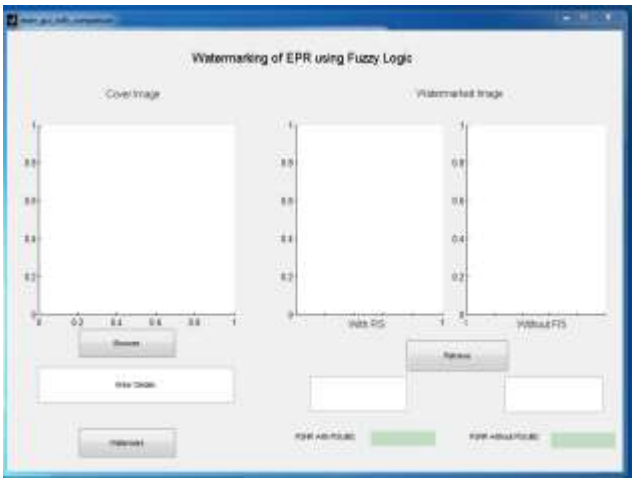

Fig 4. GUI before showing the results

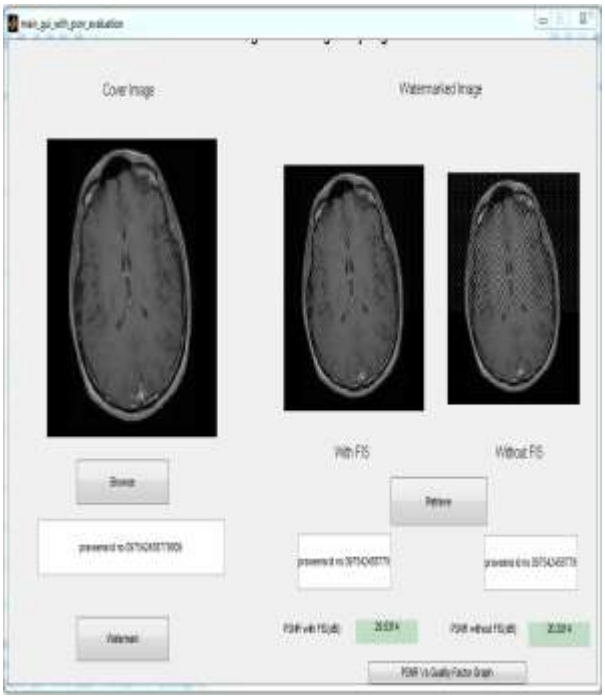

Fig 5. Final GUI showing results

A). Delimitations Of The Study

- Complicated mathematical analysis is doing for the comparison of different techniques so image enhancing is not possible up to 100%.
- Due to security problems not able to do the project with exact DICOM [3] images.

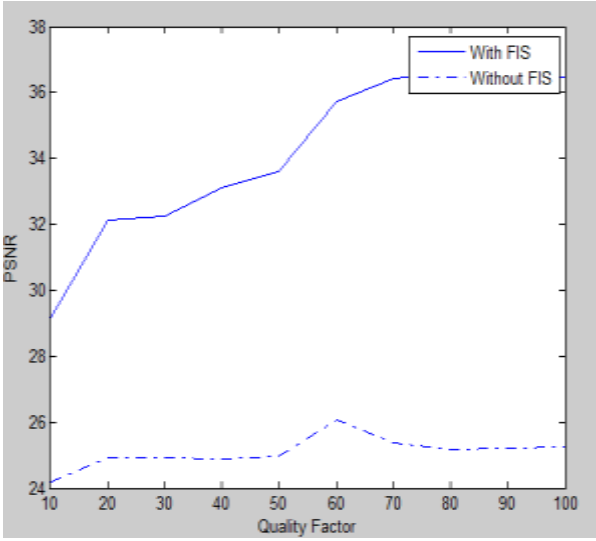

Figure 6. Performance comparison of two methods against compression for different quality factors

V. CONCLUSIONS AND FUTURE SCOPE

In this thesis tried to present a approach of blind watermarking scheme used in medical images that is robust some attacks. The FIS [7] and the HVS [3] combined are used to adjust the watermarking strength that can be embedded without noticeably degrading the quality of the image. The watermark is embedded into the mid-band frequency range of the image after being transformed by the Discrete Cosine Transform [1] (DCT). As a result, the watermark is more robust and imperceptible. The fuzzy inference [7] system is able to directly provide the power level to use, instead of the current iterative process. It is an improved technique for watermarking images. As future work; implement the new algorithm in order to obtain less degradation in the watermarked image and obtain better accuracy in the recovered watermark. Also in this the amount of data we can embed is depending upon the size f the cover image. So a better method can implement for embedding more details. From the study it is clear that the watermarking using DCT [1] with the help of FIS [7] is offering high performance than using ordinary block processing DCT by providing better PSNR [5] [8] value without degrading the quality of the image. The study also shows that the method is robust to compression attacks. The robustness is better than the method ordinary block processing DCT. This technique implemented to minimize the compression attack and improve the quality of watermarked image according to HVS [3]system

REFERENCES

[1] H.L.Desai, Pravin M. Pithiya, "*DCT Based Digital Image Watermarking, Dewatermarking & Authentication*", International Journal of Latest Trends in Engineering and Technology, Vol. 2 Issue 3 May 2013

[2] Srdjan S., O.Irena, (2010) "An application of multidimensional time- frequency analysis as base for the unified watermarking approach," *IEEE Transactions on image processing*, vol. 19, no. 3, pp. 736–745.

[3] G.Pradeepkumar, S.Usha,." EFFECTIVE WATERMARKING ALGORITHM TO PROTECT ELECTRONIC PATIENT RECORD USING IMAGE TRANSFORM" *IEEE Conference Publications, 2013 , Page(s): 1030 – 1034*

[4] Barni M., F.Bartolini, and T.Furon, (2003) "A general framework for robust watermarking security". *Signal Processing*, 83(10), pp. 2069-2084.

[5] Nallagarla.Ramamurthy and Dr.S.Varadarajan *"Effect of Various Attacks on Watermarked Images"* (IJCSIT) International Journal of Computer Science and Information Technologies, Vol. 3 (2) , 2012,3582-3587

6] Maji P., M. K. Kundu, B. Chanda, (2006) "Segmentation of Brain MR Images Using Fuzzy Sets and Modified Co-Occurrence Matrix", *Proceedings of The IET International Conference on Visual Information Engineering*, 327–332.

[7] Sameh Oueslati, Adnane Cherif, and Bassel Solaiman "MAXIMIZING STRENGTH OF DIGITAL WATERMARKS USING FUZZY LOGIC" Signal & Image Processing : An International Journal(SIPIJ) Vol.1, No.2, December 2010

[8] Baisa L Gunjal* and Dr. Suresh N Mali "Handling Various Attacks in Image Watermarking" Article CSI Communications February 2013

DEVELOPMENT OF ALGORITHMS FOR CONTRAST ENHANCEMENT OF REMOTE SENSING IMAGES

[1] Ramkumar.M.U, [2] Kavitha.N.Nair
[1]PG Scholar, Department of ECE, University College of Engineering, Muttom,Thodupuzha Kerala - 685587
[2]Lecturer, Department of ECE, University College of Engineering, Muttom, Thodupuzha, Kerala – 685587
[1]vidhunair20@gmail.com

Abstract – **For many years remote sensing images have played an important role in almost all fields such as meteorology, agriculture, geology, education etc. As the rising demand for high quality remote sensing images, contrast enhancement techniques are required for better visual perception and color reproduction. In this paper we explained some new enhancement techniques which use dominant brightness level analysis and adaptive intensity transformation with discrete wavelet transform and dual tree complex wavelet transform, DTCWT with principal component analysis (PCA), and a mathematical method for knee correction. Although various histogram equalization methods are proposed in the literature. They tend to degrade the overall image quality by exhibiting saturation artifacts in both low- and high- intensity layers. The proposed algorithms overcome this problem. In one method the DWT is performed first and then decompose the LL subband into low- middle-high- intensity layers using log-average luminance. Intensity layer transfer functions are adaptively estimated by using knee transfer function and the gamma adjustment function based on dominant brightness level on each layer .After the intensity transformation the enhance image is get back by taking Inverse DWT. We can do the decomposition using DTCWT in second method for better result. The contrast enhancement is performed with PCA and alternate knee correction method along with DWT and DTCWT for better results. The performance of every method is evaluated with parameters such Mean Square Error (MSE), Measure of Enhancement (EME), Peak Signal to Noise Ratio (PSNR) and Mean Absolute Error (MAE).**

Index Terms— **Adaptive intensity transfer function, contrast enhancement, discrete wavelet transform (DWT), dominant brightness level analysis, dual tree complex wavelet transform (DTCWT), remote sensing.**

I. INTRODUCTION

Image enhancement techniques improve the quality of an image as perceived by a human. The aim of image enhancement is to improve the interpretability or perception of information in images for human viewers, or to provide better input for other automated image processing techniques. These techniques are most useful because many satellite images when examined on a colour display give inadequate information for image interpretation. There is no conscious effort to improve the fidelity of the image with regard to some ideal form of the image. There exists a wide variety of techniques for improving image quality. The contrast stretch, density slicing, edge enhancement, and spatial filtering are the more commonly used techniques. Image enhancement is attempted after the image is corrected for geometric and radiometric distortions. The proposed paper introduces some new methods for contrast enhancement.

Histogram equalization (HE) [1] has been the most popular approach to enhancing the contrast in various application areas such as medical image processing, object tracking, speech recognition, etc. HE-based methods cannot, however, maintain average brightness level, which may result in either under- or oversaturation in the processed image. For overcoming these problems, bi-histogram equalization (BHE) [2] method have been proposed by using decomposition of two subhistograms. For further improvement, the recursive mean-separate HE (RMSHE) [3] method iteratively performs the BHE and produces separately equalized subhistograms. However, the optimal contrast enhancement cannot be achieved since iterations converge to null processing. And also proposed a modified HE method which is based on the singular-value decomposition of the LL subband of the discrete wavelet transform (DWT) [4] [5] . In spite of the improved contrast of the image, this method tends to distort image details in low- and high-intensity regions.

In remote sensing images, the common artifacts caused by existing contrast enhancement methods, such as drifting brightness, saturation, and distorted details; need to be minimized because pieces of important information are

widespread throughout the image in the sense of both spatial locations and intensity levels. For this reason, enhancement algorithms for satellite images not only improve the contrast but also minimize pixel distortion in the low- and high-intensity regions.

For achieving this goal we presented three new methods which uses adaptive intensity transfer function [6], alternate knee correction and principal component analysis along with DWT [7] and DTCWT [8] for comparative study.

II. IMAGE DECOMPOSITION TECHNIQUES

For the given three new methods we have to first perform either DWT or DTCWT for image decomposition. The theories behind the two are given in the following paragraphs.

A. Discrete Wavelet Transform (DWT)

An image is represented as a two dimensional array of coefficients, each coefficient representing the brightness level in that point. When looking from a higher perspective, the coefficients cannot be differentiated as more important one, and lesser important one. But most natural images have smooth colour variations, with the fine details being represented as sharp edges in between the smooth variations. Technically, the smooth variations in colour can be termed as low frequency variations and the sharp variations as high frequency variations. The low frequency components constitute the base of an image and the high frequency components add upon them to refine the image thereby giving a detailed image. Hence the smooth variations are demanding more importance than the details. Separating the smooth variations and details of the image can be done in many ways. One such way is the decomposition of the image using Discrete Wavelet Transform (DWT)

DWT decomposes an image into four sub-bands: approximation and detailed sub-bands- horizontal, vertical, and diagonal. The detailed sub-bands shows variations along the columns (horizontal edges), rows (vertical edges), and diagonals (diagonal edges) respectively As shown in Fig. 1 at each level, approximation sub-band is decomposed into the above mentioned four sub-bands. A low pass filter and a high pass filter are chosen, such that they exactly have the frequency range between themselves. The filter pair is called the analysis filter pair. First the low pass filter is applied for each row of data, thereby getting the low frequency components of the row. Now the high pass filter is applied for the same row of data, and similarly the high pass components are separated and placed by the side of the low pass components. This procedure is done for all rows. Next, the filtering is done for each column of the intermediate data. The resulting two dimensional arrays of coefficients contain four bands of data, each labeled as LL (low- Low), HL (high-low), LH (Low-High) and HH (High-High). The LL band can be decomposed once again in the same manner, thereby producing even more subbands. This can be done up to any level, thereby resulting in a pyramidal decomposition as shown in Fig.1. The LL band at the highest level can be classified as most important and the other detail bands can be classified as of lesser importance, with the degree of importance decreasing from the top of the pyramid to the bands at the bottom. In Fig. 1 three level decomposition is shown. Here, L & H represents low frequency and high frequency components respectively. The sub-band LL denotes the low frequency component of the image, which is the approximation sub-band of the original image. The sub-band HL is the low frequency component in horizontal direction and the high frequency component in vertical direction, which shows the horizontal edge in the original image. The sub-band LH is the high frequency component in horizontal direction and the low frequency component in vertical direction, which shows the vertical edge in the original image. The sub-band HH is the high frequency component, which manifests the diagonal edges in the original image.

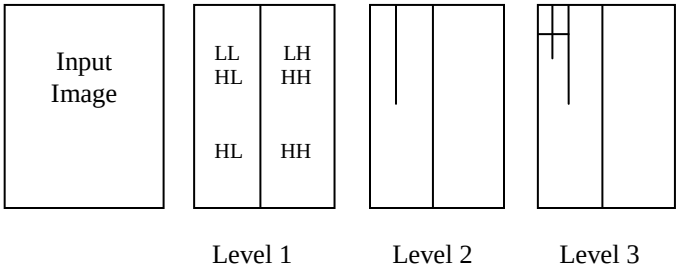

Fig. 1. Flow chart of the DWT decomposition

B. Dual tree complex wavelet transform (DTCWT)

There mainly some problems associated with DWT such as oscillations, shift variance, aliasing and lack of directionality. All these problems can be removed in DTCWT.

The dual tree approach, which is based on two filter banks and two bases is shown in Fig. 2.

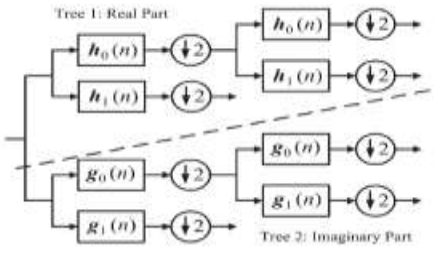

Fig. 2. 2 Level 1D DTCWT

The idea behind the dual-tree approach is quite simple. The dual tree CWT employs two real DWTs; the first DWT gives the real part of the transform while the second DWT gives the imaginary part. The decomposition image is shown in Fig 2 and it its reverse will give final result. The two real wavelet transforms use two different sets of filters. The two sets of filters are jointly designed so that the overall transform is approximately analytic. Let $h_0(n)$, $h_1(n)$ denote the low-pass/high-pass filter pair for the upper FB, and let $g_0(n)$, $g_1(n)$ denote the low-pass/high-pass filter pair for the lower FB. We denote the two real wavelets associated with each of the two real wavelet transforms as $\varphi_h(t)$ and $\varphi_g(t)$. To invert the transform, the real part and the imaginary part are each inverted the inverse of each of the two real DWTs are used to obtain two real signals. These two real signals are then averaged to obtain the final output. Note that the original signal x (n) can be recovered from either the real part or the imaginary part alone. DT-CWT produces six directional subbands, oriented at $\pm 15^0$, $\pm 45^0$ and$\pm 75^0$, while the DWT produces only three directional subbands, oriented at 0^0 , 45^0 and90^0 .

III. ALGORITHM 1-CONTRAST ENHANCEMENT USING DOMINANT BRIGHTNESS LEVEL ANALYSIS AND ADAPTIVE INTENSITY TRANSFORMATION

In this section present a novel contrast enhancement algorithm for remote sensing images using dominant brightness level-based adaptive intensity transformation as shown in Fig.3.We can use DWT or DTCWT for image decomposition. This decomposes the input image into wavelet subbands and decomposes the LL subband into low, middle, and high-intensity layers by analyzing the log-average luminance of the corresponding layer. The adaptive intensity transfer functions are computed by combining the knee transfer function [9] and the gamma adjustment function [10] [11]. All the contrast enhanced layers are fused with an appropriate smoothing, and the processed LL band undergoes inverse transform together with unprocessed LH, HL, and HH subbands to reconstruct the finally enhanced image.

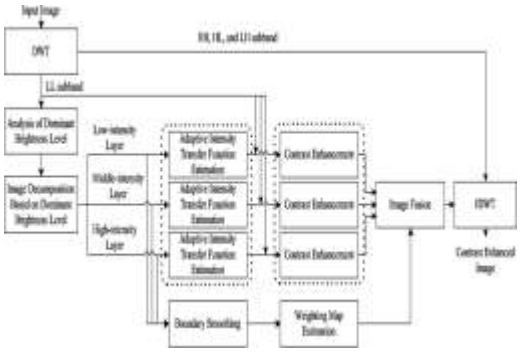

Fig.3: Block diagram of Algorithm 1

A. Analysis of Dominant Brightness Levels

If we do not consider spatially varying intensity distributions, the correspondingly contrast enhanced images may have intensity distortion and lose image details in some regions. For overcoming these problems, first decompose the input image into multiple layers of single dominant brightness levels. To use the low-frequency luminance components, perform the DWT on the input remote sensing image and then estimate the dominant brightness level using the log average luminance in the LL subband. Since high-intensity values are dominant in the bright region, and vice versa, the dominant brightness [12] [13] at the position (x, y) is computed as,

$$\mathrm{D}(x,y) = \exp\left(\frac{1}{N_L}\sum_{(x,y)\varepsilon S}\{logL(x,y) + \varepsilon\}\right) \qquad (1)$$

Where S represents a rectangular region encompassing (x, y), L(x, y) represents the pixel intensity at (x, y), N_L represents the total number of pixels in S, and ε represents a sufficiently small constant that prevents the log function from diverging to negative infinity. The low-intensity layer has the dominant brightness lower than the pre specified low bound. The high intensity layer is determined in the similar manner with the pre specified high bound, and the middle-intensity layer has the dominant brightness in between low and high bounds. The normalized dominant brightness varies from zero to one, and it is practically in the range between 0.5 and 0.6 in most images. For safely including the practical range of dominant brightness, we used 0.4 and 0.7 for the low and high bounds, respectively.

B. Edge Preserving Contrast Enhancement Using Adaptive Intensity Transformation

Based on the dominant brightness in each decomposed layer, the adaptive intensity transfer function is generated. Since remote sensing images have spatially varying intensity distributions, we estimate the optimal transfer function in each brightness range for adaptive contrast enhancement. The adaptive transfer function is

estimated by using the knee transfer and the gamma adjustment functions. For the global contrast enhancement, the knee transfer function stretches the low-intensity range by determining knee points according to the dominant brightness of each layer. More specifically, in the low-intensity layer, a single knee point is computed as,

$$P_l = b_l + w_l\ (b_l - m_l) \quad (2)$$

Where b_l represents the low bound, w_l represents the tuning parameter, and m_l represents the mean of brightness in the low intensity layer. For the high-intensity layer, the corresponding knee point is computed as,

$$P_h = b_h - w_h\ (b_h - m_h) \quad (3)$$

Where b_h represents the high bound, w_h represents the tuning parameter, and m_h represents the mean of brightness in the low intensity layer. In the middle intensity layer, two knee points are computed as,

$$P_{ml} = b_l - w_m(b_{ml} - m_m) + (p_l - p_h) \quad (4)$$

$$P_{mh} = b_h + w_m(b_{mh} - m_m) + (p_l - p_h) \quad (5)$$

Where w_m represents the tuning parameter and m_m represents the mean brightness in the middle-intensity layer.

The global image contrast is determined by tuning parameter w_i for i $\epsilon\{l, m, h\}$. Although the contrast is more enhanced as the w_i increases, the resulting image is saturated and contains intensity discontinuity. Here adjust only the middle-intensity tuning parameter wm for reducing such artifacts. Since the knee transfer function tends to distort image details in the low- and high intensity layers, additional compensations performed using the gamma adjustment function. The gamma adjustment function is modified from the original version by scaling and translation to incorporate the knee transfer function as,

$$G_k(L) = \left\{\left(\frac{L}{M_k}\right)^{1/\gamma} - \left(1 - \frac{L}{M_k}\right)^{1/\gamma} + 1\right\} \quad (6)$$

For k $\epsilon\{l, m, h\}$ Where M represents the size of each section intensity range, such as $M_l = b_l, M_m = b_h - b_l$ and $M_h = 1 - b_h$, L represents the intensity value, and γ represents the pre specified constant. The pre specified constant γ can be used to adjust the local image contrast. As γ increases, the resulting image is saturated around $b_l/2$, $b_h - b_l/2$ and $1 - b_h/2$ .Therefore, the γ value is selected by computing maximum values of adaptive transfer function in ranges $\{0 \leq L < b_l/2\ \}$, $\{b_l \leq L < (b_h - b_l/2)\}$ and $\{b_h \leq L < (1 - b_h/2)\}$ which are smaller than, $b_l/2$, $b_h - b_l/2$, and $1 - b_h/2$ respectively.

The proposed adaptive transfer function is obtained by combining the knee transfer function and the modified gamma adjustment function. Three intensity transformed layers by using the adaptive intensity transfer function are fused to make the resulting contrast-enhanced image in the wavelet domain. Extract most significant two bits from the low- , middle-, and high-intensity layers for generating the weighting map, and compute the sum of the two bit values in each layer and select two weighting maps that have two largest sums. For removing the unnatural borders of fusion, weighting maps are employed with the Gaussian boundary

smoothing filter. As a result, the fused image F is estimated as,

$$F = W_1 \times c_l + (1 - W_l) \times \{W_2 \times c_m + (1 - W_2) \times c_h\} \quad (7)$$

Where W_1 represents the largest weighting map, W_2 represents the second largest weighting map, c_l represents the contrast enhanced brightness in the low-intensity layer, c_m represents the contrast-enhanced brightness in the middle-intensity layer, and c_h represents the contrast enhanced brightness in the high-intensity layer. Since Eqn. (7) represents the point operation, the pixel coordinate (x, y) is omitted. The fused LL subband undergoes the IDWT together with the unprocessed HL, LH, and HH subbands to reconstruct the finally enhanced image.

IV. ALGORITHM 2-CONTRAST ENHANCEMENT USING DOMINANT BRIGHTNESS LEVEL ANALYSIS AND PRINCIPAL COMPONENT ANALYSIS

In this section we present a new contrast enhancement algorithm for remote sensing images using dominant brightness level- and PCA [14] as shown in Fig.4.We can use DWT or DTCWT for image decomposition. This decomposes the input image into wavelet subbands and decomposes the LL subband into low, middle, and high-intensity layers by analyzing the log-average luminance of the corresponding layer. The principal component are analyzed and contrast enhancement is. All the contrast enhanced layers are fused with an appropriate smoothing, and the processed LL band undergoes Inverse transform together with unprocessed LH, HL, and HH subbands to reconstruct the finally enhanced image.

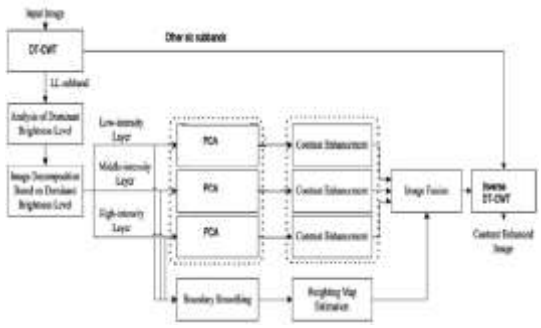

Figure 4: Contrast enhancement using DT-CWT and PCA

A. Principal Component Analysis (PCA)

Principle Component Analysis (PCA) is a statistical analytical tool that is used to explore sort and group data. PCA is a classical de-correlation technique which has been widely used for dimensionality reduction with direct applications in pattern recognition, data compression and noise reduction. What PCA does is take a large number of correlated (interrelated) variables and transform this data into a smaller number of uncorrelated variables (principal Components) while retaining maximal amount of variation, thus making it easier to operate the data and make predictions. Or as Smith (2002) puts it PCA is a way of identifying patterns in data, and expressing the data in such a way as to highlight their similarities and differences. Since patterns in data can be hard to find in data of high dimension, where the luxury of graphical representation is not available; PCA is a powerful tool for analyzing data.

B. Steps –PCA and DTCWT

1. Apply DT-CWT to the input image.
2. Find out the brightness level in LL subband using the equation (1) based on the brightness level LL subband decomposes into low, high and middle intensity layers.
3. Finding the PCA for all corresponding layers. For this Convert each layer into one dimensional vector A = $[X_1, X_2, X_3, X_4 \ldots]$ (i=1 to m*n) ,where m = number of rows, n=number of columns; Finding the mean value using this formula

$$K = \frac{1}{m*n} \sum_{i=1}^{m*n} a_i \quad (8)$$

4. Subtract the mean.
5. Calculate the covariance matrix.
6. Calculate the eigenvectors and Eigen values of the Covariance matrix
7. Finding Gaussian Factor with 5x5 Mask

$$h = \frac{1}{\sqrt{2\pi}} e^{(x^2+y^2)/2} \quad (9)$$

8. Finding maximum value of Gaussian coefficient (s1) And Eigen values (s).Multiply s1 with s .This value will be the enhanced Factor.
9. Multiplying all sub bands with this enhanced factor. Then perform fusion and Inverse DTCWT.
   We can perform it with DWT also.

V. ALGORITHM 3-CONTRAST ENHANCEMENT USING ALTERNATE KNEE CORRECTION METHOD

In this method the conventional knee point estimation is replaced by an alternate method which gives better results.

A. Knee correction By Mathematical Method

In algorithm, the knee points are estimated by using statistical methods. Statistical method means using the statistical property such as mean, variance etc of the image. Knee point is the point at which sudden change occurs. So an equivalent mathematical method for knee point estimation is proposed and is known as derivative method. In algebra y = f(x) be a function slope is given by the dy/dx that is derivative of the function. In this method calculate derivative of every point on the low, middle and high intensity layers and find out the point at which slope change occurs. These are the knee points of low, high and middle intensity layers. Derivative of each points are estimated by using gradient method. This knee point together with gamma function is used for the contrast enhancement of the LL layer and after appropriate smoothening and fusion process the final image is got by the inverse of the corresponding inverse transform. The block diagram of this method is given in Fig.5.

B. Steps-Alternate knee correction Method

1. Apply DT-CWT or DWT to the input image.
2. Find out the brightness level in LL subband using the equation (1) based on the brightness level LL subband decomposes into low, high and middle intensity layers.
3. Apply alternate knee correction method to find knee point
4. Calculate the gamma correction function.
5. Combining the knee and gamma to obtain contrast enhancement
6. Perform Smoothing filtering of layers.
   Finally perform fusion and Inverse DTCWT

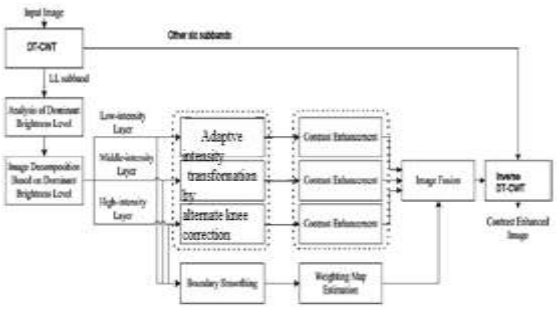

Fig. 5: Contrast enhancement using Alternate knee correction

VI. EXPERIMENTAL RESULTS

For evaluating the performance of the proposed algorithm, we tested low-contrast remote sensing images as shown in Fig. 6. The performance [15] of the proposed algorithms is compared with existing well-known algorithms including standard HE, BHE, RMSHE and DWT-SVD Methods.

The proposed method is evaluated using the Peak Signal to Noise Ratio (PSNR), Mean Square Error (MSR), Measure of Enhancement (EME), Mean Absolute Error (MAE). PSNR is the quality measurement between the original image and the reconstructed image which is calculated through the Mean Squared Error (MSE). The MSE represents the cumulative squared error between the compressed and the original image, whereas PSNR represents a measure of the peak error. The EME [16] represents the overall image quality enhanced with preserving the average brightness level and edge details in all intensity ranges and MAE represents mean of the difference existing between two images. These parameters are calculated as follows:

$$\text{EME}=\frac{1}{k1k2}\sum_{i=1}^{k2}\sum_{k=1}^{k1}\frac{I_{max}\,(k,l)}{I_{min}\,(k,l)}\ln\frac{I_{max}\,(k,l)}{I_{min}\,(k,l)+c} \quad (10)$$

Where k1, k2 represents the total number of blocks in an image, $I_{max}\,(k,l)$ represents the maximum value of the block, $I_{min}\,(k,l$ represents the minimum value of the block, and c represents a small constant to avoid dividing by zero.

$$\text{MSE} = \frac{1}{MN}\sum_{i=0}^{M-1}\sum_{j=0}^{N-1}[I(i,j)-K(i,j)]^2 \quad (11)$$

$$\text{MAE} = \frac{1}{MN}\sum_{i=0}^{M-1}\sum_{j=0}^{N-1}|I(i,j)-K(i,j)| \quad (12)$$

$$\text{PSNR} = 10\log\frac{255^2}{MSE} \quad (13)$$

Where I(i, j) is the input image and K(i, j) is the output image. The development of the system includes the generation the codes for each of the above steps and finally we can measure the performance of the proposed method and we can do a comparison with the older methods for better distinguishing. The performance measure includes MSE, MAE, PSNR and EME. For contrast enhancement purposes the better method for evaluating the performance is EME that is the measure of enhancement.

For the experiment, we used γ = 1.4, b_l = 0.4, and b_h = 0.7. For three different intensity layers, w_l = 1, w_m = 3, and w_h = 1 were used. The results of the standard HE method show under- or oversaturation artifacts because it cannot maintain the average brightness level. Although RMSHE and GC-CHE methods can preserve the average brightness level, and better enhance overall image quality, they lost edge details in low- and high-intensity ranges On the other hand, Demirels method could not sufficiently enhance the low-intensity range because of the singular-value constraint of the target image. Fig.6 (a) - (e) [17] shows the results of the proposed contrast enhancement method. The overall image quality is significantly enhanced with preserving the average brightness level and edge details in all intensity ranges. Here the knee point estimation is did using statistical methods. An alternate method for knee correction that is derivative method is also tested with the same image. Resultant contrast enhanced image using alternate knee correction as shown in Fig. 9. Using this knee correction contrast is not significantly improved but some brightness preservation satisfied and also improved the visual interpretation as shown in Fig.9. Fig.7 shows the enhancement using adaptive method with DTCWT. Fig.8 shows the results of enhancement using DTCWT and PCA. Here 4 LEVEL DTCWT is used. The DTCWT-PCA can achieve the sharpest enhancement result compared to other enhancement methods. EME values for different enhancement methods are listed in Table I.We also include the value of PSNR, MAE and MSE. Comparison of EME values show that the proposed Method outperforms existing enhancement methods.

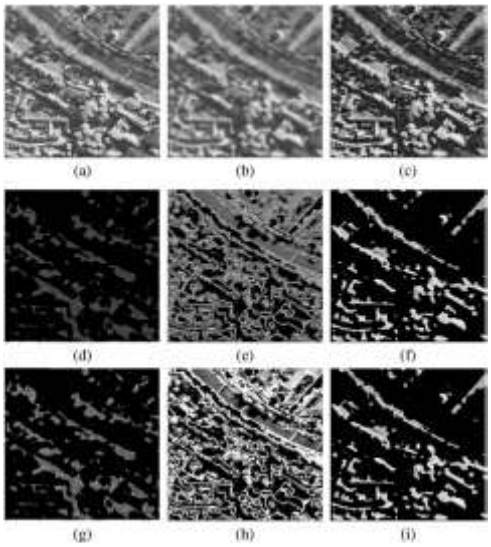

Fig. 6: Image decomposition based on the dominant brightness levels and contrast enhancement results. (a) Original image. (b) Dominant intensity analysis.(c) Enhanced result image. (d-f) Low-, middle-, and high- intensity layers. (g-i) Enhanced low-, middle-, and high intensity layers.

Fig.7: Enhanced image DTCWT and adaptive intensity transformation

Fig. 8: Enhanced image using DTCWT and PCA

Fig. 9: Enhanced image using alternate knee correction

TABLE I: COMPARISON OF RESULTS BETWEEN PROPOSED METHODS AND EXISTING METHODS

Method	EME	MSE	PSNR	MAE
DTCWT-PCA	1.3265	22.43	20.14	26.13
Alternate knee correction	0.6347	27.43	24.12	28.14
Adaptive intensity method	0.7313	24.65	20.32	24.23
SVD-DWT	0.626	42.05	15.66	35.70
RMSHE	0.680	64.31	10.12	54.06
BHE	0.690	63.17	12.15	52.34
HE	0.689	42.17	15.54	37.92

VII.CONCLUSION

In this paper we have presented different contrast enhancement method for remote sensing images. The existing algorithm decomposes the input image into four wavelet subbands and decomposes the LL subband into low-, middle-, and high-intensity layers by analyzing the log-average luminance. The adaptive intensity transfer functions are computed by combining the knee transfer function and the gamma adjustment function. All the contrast enhanced layers are fused with an appropriate smoothing, and the processed LL band undergoes the IDWT together with unprocessed, HL, LH and HH subbands. This method utilizes DWT for image decomposition. But DWT produces some artifacts. To avoid the draw backs of DWT a new

transform called dual tree complex wavelet transform (DTCWT) is used. The transfer function is applied for the every pixel of the image and it does not deals with which are more important one and lesser important one. To separate correlated and uncorrelated parts of an image a statistical method is used called principal component analysis (PCA). A new enhancement method is proposed based on DTCWT and PCA. Using this, dimensionality reduction is also achieved and it can effectively enhance the overall quality and visibility of local details better than existing state-of-the-art methods including HE, BHE and RMSHE. Experimental results demonstrate that the proposed algorithms can enhance the low contrast satellite images and is suitable for various imaging devices such as consumer camcorders, real-time 3-D reconstruction systems, and computational cameras.

REFERENCES

[1] R. Gonzalez and R.Woods, Digital Image Processing, 3rd ed. Englewood Cliffs, NJ: Prentice-Hall, 2007.

[2] Y. Kim, Contrast enhancement using brightness preserving bi-histogram equalization, IEEE Trans. Consum. Electron., vol. 43, no. 1, pp. 18, Feb. 1997

[3] S. Chen and A. Ramli, Contrast enhancement using recursive mean separate histogram equalization for scalable brightness preservation, IEEE Trans. Consum. Electron. vol. 49, no. 4, pp. 13011309, Nov. 2003.

[4] H. Demirel, C. Ozcinar, and G. Anbarjafari, Satellite image contrast enhancement using discrete wavelet transform and singular value decomposition, IEEE Geosci. Reomte Sens. Lett., vol. 7, no. 2, pp. 3333337, Apr. 2010.

[5] H. Demirel, G. Anbarjafari, and M. Jahromi, Image equalization based on singular value decomposition, in Proc. 23rd IEEE Int. Symp. Comput. Inf. Sci., Istanbul, Turkey, Oct. 2008, pp. 15.

[6] Eunsung Lee, Sangjin Kim, Wonseok Kang, Doochun Seo, and Joonki Paik, Contrast Enhancement Using Dominant Brightness Level Analysis and Adaptive Intensity Transformation for Remote Sensing Images, IEEE Transactions on Geosciences and remote sensing letters, vol.10,no.1,january 2013.

[7] G.Veena, V.Uma, Ch. Ganapathy Reddy, Contrast Enhancement for Remote Sensing Images with Discrete Wavelet Transform, International Journal of Recent Technology and Engineering (IJRTE) ISSN: 2277- 3878, Volume-2, Issue-3, July 2013.

[8] Ivan W. Selesnick, Richard G. Baraniuk, and Nick G. Kingsbury. Dual-Tree Complex Wavelet Transform.

[9] Y.Monobe,H.Yamashita, T.Kurosawa and H.Kotera, Dynamic range compression preserving local image contarst for digital video camera, IEEE Trans.Consum.Electron.Vol.51 ,no.1.pp.110,Feb.2005.

[10] S. Lee, An efficient contrast-based image enhancement in the compressed domain using retinex theory, IEEE Trans. Circuit Syst. Video Technol., vol. 17, no. 2, pp. 199213, Feb. 2007.

[11] W. Ke, C. Chen, and C. Chiu, BiTA/SWCE: Image enhancement with bilateral tone adjustment and saliency weighted contrast enhancement, IEEE Trans. Circuit Syst. Video Technol., vol. 21, no. 3, pp. 360364, Mar. 2010.

[12] L.Meylan and S. Susstrunk, High dynamic range image rendering with a retinex-based adaptive filter, IEEE Trans. Image Process., vol. 15, no. 9, pp. 28202830, Sep. 2006.

[13] S. Chen and A. Beghdadi, Nature rendering of color image based on retinex, in Proc. IEEE Int. Conf. Image Process., Nov. 2009, pp. 18131816.

[14] R.Vani, K.Soundara Rajan, DWT and PCA Based Image Enhancement with Gaussian Filter, International Journal of Science and Modern Engineering (IJISME) ISSN: 2319-6386, Volume-1, Issue-3, February 2013. [15] S. Kim, W. Kang, E. Lee, and J. Paik, Wavelet-domain color image enhancement using filtered directional bases and frequency-adaptive shrinkage, IEEE Trans. Consum. Electron., vol. 56, no. 2, pp. 1063 1070, May 2010.

[16] S. S. Agaian, B. Silver, and K. A. Panetta, Transform coefficient histogram-based image enhancement algorithms using contrast entropy, IEEE Trans. Image Process., vol. IP-16, no. 3, pp. 741–758, Mar. 2007.

[17] Computer Vision Group-University of Granada (CVG-UGR) Image Database. [Online]. Available: http://decsai.ugr.es/cvg/dbimagenes.

ROI CODING OF REMOTE SENSING 2-D IMAGES USING SHAPE ADAPTIVE REVERSIBLE INTEGER LAPPED TRANSFORM

[1]Vaisakhan.B, [2]Kavitha N Nair
[1]PG Scholar, Department of ECE, University College of Engineering, Muttom,Thodupuzha Kerala - 685587
[2]Lecturer, Department of ECE, University College of Engineering, Muttom, Thodupuzha, Kerala – 685587
[1]vysaknb@gmail.com

Abstract – **Image compression is the application of data compression on digital images. Image compression can be lossy or lossless. Raw data from an image sensor obviously contains information about a scene, but it is not intrinsically recognizable to the human eye. This thesis proposes a new shape-adaptive (SA) transform, shape-adaptive reversible integer lapped transform (SA-RLT) method. Region-of interest (ROI) coding algorithms have also been proposed, since observers are always more concerned about some special areas, i.e, ROI than the background (BG) area. Based on SA-RLT and object-based set partitioned embedded block coder (OBSPECK), a new ROI compression scheme can be designed for 2D remote sensing images. A new ROI segmentation algorithm is used here to segment out ROI other than hand segmentation.**

Keywords- **Image Compression;Discrete Wavelet Transform (DWT); Discrete Cosine Transform (DCT); Region of interest (ROI); Shape Adaptive Reversible Lapped Transform (SARLT).**

I. INTRODUCTION

Remote sensing images have an important role in many fields such as environmental monitoring, geology detection, urban planning etc. Since these images will take up a great deal of storage space and bandwidth with increase in spatial resolution, compression techniques have been widely researched. Region of interest (ROI) coding algorithms also have much importance since observers are always more concerned about some special areas than background areas. A better lossless compression technique for remote sensing images based on shape adaptive reversible lapped transform (SA-RLT) which is having more advantages than other present SA transform methods is proposed. A comparison between the existing SA transforms such as SA-DWT, SA-DCT and the new SA-RLT method is made and it is analyzed that SA-RLT has preserved the information and is better than the other transforms. The proposed thesis includes a new SA-RLT based ROI coding scheme for 2-D remote sensing images.

The aim of source coding or data compression is to represent discrete signal s(n) with only a small expected number of bits per sample (the so called bit rate), with either no distortion (lossless compression), or as low distortion as possible for a given rate (lossy compression). Since we try to optimize the trade-off between distortion and rate on the average, we regard signals as random which we describe by their statistical properties. The essential step in source coding is quantization.

In PCM strong statistical dependencies exists between signal samples. Normally in PCM sample is quantized individually at a fixed number of bits, e.g. eight bits for grey level images[1].

Most signals representing meaningful information, however, exhibit strong statistical dependencies between signal samples. In images, for instance, the grey levels of neighbouring pixels tend to be similar. To take such dependencies into account, possibly large sets of adjacent samples should be quantized together. Unfortunately, this unconstrained approach leads to practical problems even for relatively small groups of samples.

In transform coding, the signals or images are first decomposed into adjacent blocks or vectors of N input samples each. Each block is then individually trans- formed such that the statistical dependencies between the samples are reduced, or even eliminated. Also, the signal energy which generally is evenly distributed over all signal samples s(n) should be repacked into only a few transform coefficients. The transform coefficients S(k) can then be quantized individually. Each quantizer output consists of an index i(k) of the quantization interval into which the corresponding transform coefficient falls. These indices are

then coded, e.g. by a fixed length code or an entropy code[2][3].

The decoder then first reconverts the incoming bit stream into the quantization indices, and then replaces the quantization index i(k) for each transform coefficient S(k) by the centroid V(i(k)) of the indexed quantization interval, which serves as approximation, or better, estimate, bS(k) = V (i(k)) of S(k). The relation between the indices i(k) and the centroid V (i(k)) is stored in a look-up table called a codebook[2]. An inverse transform then calculates the reconstructed signal. Clearly, due to quantization, the compression technique is lossy. Optimizing a transform codec needs to address choosing an optimal transform and optimal scalar quantization of the transform coefficients. Practical transform codec employ linear unitary or orthogonal transforms. Linear transforms explicitly influence linear statistical dependencies, that is, correlations

The principles of image compression are based on information theory. The amount of information that a source produce is Entropy. The amount of information one receives from a source is equivalent to the amount of the uncertainty that has been removed.

A source produces a sequence of variables from a given symbol set. For each symbol, there is a product of the symbol probability and its logarithm. The entropy is a negative summation of the products of all the symbols in a given symbol set. Compression algorithms are methods that reduce the number of symbols used to represent source information, therefore reducing the amount of space needed to store the source information or the amount of time necessary to transmit it for a given channel capacity. The mapping from the source symbols into fewer target symbols is referred to as Compression and Vice-versa Decompression.

Image compression refers to the task of reducing the amount of data required to store or transmit an image. At the system input, the image is encoded into it's compressed from by the image coder. The compressed image may then be subjected to further digital processing, such as error control coding, encryption or multiplexing with other data sources, before being used to modulate the analog signal that is actually transmitted through the channel or stored in a storage medium. At the system output, the image is processed step by the step to undo each of the operations that were performed on it at the system input. At the final step, the image is decoded into its original uncompressed form by the image decoder. If the reconstructed image is identical to the original image the compression is said to be lossless, otherwise, it is lossy[1].

ROI coding of 2-D remote sensing images based on SA-RLT performs better than other existing methods. However, it comes along with some drawbacks. ROI area is segmented by hand in the method. This will create more complexity in studying a particular region from the image as hundreds of images are obtaining at same instance from satellite. Also it will be much difficult to find out the particular region of interest from the satellite image with the help of human eye. So, hand segmenting the ROI area will create more complexity and consume more time.

The method can be used for any type of imaging devices but concentration in the field of satellite images. For several decades remote sensing images have played an important role in many fields such as meteorology, agriculture, geology, education etc. Because of the rising demand for high quality remote sensing images without losing any information while compression. Demand for ROI coding algorithms have increased as observers are always more concerned about some special areas than background areas

II. METHODOLOGY

In this section the detailed procedure for compression and segmentation of images are given.

A. Image Compression

In the compression procedure, lossless compressions are introduced. DWT and RLT algorithms are used to implement compression of images.

Compression techniques have been widely researched since images will take up a great deal of storage space and bandwidth particularly with the increase of spatial resolution. Among various compression techniques, lossy-to-lossless compression technique exhibits great flexibility, because it is able to compress images at a high compression ratio at the cost of losing some minor information and it is also able to realize lossless compression without any information distortion. Region-of interest (ROI) coding algorithms have also been proposed, since observers are always more concerned about some special areas (i.e., ROI) than the background (BG) area.

B. RTDLT

RTDLT [4][5] belongs to block transform. Thus the source image will be segmented into adjacent non overlapping blocks before transforming. First, reversible integer prefiltering is done on neighboring blocks to reduce redundancy. Floating point prefilter may be defined as,

$$F = \begin{bmatrix} I & J \\ I & -J \end{bmatrix} \begin{bmatrix} I & 0 \\ 0 & V \end{bmatrix} \begin{bmatrix} I & J \\ J & -I \end{bmatrix} \qquad (3.1)$$

V is defined as,

$$V = \begin{bmatrix} J(C_N 11)TD_S C_N J & O_{N\left(\frac{M}{2}-N\right)} \\ O_{\left(\frac{M}{2}-N\right)} & I_{\left(\frac{M}{2}-N\right)\left(\frac{M}{2}-N\right)} \end{bmatrix} \quad (3.2)$$

$$C_N(n,k)=\sqrt{2/N}.\varepsilon K.\cos(2nH)\, k/2n \quad (3.3)$$

where $n, k = 0,1,2, \ldots\ldots\ldots\ldots N-1$

$\epsilon k = \sqrt{1/2}$ if k=o; otherwise $\varepsilon = 1$ (3.3)

$$C_N(n,k)=\sqrt{2/N}.\cos \pi(2n+1)(2K+1)/4N \quad (3.4)$$

where $n, k = 0,1,2, \ldots\ldots\ldots\ldots N-1$

Now 2-D reversible integer DCT is performed on each block by cascading 1-D RDCT along vertical and horizontal directions separately.

C. PROPOSED SA-RLT

Based on RTDLT, we propose SA-RLT with the same concept as used in SA-DCT and SA-DWT. However, SA-RLT has its special advantages .The first one is that SARLT belongs to block transform; as a result, its computational memory requirement is lower than that of global transforms, and its hardware implementation can be parallel processed. The second one is that SA-RLT exploits the correlation between neighboring blocks; therefore, it can improve the efficiency of conventional block-based transforms. Moreover, SA-RLT can realize reversible integer-to-integer transform. How to realize SA-RLT is discussed as follows.

We first compute prefilter and DCT matrices of different sizes. Segmenting image into 8 ×8 blocks has been proved to be the best trade of between transform performance and computational complexity in conventional DCT based compression schemes such as JPEG. Therefore, in our scheme, basic transform matrices with a size of $2 \times 2 - 8 \times 8$are computed first. Second, we design a multilifting scheme for prefilter and DCT matrices obtained from the first step. To do this, we use the matrix factorization method to factorize basic matrices into TERMs. Suppose that matrix L is a lower TERM factorized from basic transform matrix with a size of 3 × 3. Then, its multilifting scheme can be obtained [5].

C..*Discrete Cosine Transform (DCT)*

The discrete cosine transform (DCT) [6] is a technique for converting a signal into elementary frequency components. It is widely used in image compression. Here we develop some simple functions to compute the DCT and to compress images. Image Compression is studied using 2-D discrete Cosine Transform. The original image is transformed in 8-by-8 blocks and then inverse transformed in 8-by-8 blocks to create the reconstructed image. The inverse DCT would be performed using the subset of DCT coefficients. The discrete cosine transform (DCT) helps separate the image into parts (or spectral sub-bands) of differing importance (with respect to the image's visual quality). The DCT is similar to the discrete Fourier transform: it transforms a signal or image from the spatial domain to the frequency domain[7] Fig. 2.

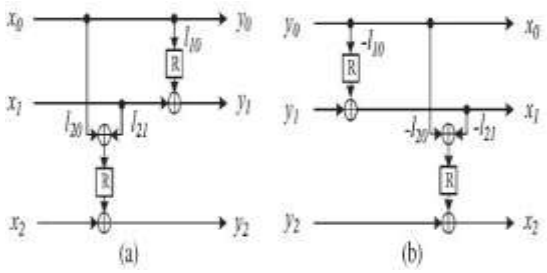

In this way, reversible integer prefilter and DCT for 1-D arbitrary-length vectors have been obtained. A 2-D transform can be obtained by cascading 1-D transform along the vertical and horizontal directions, respectively. It should be noted that the lengths of vertical and horizontal vectors may be different, and each length should be figured out by scanning the vector before transform. Up to now, we have achieved reversible integer prefilter and DCT for arbitrarily shaped image area. In one arbitrarily shaped image area, there exist two types of blocks. The first type of block is incomplete, which is along the area boundary; the second type of block is full, which is inside the image area. We employ different strategies on these two types of blocks. On one hand, we use SA-RDCT for incomplete blocks and use RTDLT for full blocks. Thus, strictly speaking, SA-RLT means the integration of SA-RDCT and RTDLT [5]. In fact, we have taken experiments to perform SA-R-Filter on incomplete blocks along object edges, but the performance improvement is very limited. Therefore, to reduce complexity, we perform SA-RLT employing the aforementioned strategies. There exists no truncation error in the transformation process, since SA-RLT can realize completely reversible integer to- integer transform on both incomplete and full blocks in arbitrarily shaped image area. Therefore, SA-RLT[8] can be applied in both lossy and lossless compressions.

D. SA-RLT BASED ROI CODING FOR RSI

One advantage of the proposed scheme over JPEG2000-ROI coding is that it codes ROI[9] and BG separately; therefore, bit rate can be controlled more flexibly, and ROI can be coded losslessly without BG. First, we apply SA-RLT to ROI and BG, respectively.

Coefficients will be distributed in a blocky structure after transforming. Most energy will be concentrated in the left-upper corner of each block. In order to code the transform coefficients of SA-RLT using wavelet-based codec, we reorganize the blocky coefficients into sub band structure like that in wavelet transform. Second, we code these coefficients using object-based set partitioned embedded block (OB-SPECK).OB-SPECK [10][11] is an efficient algorithm for coding arbitrarily shaped object. It can be proved that OB-SPECK performs better than the state of-the-art image compression techniques such as traditional SPIHT, SPECK, and JPEG2000 for region-based digital mammography. Moreover, it possesses characteristics of low complexity and embedded/progressive bit streams. A binary shape mask, which corresponds to the ROI area, is coded by OB-SPECK independently and transmitted with the whole bit stream.

E. OBJECT-BASED SPECK ALGORITHM

A straightforward extension of the SPECK[11] algorithm to coding of video objects of arbitrary shape is that we set all the coefficients outside the object in each sub band to zero. Then the original SPECK algorithm can be applied just as if the support of the object were rectangular[12]. No modification of the algorithm would be required.

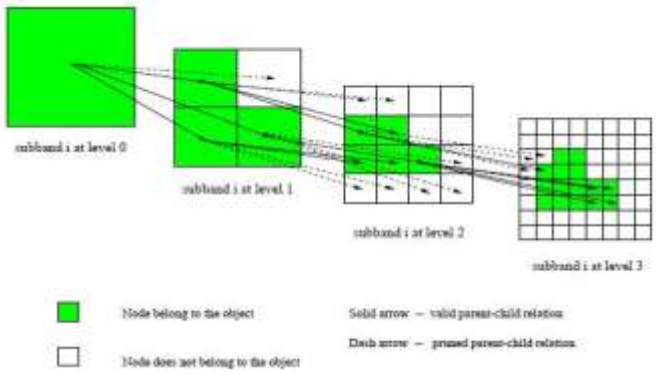

In the parent-child relation in the OB-SPECK algorithm, the branches, which correspond to the nodes outside the object (represented by the dash arrows), are pruned before the coding process begins.

This method is in efficient, since one bit must be transmitted to tell the decoder that the node or branch outside the object is insignificant under each threshold. In this scheme, the shape information of object area in the wavelet domain is integrated into the coding process[13]. Similar to the object-based wavelet decomposition, the shape image is also decomposed into a pyramid of sub bands, called the shape mask pyramid .In this way, the regions which belong to the object in each sub band are known by both the encoder and the decoder. Each pixel of the shape mask has a 2-bit mask value: 1 bit is used to distinguish if the current wavelet coefficient is within the object; and the other bit is used to tell if its child branch is within the object. When the spatial orientation tree is constructed, which node and/or child branch are inside/outside the video object is known. Before the coding process, we prune the node and branch which are outside the video object. During the sorting pass in theSPECK algorithm, those nodes and branches are not added into any list of LSP, LIP and LIS[14]. Therefore, no information about these nodes and branches are transmitted. When the encoder and decoder scan these nodes and branches, they will be informed by the shape mask pyramid and skip over them[15].

III. RESULT AND DISCUSSION

DCT, DWT, SARLT compression were done on input remote sensing image and a comparison study was done. ROI coding based on SARLT was carried out

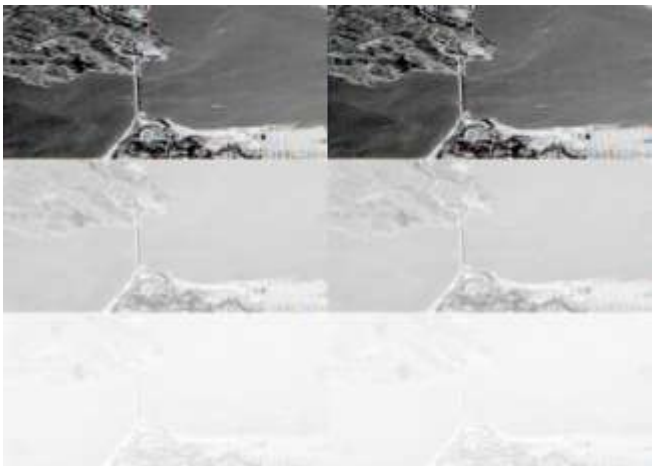

Fig 4.1: Input image

Compression techniques have been widely researched since images will take up a great deal of storage space and bandwidth particularly with the increase of spatial resolution. Among various compression techniques, lossy-to-lossless compression technique exhibits great flexibility, because it is able to compress images at a high compression ratio at the cost of losing some minor information and it is also able to realize lossless compression without any information distortion.

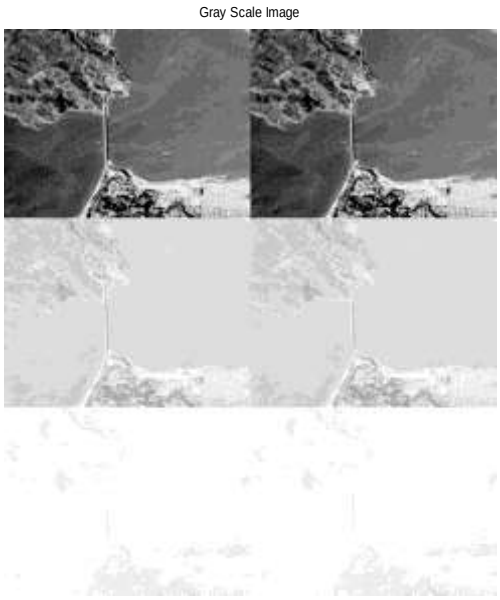

Fig 4.2: Grey Scale Image

Remote sensing images are compressed in order to reduce size. Usually DCT, DWT, LT compressions are done on RSI. Before compression RSI are converted to Grey scale

images and to filtered images. Grey scale and filtered images of input RSI are shown in Fig 4.2 and Fig 4.3.

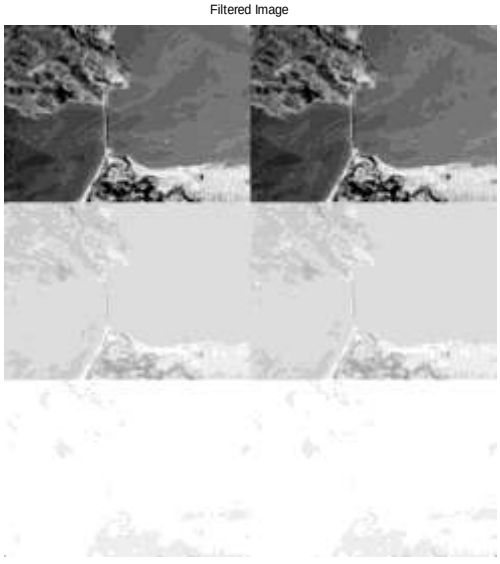

Fig 4.3: Filtered image

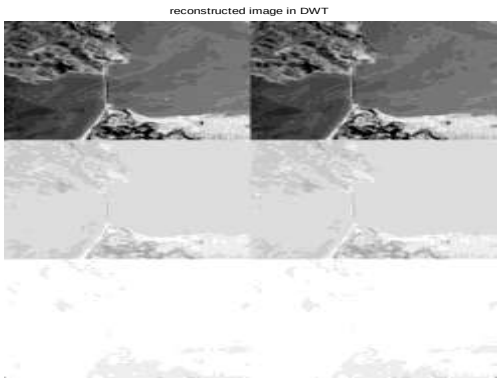

Fig 4.4: DWT compressed image

Shape-adaptive wavelet coding is needed for efficiently coding arbitrarily shaped visual objects, which is essential for object-oriented multimedia applications. The challenge is to achieve high coding efficiency while satisfying the functionality of representing arbitrarily shaped visual texture. One of the features of the SA-DWT's is that the number of coefficients after SA-DWT's is identical to the number of pixels in the original arbitrarily shaped visual object.

Another feature of the SA-DWT is that the spatial correlation, locality properties of wavelet transforms, and self-similarity across sub bands are well preserved in the SA-DWT. Also, for a rectangular region, the SA-DWT becomes identical to the conventional wavelet transforms.

There are two components in the SA-DWT. One is a way to handle wavelet transforms for arbitrary length image segments. The other is a sub sampling method for arbitrary length image segments at arbitrary locations. The SA-DWT allows odd- or small-length image segments to be decomposed into the transform domain in a similar manner to the even- and long-length segments, while maintaining the number of coefficients in the transform domain identical to the number of pixels in the image domain.

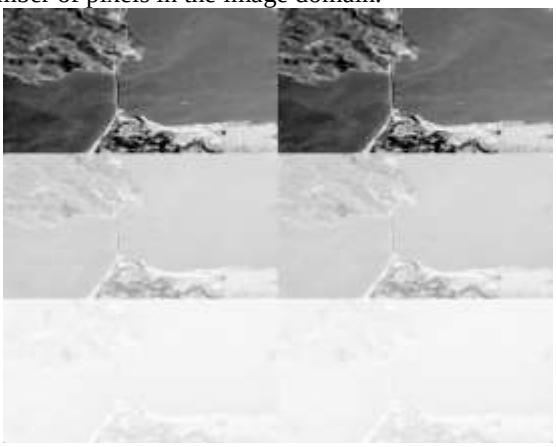

Fig 4.5: SARLT compressed RSI

We first compute pre filter and DCT matrices of different sizes. Segmenting image into 8 ×8 blocks has been proved to be the best trade of between transform performance and computational complexity in conventional DCT based compression schemes such as JPEG. Therefore, in our scheme, basic transform matrices with a size of $2 \times 2 - 8 \times 8$are computed first. Second, we design a multi lifting scheme for pre filter and DCT matrices obtained from the first step. To do this, we use the matrix factorization method to factorize basic matrices into TERMs. Suppose that matrix L is a lower TERM factorized from basic transform matrix with a size of 3×3. Then, its multi lifting scheme can be obtained.

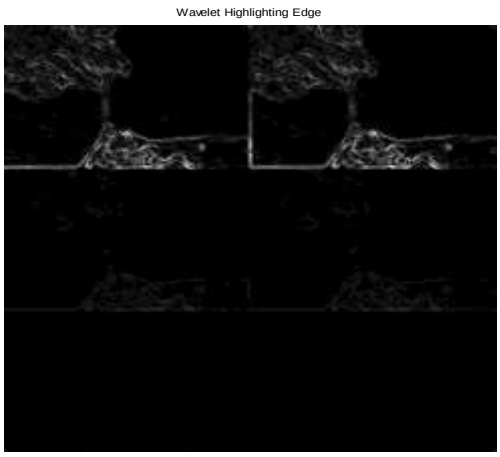

Fig 4.6: ROI segmentation using SARLT

Region merging, region splitting and a combination of region merging and splitting are well known region detection techniques. In characteristic feature thresholding or clustering, threshold level schemes are based on grey level histogram and local properties. Edge detection is the simple and basic technique used in segmentation of images. It is a useful segmentation method used for simple image.

CONCLUSION

In the method, a shape adaptive reversible integer lapped transform (SA-RLT) method for compression of 2-D remote sensing images is proposed. Based on SA-RLT and object based set partitioned embedded block coder, a new region of interest (ROI) compression scheme is designed for 2-D remote sensing images. Experimental results demonstrate that the proposed transform (SA-RLT) performs better than other existing SA transforms such as shape adaptive discrete cosine transform (SA-DCT), shape adaptive discrete wavelet transform (SA-DWT). A new segmentation method for segmenting the region of interest (ROI) based on colour intensity is proposed here. The new proposed method overcomes the limitations of hand segmentation such as complexity and time to a large extent. The proposed algorithm can effectively improve the overall quality and details of the satellite images since the compression technique used here is lossless. . The delimitations of the proposed model were also analyzed clearly and the simulation tool is selected to perform comprehensive simulations.

REFERENCES

[1]Nageswara Rao Thota, Srinivasa Kumar Devireddy, " Image compression using DCT", IEEE Trans. Signal Process, vol. 52,no 6,may 2007

[2] Ryszard Stasinski and Hoegskolen Narvik,"Shape Adaptive Discrete Fourier Transform for coding of irregular image segments"

[3] Xiongwen Li, Eran Edirisinghe, Helmut Bez, "Shape adaptive integer transform for coding arbitrarily shaped objects in H.264/AVC ",

[4] Lei Wangn, Licheng Jiao,Jiaji Wu,Guang ming Shi,Yanjun Gong,"Lossy-to- lossless image compression based on multiplier-less reversible integer time do-main lapped transform",Signal Processing: Image Communication 2010,622632.

[5] Rafael Galvao de Oliveira, Beatrice Pesquet-Popescu, Maria Trocan, Inter prediction using lapped transforms for advanced video coding,18th IEEE International Conference on Image Processing 2011.

[6] Gilbert Strang,"The Discrete Cosine Transform",SIAM REVIEW Society for Industrial and Applied Mathematics Vol.41, No.1,1999.

[7] B.Penna, T.Tillo, E.Magli, and G.Olmo, "Transform coding techniques for lossy hyperspectral data compression," IEEE trans. Geosci. Remote Sens, vol 45, no 5, pp 1408-1421, may 2007

[8] I. Baeza, J. Verdoya, J.Villanueva Oller, R.J Villanueva,"ROI-based procedures for progressive transmission of digital images:A comparison", Mathematical and Computer Modelling 2009.

[9] Hui-Cheng Hsu, Kun-Bin Lee, Nelson Yen-Chung Chang, and Tian-Sheuan Chang,"Architecture Design of Shape-Adaptive Discrete Cosine Transform and Its Inverse for MPEG-4 Video Coding",IEEE transactions on circuits and systems for video technology, vol. 18, no. 3, march 2008.

10] T.Sikora and B.Makai, " SA-DCT for generic coding of video," IEEE trans. Circuits system video tech., vol.5,no-1,pp.59-62, Feb 1995

[11] Abu-Hajar and R.Sankar, "Integer to integer shape adaptive wavelet transform for region of interest image

[12] S.Li and W.Li, "Shape adaptive discrete wavelet transform for arbitrarily shaped visual object coding.

[13] Dominik Engel, Andreas Uhl, "Adaptive image compression of arbitrarily shaped objects using wavelet packets", In Proceedings of the 23rd International Picture Coding Symposium 2003, pp. 283 – 288

[14] V.Srinivasa rao, Dr P.Rajesh Kumar, G.V.H.Prasad, M.Prema Kumar, S.Ravichand,"Discrete Cosine Transform Vs Discrete Wavelet Transform: An Objective Comparison of Image Compression Techniques for JPEG coding with SPECK"

[15] Z.Lu and W.A Pearlman, "Wavelet video coding of video object by object based SPECK algorithm," in proc. PCS, Seoul, Korea, Apr.2001, pp. 413-416

coding," IEEE 10th digital signal process workshop 2002

● ● ●

CONTRAST ENHANCEMENT BASED ON GAUSSIAN MIXTURE MODELING WITH NOISE ADAPTIVE FUZZY SWITCHING MEDIAN FILTER

[1]Jayasilpa S, [2]Kavitha N Nair
[1] M Tech(pursuing), Department of ECE,Mahatma Gandhi University College Of Engineering, Thodupuzha, kerala
[2]Lecturer, Mahatma Gandhi University College Of Engineering, Thodupuzha, kerala
[1]vysaknb@gmail.com

***Abstract*—The proposed algorithm automatically enhances the contrast in an input image. The algorithm uses the Gaussian mixture model to model the image gray-level distribution. In a mixture distribution, its density function is just a convex combination (a linear combination in which all coefficients or weights sum to one) of other probability density functions. The Gaussian components with small variances are weighted with smaller values than the Gaussian components with larger variances By enhancing the contrast of an image in such a way might amplify noise if present and produce worse results. A noise adaptive fuzzy switching median filter is used for salt-and-pepper noise removal. It is able to suppress high-density of salt-and-pepper noise, at the same time preserving fine image details, edges and textures.**

Keywords- Gaussian Mixture Model (GMM), Noise Adaptive Fuzzy Switching Median (NAFSM), Bihistogram Equalization (BBHE), Minimum Mean Brightness Error Bi-Histogram Equalization (MMBEBHE). Recursive Mean Separate Histogram Equalization (RMSHE)

I. INTRODUCTION

Generally, an image may have poor dynamic range or distortion due to the poor quality of the imaging devices or the adverse external conditions at the time of acquisition. Whenever an image is converted from one form to other such as digitizing the image some form of degradation occurs at output. The main goal of image enhancement technique is to improve the characteristics or quality of an image, such that the resulting image is better than the original image. There are two broad categories of image enhancement techniques: (1) Spatial domain techniques and (2) frequency domain techniques.

Several image enhancement techniques were proposed in the past. Histogram equalization (HE) [1] is a very popular technique for image enhancement. One problem of the histogram equalization is that the brightness of an image is changed after the histogram equalization, hence not suitable for consumer electronic products, where preserving the original brightness and enhancing contrast are essential to avoid annoying artifacts. . So Bi-histogram equalization (BBHE) has been proposed which can preserve the original brightness to a certain extend. However, there are still cases that are not handled well by BBHE [2], as they require higher degree of preservation. The extension of BBHE is Minimum Mean Brightness Error Bi-Histogram Equalization (MMBEBHE). The result of MMBEBHE [3] is bad for the image with a lot details. Recursive Mean-Separate Histogram Equalization (RMSHE) [3] is another improvement of BBHE. However, it also is not free from side effects.

Although these methods can achieve good contrast enhancement, they also generate annoying side effects depending on the variation in the gray-level distribution. may create problems when enhancing a sequence of images, when the histogram has spikes, or when a natural-looking enhanced image is required. In this paper a contrast enhance ment algorithm using GMM is proposed along with a noise adaptive fuzzy switching median filter. Images with low contrast are automatically improved in terms of an increase in the dynamic range. The proposed algorithm is free from parameter setting. The NAFSM filter is able to suppress high density salt-and-pepper noise,and at the same time it preserves fine image details, edges and textures well. Also, it does not require any further tuning or training of parameters once optimized.

The rest of the paper is organised as follows: Section II presents the proposed algorithm. Section III presents the results of algorithm. Section IV concludes this paper.

II. PROPOSED ALGORITHM

Let us consider an input image, $X = \{x(i,j) \mid 1 \le i \le H, 1 \le j \le W\}$, of size $H \times W$ pixels, where $x(i,j) \in R$. Assume that X has a dynamic range of $[x_d, x_u]$ where $x(i,j) \in [x_d, x_u]$. The main objective of the proposed algorithm is to generate an enhanced image, $Y = \{y(i,j) \mid 1 \le i \le H, 1 \le j \le W\}$, which has a better visual quality with respect to X. The dynamic range of Y can be stretched or tightened into the interval $[y_d, y_u]$, where $y(i,j) \in [y_d, y_u]$, $y_d < y_u$ and $y_d, y_u \in R$.

III. DENOISING

A noise adaptive fuzzy switching median (NAFSM) filter for salt-and-pepper noise removal. It is a recursive double-stage filter. The NAFSM filter is a hybrid between the simple adaptive median filter and the fuzzy switching median filter. The adaptive behavior enables the NAFSM filter to expand the size of its filtering window according to the local noise density, making it possible to filter high-density of salt-and-pepper noise. Meanwhile, the inherited switching median behavior will speed up the filtering process at the same time preserving image details by selecting only "noise pixels" for processing. In addition, the resorted fuzzy reasoning deals with the uncertainty presence in the local information and helps to produce an accurate correction term when restoring detected "noise pixels"[4].

The detection stage starts by searching for two salt and- pepper noise intensities or local maximums L_{max} and L_{min} from both ends of the noisy image histogram. The search is directed towards the center of the histogram. Once these intensities were found the search is stopped. Based on these possible noise pixels of image are identified. A binary noise mask $N(i,j)$ will be created to mark the location of "noise pixels" by using

$$N(i,j) = \begin{cases} 0, X(i,j) = L_{salt} \text{ or } L_{pepper} \\ 1, \text{otherwise} \end{cases} \quad (1)$$

where $N(i,j) = 1$ represents noise free pixels and $N(i,j) = 0$ represents noise pixels. When a "noise pixel" is detected, it is subjected to the next filtering stage. Otherwise, when a pixel is classified as "noise-free," it will be retained and the filtering action is spared to avoid altering any fine details and textures that are contained in the original image.

In the filtering stage noise pixel marked with $N(i,j) = 0$ will be replaced by an estimated correction term. A square filtering window is used here. Then the number of noise free pixels in the window is counted. If the current filtering window does not have a minimum number of one noise-free pixel ,then the filtering window will be expanded by one pixel at each of its four sides . This procedure is repeated until the criterion of having a minimum one noise-free pixel is met. For each detected noise pixel, the size of the filtering window is initialized to 3×3. These "noise-free pixels" will all be used as candidates for selecting the median pixel, $N(i,j)$ given by

$$M(i,j) = median\{X(i+m, j+n)\} \quad (2)$$

with $N(i+m, j+n) = 1$

where $m, n \in (-s, \cdots\cdots, o, \cdots\cdots s)$.

Fuzzy reasoning is applied to the extracted local information. Finally, the correction term to restore a detected noise pixel is a linear combination between the processing pixel $X(i,j)$ and median pixel $M(i,j)$.

IV. MODELING

Gaussian mixture model is used for image modeling. Like K-Means, Gaussian Mixture Models (GMM) can be regarded as a type of unsupervised learning or clustering methods. They are among the most statistically mature methods for clustering. But unlike K-Means, GMMs are able to build soft clustering boundaries, i.e., points in space can belong to any class with a given probability. In statistics, a mixture model is a probabilistic model which assumes the underlying data to belong to a mixture distribution. In a mixture distribution, its density function is just a convex combination (a linear combination in which all coefficients or weights sum to one) of other probability density functions. Each of the Gaussian components has a different mean, standard deviation, and proportion (or weight) in the mixture model.

The human eye is not sensitive to small variations around dense data but is more sensitive to widely scattered fluctuations. Thus, in order to increase the contrast while retaining image details, dense data with low standard deviation should be dispersed, whereas scattered data with high standard deviation should be compacted. While doing this the gray-level distribution should be retained[5].

The grey-level distribution p (x), where x ∈ X, of the input image X can be modeled as a density function composed of a linear combination of N functions using the GMM, i.e.,

$$p(x) = \sum_{n=1}^{N} P(\omega_n) p(x|\omega_n) \quad (3)$$

where (w_n) is the prior probability of the data points generated from component w_n of the mixture and p ($x|w_n$) is the nth component density and is given by

$$p(x|\omega_n) = \frac{1}{\sqrt{2\pi\sigma_{\omega_n}^2}} exp\left(-\frac{(x-\mu_{\omega_n})^2}{2\sigma_{\omega_n}^2}\right) \quad (4)$$

Here μ_{Wn} and σ^2_{Wn} are respectively the mean and the variance of the nth component. Therefore a GMM is completely specified by its parameters

$$\theta = \{p(\omega_n), \mu_{\omega_n}, \sigma^2{}_{\omega_n}\}_{n=1}^{N} \quad (5)$$

The Figueiredo-Jain (FJ) algorithm [6] is used for parameter estimation which tries to overcome three major weaknesses of the basic EM algorithm. The EM algorithm requires the user to set the number of components and the number will be fixed during the estimation process. The FJ algorithm adjusts the number of components during the estimation by annihilating components that are not supported by the data. This leads to the other EM failure point, the boundary of the parameter space. FJ avoids the boundary when it annihilates components that are becoming singular. FJ also allows to start with an arbitrarily large number of components, which tackles the initialization issue with the EM algorithm. The classical way to select the number of mixture components is to adopt the "modelclass/ model" hierarchy, where some candidate models (mixture PDFs) are computed for each model-class (number of components), and then select the "best" model. The idea behind the FJ algorithm is to abandon such hierarchy and to find the "best" overall model directly by using the minimum message length criterion and applying it to mixture models.

(a)

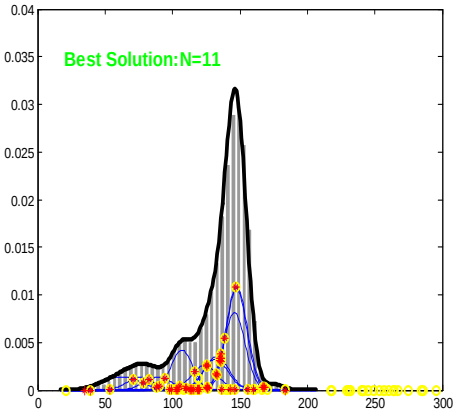

Fig 1. (a) Gray-level image and (b) its histogram and GMM fit

Fig. 1(a) and (b) illustrates an input image and its histogram, together with its GMM fit, respectively. The histogram is modeled using eleven Gaussian components, i.e., N=11. The close match between the histogram (shown as rectangular vertical bars) and the GMM fit (shown as solid black line) is obtained using the FJ algorithm.

V. PARTITIONING

The goal of partion is to change the representation of an image into something that is easier to analyze. The result of image partion is a set of segments that collectively cover the entire image. For partioning the intersection points are selected from different Gaussian components. The intersection points between two Gaussian components w_m and w_n are found by solving

$$P(\omega_m)p\big((x|\omega_m)\big) = P(\omega_n)p\big((x|\omega_n)\big) \quad (6)$$

or equivalently

$$-\frac{(x-\mu_{\omega m})^2}{2\sigma^2_{\omega m}} + \frac{(x-\mu_{\omega n})^2}{2\sigma^2_{\omega n}} = ln\left(\frac{P(\omega_n)\sigma_{\omega m}}{P(\omega_m)\sigma_{\omega n}}\right) \quad (7)$$

The second order parametric equation has two roots, *i.e.*,

$$x^{(1)}_{m,n} = \frac{-b+\sqrt{b^2-4ac}}{2a} \text{ and } x^{(2)}_{m,n} = \frac{-b-\sqrt{b^2-4ac}}{2a} \quad (8)$$

On solving the above equation, we obtain the numerical values of intersection points. The total number of intersection points thus calculated is N(N-1). From this significant intersection points are selected to cover the entire dynamic range of the image. For a given intersection point $x^{(k)}_{m,n}$, where k={1,2}, between Gaussian components ω_m and ω_n , it is selected as a significant intersection point if and only if it is a real number in the dynamic range of the ·components ω_m and ω_n contain the maximum value in the mixture for point $x^{(k)}_{m,n}$, i.e.,

$$P(\omega_m)p\left(x_{m,n}^k|\omega_m\right) = P(\omega_n)p\left(x_{m,n}^k|\omega_n\right)$$
$$P(\omega_m)p\left(x_{m,n}^k|\omega_m\right) > P(\omega_n)p\left(x_{m,n}^k|\omega_n\right) \quad (9)$$

The significant intersection points are sorted in ascending order of their value and are partitioned into gray-level intervals to cover the entire dynamic range of X. The consecutive pairs of significant intersection points are used to partition the dynamic range of X into subintervals, i.e.,$[x_d, x_u] = [x_s^1, x_s^2]\ U\ [x_s^2, x_s^3]\ U$ ····· $\left[x_s^{(k-2)}, x_s^{(k-1)}\right]$ $U\left[x_s^{(k-1)}, x_s^k\right]$. Thus the dynamic range of input image is represented by the union of all intervals where k is the maximum number of significant intersection points. For each input gray level interval there is only one Gaussian component that is dominant with respect to the others which represents the data within that interval. Subinterval $[x_s^{(k-1)}, x_s^{(k)}]$ is represented by a Gaussian component w_k, which is dominant with respect to the other Gaussian components in it. The dominant Gaussian component is found by considering the a posteriori probability of each component in specified interval.

VI. MAPPING

Enhanced image is obtained by mapping each input interval to corresponding output interval by adding weight which depends on the rate of the total number of pixels that fall into interval and the standard deviation of the dominant Gaussian component ω_k.

$$\alpha_k = \frac{\sigma_{\omega_k}^{\gamma}}{\sum_{i=1}^{N}\sigma_{\omega_i}^{\gamma}} \frac{F\left(x_s^{(k+1)}\right) - F\left(x_s^{(k)}\right)}{\sum_{is=1}^{k-1} F\left(x_s^{(i+1)}\right) - F\left(x_s^{(i)}\right)} \quad (10)$$

The first term adjusts the brightness of the equalized image,and $\gamma \in [0,1]$ is brightness constant. The lower the value of γ , the brighter the output image is. The second term in (19) is related to the gray-level distribution and is used to retain the overall content of the data in the interval. Equation (19) maintains a balance between the data distribution and the variance of the data in a certain interval. Since the human eye is more sensitive to sudden changes in widely scattered data and less sensitive to smooth changes in densely scattered data, larger weights are given to widely scattered data and vice versa.

Using , the input interval $[x_s^{(k-1)}, x_s^{(k)}]$ is mapped onto the output interval $[y^{(k-1)}, y^{(k)}]$ according to

$$y^{(k)} = y_d + (y_u - y_d)\sum_{i=1}^{k-1}\alpha_i$$
$$y^{(k+1)} = y^k + \alpha_k(y_u - y_d) \quad (11)$$

Where m=1, 2…….M – 1.

The gray levels of the pixels in each input interval are transformed according to the dominant Gaussian component and the CDF of the interval to obtain the contrast-equalized image. Let the Gaussian distribution with parameters $\mu_{\omega_{n'}}$ and $\sigma^2{}_{\omega_{n'}}$ represent the Gaussian component in range $[y^{(k-1)}, y^{(k)}]$ .The new parameters of the Gaussian distribution are computed as follows:

$$\mu_{\omega_{k'}} = \frac{\left(\frac{x_s^{(k)} - \mu_{\omega_k}}{x_s^{(k+1)} - \mu_{\omega_k}} y^{k+1} - y^{(k)}\right)}{\left(\frac{x_s^{(k)} - \mu_{\omega_k}}{x_s^{(k+1)} - \mu_{\omega_k}} - 1\right)} \quad (12)$$

$$\sigma_{\omega_{k'}} = \frac{\left(y^{(k)} - \mu_{\omega_{k'}}\right)}{\left(x_s^{(k)} - \mu_{\omega_k}\right)}\sigma_{\omega_k}$$

Thus final mapping is done by linearly transforming each input interval to corresponding output interval so as to get an equalized and contrast enhanced image. It is achieved by considering all Gaussian components in the GMM to retain the pixel distributions in input and output intervals equal by using the superposition of distributions i.e.,

$$y = \sum_{i=1}^{N}\left(\left(\frac{x - \mu_{\omega_{i'}}}{\sigma_{\omega_{i'}}}\right)\sigma_{\omega_{i'}} + \mu_{\omega_{i'}}\right)P_{\omega_{i'}} \quad (13)$$

As shown in Fig.1(b) all intersection points between Gaussian components that fall within the dynamic range of the input image are denoted by yellow circles, and significant intersection points that are used in dynamic range representation are denoted by orange points. The proposed method is extended to color images by applying the method to their luminance component only and preserve the chrominance components.

RESULTS AND DISCUSSION

A data set comprising of standard test images from [7] is used to evaluate the proposed algorithm. An output image is said to have been enhanced over the input image if it enables the image details to be better perceived. An assessment of image enhancement is not an easy task as an improved perception is difficult to quantify. Some contrast enhancement results on grayscale images are shown in Figs. 2-3. For comparison purpose techniques like histogram equalizationand Brightness Preserving Dynamic Fuzzy Histogram Equalization (BPDFHE) are used.

The input image in Fig. 2(a) shows an ariel view of a tank. There are three main gray tones in the input image corresponding to the tank, its shadow, and the image background. The other gray-level tones are distributed around the three main tones. By using the proposed algorithm, the dynamic range of the input image is modeled with the GMM, which makes it possible to model the intensity values of shadow, background and tank differently. Input gray-level values are assigned to output gray-level values according to their representative Gaussian components. The nonlinear mapping is designed to utilize the full dynamic range of the output image. Thus, the proposed algorithm improves the overall contrast while preserving image details. The HE method over enhances the image and destroys the natural appearance of the image.

The bright input image in Fig. 3(a) shows an aerial view of a junction in a city . Visual verification shows that natural look of the enhanced image is retained by the proposed algorithm in Fig. 3(c) by preserving the overall shape of the gray-level distribution and redistribution of the gray levels of the input image within the dynamic range. The BPDFHE does not darken the image as done by competing methods.

But HE method produces sufficient contrast for the different objects to be recognized.

(a)

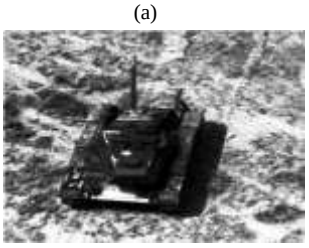

(b)

(c)

(d)

Fig 2. Contrast enhancement for grey image *tank*: (a) Original image, (b) Histogram Equalization (c) BPDFHE and (d) Enhanc[illegible]ethod.

(a)

(b)

(c)

(d)

TABLE I PSNR VALUES OF TEST IMAGE ELAINE

Percentage Of Noise	Type Of Filter		
	Median	***HMF***	***NAFSM***
10%	22.92	34.27	39.10
50%	14.82	14.89	31.06
90%	6.65	6.61	22.66

TABLE II MSE VALUES OF TEST IMAGE ELAINE

Noise(%)	***Median***	***HMF***	***NAFSM***
10%	331.3	24.29	7.98
50%	0.0021	2.10	50.89
90%	0.00014	1.41	352.40

Fig 3. Contrast enhancement for grey image *city* (a) Original image (b) Histogram Equalization (c) BPDFHE and (d) Enhanced output using proposed method.

The PSNR (dB) evaluation scheme is used to assess the strength of the filtered image. Since image is subjective to the human eyes, visual inspection is carried out on the filtered images as to judge the effectiveness of the filters in removing salt-and-pepper noise.The performance of the NAFSM filter was evaluated on the basis of comparison of PSNR with existing techniques like aconventional median filter, hybrid median (HMF) filter.

Fig 4. (a), (b) and (c) shows the test image Elaine
corrupted with 90%, 50% and 10% salt and pepper noise respectivley. Table I shows the PSNR values for the same image for a conventional median filter, hybrid media sameimage for a conventional median filter, hybrid median(HMF) filter and the NAFSM filter. It is clear that NAFSM has better noise filtering action compared to other filters like HMF and conventional median filter. From Fig. (d), (e) and(f) and the high PSNR values shows that the implemented filter (NAFSM) is capable of removing high density salt and pepper noise.

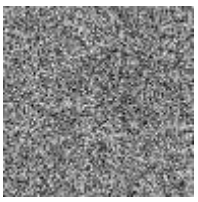

(a)

(b)

(d)

(e)

(e)

(f)

Fig 4. Test image Elaine corrupted with (a) 90% (b) 50% (c) 10% noise respectivley and (d),(e),(f) represents the corresponding images after NAFSM filtering

CONCLUSION

The automatic image enhancement algorithm using Gaussian mixture modelling of an input image to perform non-linear data mapping generates visually pleasing enhancement on different types of images. A noise adapyive fuzzy median filtering was implemented to remove salt and pepper noises. It is able to suppress high-density of salt-and-pepper noise, at the same time preserving fine image details, edges and textures. This methodology can not only enhance the details, but also maintains the naturalness for the nonuniform illumination images. The images enhanced by this methodology are visually pleasing, artefact free and natural looking. It doesnt require parameter tuning. Future works focuses on applying the algorithm to color images and for rendering HDR images on conventional displays.

REFERENCES

.R. C. Gonzalez and R. E. Woods, Digital Image Processing. Upper Saddle River, NJ: Prentice-Hall, 2006.

Y.-T. Kim, "Contrast enhancement using brightness preserving bi-histogram equalization," IEEE Trans. Consumer Electron., vol. 43, no. 1, pp. 1–8, Feb 1997.

S.-D. Chen and A. Ramli, "Contrast enhancement using recursive Mean-Separate histogram equalization for scalable brightness preservation," IEEE Trans. on Consumer Electronics, vol. 49, no. 4, pp. 1301-1309, Nov. 2003.

Kenny Kal Vin Toh and Nor Ashidi Mat Isa, "Noise Adaptive Fuzzy Switching Median Filterfor Salt-and-Pepper Noise Reduction," IEEE Signal Processing Letters, vol. 17, no. 3, march 2010.

Turgay Celik and Tardi Tjahjadi "Automatic Image Equalization and Contrast Enhancement Using Gaussian Mixture Modeling," IEEE Transactions On Image Processing, Vol. 21, No. 1, January 2012.

M. Figueiredo and A. Jain, "Unsupervised learning of finite mixture models," IEEE Trans. Pattern Anal. Mach. Intell., vol. 24, no. 3, pp. 381–396, Mar. 2002.

[Online].Available:http://www.imagecompression.info/test_image.

EFFICIENT COMPRESSION AND ENCRYPTION METHOD FOR SECURE TRANSMISSION OF IMAGES

[1] Meera Mohan,[2]Kavitha N Nair
[1] PG Scholar, Department of ECE, University College of Engineering, Muttom, Kerala - 685587
[2]Lecturer, Department of ECE, University College of Engineering, Muttom, Thodupuzha, Kerala – 685587
[1]meeramohan1731@gmail.com

Abstract - **Traditional data transmission over an insecure noiseless channel consists of first compressing data for efficiency and then encrypting it for security. Multimedia data requires considerable storage capacity and transmission bandwidth. The data are in the form of graphics, audio, video and image. These types of data have to be compressed during the transmission process. Large amount of data cannot be stored if there is low storage capacity. Compression is minimizing the size in bytes of a graphics file without degrading the quality of image to an unacceptable level. This work proposes a novel scheme for efficient encryption and compression of an image for secure transmission. Linear encoding and pseudorandom permutation is used to encrypt an original image which provides more efficiency and then the image is compressed with the use of DCT and DWT. After receiving the compressed data, with the use of inverse compression algorithm and linear decoding, a receiver can reconstruct the principal content of the original image. In this paper, DCT and DWT are compared on the basis of performance parameters, Peak signal to noise ratio, Mean square error and Time of the compressed images of DCT and DWT.**

Keywords- **Image Encryption; Image Compression; Linear Encoding; Pseudorandom Permutation; Discrete Wavelet Transform (DWT); Discrete Cosine Transform (DCT)**.

I. INTRODUCTION

In recent years, compression of encrypted data has attracted considerable research interest. The traditional way of securely and efficiently transmitting redundant data is to first compress the data to reduce the redundancy, and then to encrypt the compressed data to mask its meaning. At the receiver side, the decryption and decompression operations are orderly performed to recover the original data. However, in some application scenarios, a sender needs to transmit some data to a receiver and hopes to keep the information confidential to a network operator who provides the channel resource for the transmission. That means the sender should encrypt the original data and the network provider may tend to compress the encrypted data without any knowledge of the cryptographic key and the original data. At receiver side, a decoder integrating decompression and decryption functions will be used to reconstruct the original data.

Image compression is very important for efficient transmission and storage of images. Demand of communication of multimedia data through telecommunication network and data accessing through internet is explosively growing. Image compression is minimizing the size in bytes of a graphics file without degrading the quality of image to an unacceptable level. Large amount of data can't be stored if there is low storage capacity present. A gray scale image that is 256 x 256 pixels have 65, 536 elements to store and a typical 640 x 480 color image have nearly a million. Downloading of these files from internet can be very time consuming task. The compression offers a means to reduce the cost of storage and increase the speed of transmission. There are two types of image compression is present. These are lossy and lossless [1]. In lossless compression technique the reconstructed image after compression is identical to original image. These images are also called noise less, since they do not add noise to signal image. This is also known as entropy coding. Loss less compression technique is used only for a few applications with stringent requirement such as medical imaging. **:** Lossy compression technique is widely used because the quality of reconstructed images is adequate for most applications. In general, lossy techniques provide for greater compression ratios than lossless techniques that are lossless compression gives good quality of compressed images but yields only less compression whereas the lossy

compression techniques lead to loss of data with higher compression ratio [2].

Several techniques for compressing/decompressing encrypted data have been developed. It has been shown in [3] that, based on the theory of source coding with side information at the decoder, the performance of compressing encrypted data may be as good as that of compressing non encrypted data in theory. Two practical approaches to lossless compression of encrypted black and white images and to lossy compression of encrypted Gaussian sequence are also introduced. In the former approach, the original binary image is encrypted by adding a pseudorandom string, and the encrypted data are compressed by finding the syndromes with respect to low-density parity-check (LDPC) channel code [4]. In the latter one, the original data is encrypted by adding an i.i.d. Gaussian sequence, and the encrypted data are quantized and compressed as the syndromes of trellis code. By employing LDPC codes into various bit-planes and exploiting the spatial and cross-plane correlation among pixels, a few methods for lossless compression of encrypted gray and color images are also introduced. In [5], a compressive sensing technique is introduced to achieve lossy compression of encrypted image data, and a basis pursuit algorithm is appropriately modified to enable joint decompression and decryption.

In most of the above-mentioned schemes for compressing encrypted image, the syndrome of channel code is exploited to generate the compressed data in lossless manner. In this work, a novel system for lossy and lossless compression of encrypted image is proposed. The network provider may remove the redundant and trivial data from the encrypted image, and a receiver can retrieve the principal content of the original image. The compression ratio and the quality of the reconstructed image are dependent on the values of compression parameters. Here DWT and DCT compression methods are compared by using some performance parameters.

The structure of this paper is organized as follows. Section 2 explains about the methodology. Section 3 discusses the experimental results. Finally, conclusion and suggestion for future works are given in Section 4.

II. METHODOLOGY

In this section the detailed procedure for encryption and compression of images are given.

A. Image Encryption

Assume the original image is in uncompressed format and each pixel with a gray value falling into [0, 255] is represented by 8 bits. Denote the numbers of the rows and the columns in the original image as N_1 and N_2 , and the number of all pixels as N, ($N = N_1 \times N_2$). Then, the amount of bits of the original image is $8.N$. For image encryption, the data sender pseudorandomly permutes the pixels and the permutation way is determined by a secret key [7]. The permuted pixel-sequence is viewed as the encrypted data. A number of permutation-based image encryption methods can be used here. Since only the pixel positions are permuted and the pixel values are not masked in the encryption phase, an attacker without knowledge of the secret key can know the original histogram from an encrypted image. To improve the secrecy, the pixel values can be masked or changed using a linear encoding algorithm shown in Fig.1. The linear encoding algorithm performs in the column vector.

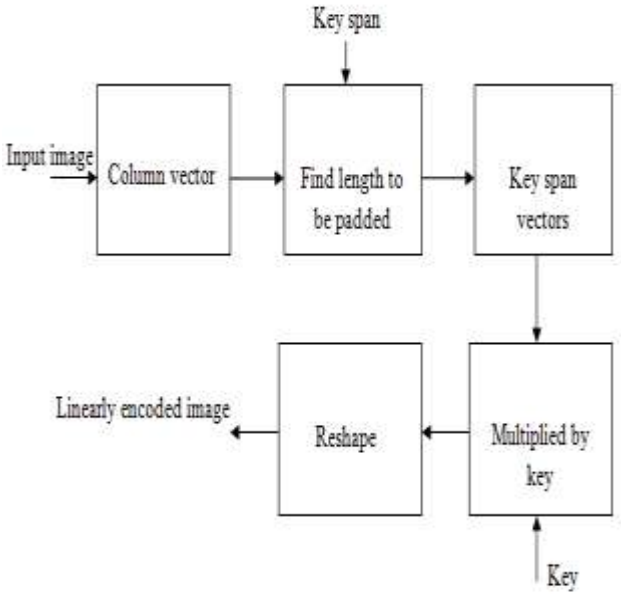

Fig. 1. Linear Encoding

In linear encoding, image is converted into a column vector. The pixels are grouped into a particular size specified by a key-span. If extra pixels are required to complete the specified group then padding is used, for that the length to be padded is find. These sets are then multiplied by a lower triangular matrix which is generated in the encoding algorithm by the use of key and serves as the secret key for pixel value encryption. The pixels are then transformed to original image format.

B. Image Compression

In the compression procedure, both lossy and lossless compressions are introduced. DCT and DWT algorithms are used to implement compression of images.

1. Discrete Cosine Transform (DCT)

The discrete cosine transform (DCT) [1] is a technique for converting a signal into elementary frequency

components. It is widely used in image compression. Here we develop some simple functions to compute the DCT and to compress images. Image Compression is studied using 2-D discrete Cosine Transform. The original image is transformed in 8-by-8 blocks and then inverse transformed in 8-by-8 blocks to create the reconstructed image. The inverse DCT would be performed using the subset of DCT coefficients. The discrete cosine transform (DCT) helps separate the image into parts (or spectral sub-bands) of differing importance (with respect to the image's visual quality). The DCT is similar to the discrete Fourier transform: it transforms a signal or image from the spatial domain to the frequency domain Fig. 2.

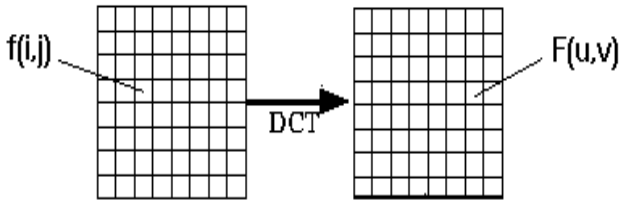

Fig. 2. Transformation of function into DCT

A discrete cosine transform (DCT) expresses a sequence of finitely many data points in terms of a sum of cosine functions oscillating at different frequencies. The 2-D discrete cosine transform (DCT) is an invertible linear transform and is widely used in many practical image compression systems because of its compression performance and computational efficiency. DCT converts data (image pixels) into sets of frequencies. The first frequencies in the set are the most meaningful; the latter, the least. The least meaningful frequencies can be stripped away based on allowable resolution loss. DCT-based image compression relies on two techniques to reduce data required to represent the image. The first is quantization of the image's DCT coefficients; the second is entropy coding of the quantized coefficients [1].

The forward 2D_DCT transformation is given by the following equation:

$$C(u,v) = D(u)D(v)\sum_{x=0}^{N-1}\sum_{y=0}^{N-1} f(x,y)\cos\left[\frac{\pi.u}{2N}(2x + 1\cos\pi.v2N2y+1\right] \quad (1)$$

Where, $u, v = 0,1,2,3, \ldots . N-1$

The inverse 2D-DCT transformation is given by the following equation:

$$f(x,y) = \sum_{u=0}^{N-1}\sum_{v=0}^{N-1} D(u)D(v)D(u,v)\cos\left[\frac{\pi u}{2N}(2x + 1\cos\pi v2N2y+1\right] \quad (2)$$

Where

$$D(u) = \left(\frac{1}{N}\right)^{\frac{1}{2}} \; for\; u = 0$$

$$D(v) = \left(\frac{2}{N}\right)^{\frac{1}{2}} \; for\; u = 1,2,3 \ldots . (N-1)$$

The basic operation of the DCT is as follows:

- The input image is N by M
- f (i,j) is the intensity of the pixel in row i and column j
- F (u,v) is the DCT coefficient in row k1 and column k2 of the DCT matrix.
- For most images, much of the signal energy lies at low frequencies; these appear in the upper left corner of the DCT.
- Compression is achieved since the lower right values represent higher frequencies, and are often small - small enough to be neglected with little visible distortion.
- The DCT input is an 8 by 8 array of integers. This array contains each pixel's gray scale level
- 8 bit pixels have levels from 0 to 255.
- When desired, the image is reconstructed through decompression, a process that uses the Inverse Discrete Cosine Transform (IDCT).

2. Discrete Wavelet Transform (DWT)

Wavelet Transform has become an important method for image compression. Wavelet based coding provides substantial improvement in picture quality at high compression ratios mainly due to better energy compaction property of wavelet transforms [8]. Wavelets are functions which allow data analysis of signals or images, according to scales or resolutions. The DWT represents an image as a sum of wavelet functions, known as *wavelets*, with different location and scale. It represents the data into a set of high pass (detail) and low pass (approximate) coefficients. Mathematically DWT can be expressed as:

$$\mathrm{DWT}_{\mathrm{X(n)}} = \mathrm{d_{j,k}} = \sum \mathrm{x(n)h_j^*\,(n - 2^j k)} \quad (3)$$

$$\mathrm{DWT}_{\mathrm{X(n)}} = \mathrm{a_{j,k}} = \sum \mathrm{x(n)g_j^*\,(n - 2^j k)} \quad (4)$$

The coefficients $d_{j,k}$ are called detail components of signal x(n) and coefficients $a_{j,k}$ are called approximation components. The functions g(n) and h(n) refer to the coefficients of low pass and high pass filters with parameters j and k as wavelet scale and translation factors.

The input data is passed through set of low pass and high pass filters. The output of high pass and low pass filters are down sampled by 2.The output from low pass filter is an approximate coefficient and the output from the high pass filter is a detail coefficient. This procedure is one dimensional (1-D) DWT. but in this research work we are using two dimensional (2-D) DWT. In case of in two directions, both rows and columns. The outputs are then down sampled by 2 in each direction as in case of 1-D DWT. Output is obtained in set of four coefficients LL, HL, LH, HH. The first alphabet represents the transform in row where as the second alphabet represents transform in column. The alphabet L means low pass signal and H means high pass signal. LH signal is a low pass signal in row and a high pass in column. Hence, LH signal contain horizontal elements. Similarly, HL and HH contains vertical and diagonal elements, respectively [9]. As shown in Fig.3 at each level, approximation sub-band is decomposed into the above mentioned four sub-bands.

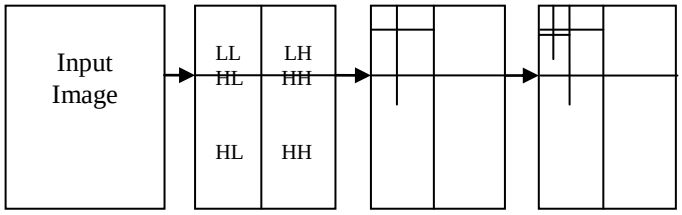

Fig. 3. Flow chart of the DWT decomposition

In this research work, haar wavelet is used [10], each block of the image is then passed through the two filters: high pass filter and low pass filter. The first level decomposition is performed to decompose the input data into an approximation and the detail coefficients. After obtaining the transformed matrix, the detail and approximate coefficients are separated as LL, HL, LH, and HH coefficients. All the coefficients are discarded, except the LL coefficients. The LL coefficients are further transformed into the second level. The process continues for one more level. The coefficients are then divided by a constant scaling factor (SF) to achieve the desired compression ratio. Finally, for data reconstruction, the data is rescaled and padded with zeros, and passed through the wavelet filter.

3. Performance Measure

The performance of both DCT and DWT compression are measured on the basis of performance parameters Peak signal to noise ratio (PSNR), Mean square error (MSE) and Time of the compressed images of DCT and DWT. PSNR is the quality measurement between the original image and the reconstructed image which is calculated through the Mean Square Error (MSE). The MSE represents the cumulative squared error between the compressed and the original image, whereas PSNR represents a measure of the peak error. It is most easily defined via the mean squared error (MSE) which for two $m \times n$ monochrome images I and K where one of the images is considered a noisy approximation of the other is defined as:

$$\mathrm{MSE} = \frac{1}{\mathrm{MN}} \sum_{\mathrm{i}=0}^{\mathrm{M}-1} \sum_{\mathrm{j}=0}^{\mathrm{N}-1} [\mathrm{I}(\mathrm{i},\mathrm{j}) - \mathrm{K}(\mathrm{i},\mathrm{j})]^2 \quad (5)$$

$$\mathrm{PSNR} = 10 \log \frac{255^2}{\mathrm{MSE}} \quad (6)$$

Where I(i, j) is the input image and K(i, j) is the output image. The development of the system includes the generation of the codes for each of the above steps and finally we can measure the performance of the proposed method.

III. RESULT AND DISCUSSION

Two test images, Bats man and Tiger are used to evaluate the proposed work with size 256×256 ,shown in Fig.4; Fig. 5. Shows the encrypted images of Fig.4 (a) with and without linear encoding. The output images are shown in Fig.6, which includes the compressed, decompressed and decrypted images of DCT algorithm.Fig.7, shows the output images of DWT algorithm.

(a) (b)

Fig. 4. Test Images: (a) Bats man, (b) Tiger

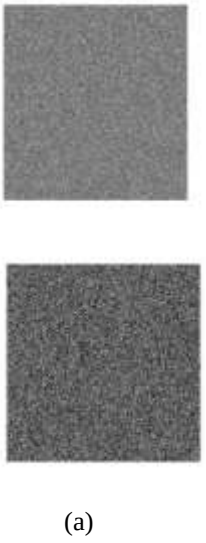

(a) (b)

Fig. 5. Encrypted Images: (a) without linear encoding, (b)with linear encoding

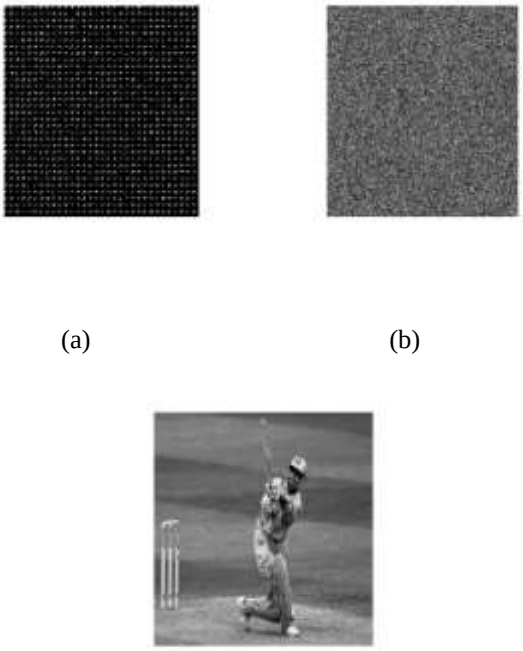

(a) (b)

(c)

Fig. 6. Output Images of DCT: (a)Compressed image, (b)Decompressed image, (c)Decrypted image

.

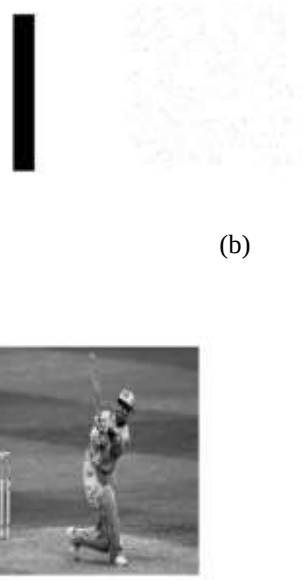

(a) (b)

(c)

Fig. 7. Output Images of DWT: (a) Compressed image, (b) Decompressed image, (c)Decrypted image

Table.1.Comparison based on *Mean Square Error (MSE), Peak Signal to Noise Ratio (PSNR) and Execution Time*

Parameters / **Images**		*Mean Square Error (MSE)*	*Peak Signal to Noise Ratio (PSNR in db)*	*Execution Time (in sec)*
DCT	Bat man	0.0036	24.46	527.83
	Tiger	0.0036	24.45	524.73
DWT	Bats man	0.0006	31.71	5.58
	Tiger	0.0006	31.72	6.29

The performance of both DWT and DCT are evaluated using the PSNR and MSE. The Table.1 shows the comparison of DCT and DWT methods. PSNR is high for DWT and also the execution time is less. Since the MSE of DWT is much smaller, there is no degradation in the reconstructed image compared to DCT.

CONCLUSION

This work proposes a novel idea for efficiently compressing and securely encrypting image and designed a practical scheme made up of image encryption and compression. The original image is encrypted by pseudorandom permutation and linear encoding, and then compressed by DCT and DWT compression algorithm. In the encryption phase of the proposed system, the pixel positions are shuffled and the pixel values are masked.Thus by providing a secure encryption scheme. DWT provides higher compression ratios & avoids blocking artifacts. DCT produces some degradation in the reconstruction whereas DWT does not, and also DCT need more execution time than DWT. Thus for image compression, DWT is more suitable. Still the DCT and DWT offers new research directions that are being explored in the current and upcoming image/video coding standards.

REFERENCES

[1]Abhishek Kaushik, Maneesha Gupta,"Analysis of Image Compression Algorithms", International Journal of Engineering Research and Applications (IJERA) , Vol. 2, Issue 2,Mar-Apr 2012, pp.773-779.

[2] M. Mozammel Hoque Chowdhury and Amina Khatun, "ImageCompression Using Discrete Wavelet Transform", International Journal of Computer Science Issues, Vol. 9, Issue 4, No 1, July 2012

[3]R. Lazzeretti and M. Barni, "Lossless compression of encrypted grey-level and color images," in Proc.16th Eur. Signal Processing Conf. (EUSIPCO 2008), Lausanne Switzerland, Aug. 2008.

[4]D. Schonberg, S. C. Draper, and K. Ramchandran, "On blind compression of Encrypted correlated data approaching the source entropy rate," in Proc. 43rd Annu.Allerton Conf, Allerton, IL, 2005.

[5]D. Schonberg, S. C. Draper, C. Yeo, and K. Ramchandran, "Toward compression of encrypted images and video sequences", IEEE Trans.Inf. Forensics Security, vol. 3, no. 4, pp. 749–762, Dec. 2008.

[6]Mohammad Ali Bani Younes and Aman Jantan, "Image Encryption Using Block-Based Transformation Algorithm", IAENG International Journal of Computer Science, 35:1, IJCS_35_1_03, Jul 2007.

[7]Xinpeng Zhang, " Lossy Compression and Iterative Reconstruction for Encrypted Image", IEEE Trans.Inf. Forensics Security , vol. 6, no. 1, March 2011.

[8] N. Lavanyadevi**,** SP. Priya & K. Krishanthana, "Performance Analysis of Face Matching and Retrieval In Forensic Applications", Department of ECE, Mepco Schlenk Engineering College, Sivakasi

[9] J.Madhavan, K.Porkumaran," Performance comparison of PCA, DWT- PCA and LWT-PCA for Face Image Retrieval", Computer Science & Engineering: An International Journal (CSEIJ), Vol.2, No.6, December 2012.

[10] Bhonde Nilesh, Shinde Sachin, Nagmode Pradip, D.B. Rane, "Image Compression Using Discrete Wavelet Transform", International Journal of Computer Technology and Electronics Engineering (IJCTEE) Volume 3, Special Issue, March-April 2013

IMPLEMENTATION OF HIGH PRECISION FIXED WIDTH MULTIPLIER FOR DSP APPLICATIONS

[1] G.Niharika,[2] B.Santosh Kumar
[1] PG Scholar, Department of Electronics & Communication, Vaagdevi College of Engineering Warangal India-506005
[2] Assistant Professor, Department of Electronics & Communication, Vaagdevi College of Engineering Warangal India-506005
[1] niharika_rec@hotmail.com, [2]Santosh_b34@yahoo.com

Abstract: **Significant improvements in area, delay, and power can be achieved with truncated multipliers. Fixed-width multipliers generate n-bit (instead of 2n-bit) products with low product error, but use only about half the area and less delay when compared with a standard parallel multiplier. In them, cost-effective carry-generating circuits are designed, respectively, to make the products generated more accurately and quicklyThe proposed method aims at tree reduction using proper ratio of full adders and half adders. The advantage of doing so, is experimentally we can achieve better area. The output is in the form of LSB and MSB. Using the most significant methods like reduction, deletion, truncation, rounding and final addition in order to compress the LSB part. In previous related papers, to reduce the truncation error we use error compensation circuits. But here, there is no need of error compensation circuits, and the final output is precise.**

*Keywords:***Computer arithmetic, faithful rounding, fixed- width multiplier, tree reduction, and truncated multiplier.**

I. INTRODUCTION

MULTIPLICATION is one of the most area consuming arithmetic operations in high-performance circuits. As a consequence many research works deal with low power design of high speed multipliers. Multiplication involves two basic operations, the generation of the partial products and their sum, performed using two kinds of multiplication algorithms, serial and parallel.

Serial multiplication algorithms use sequential circuits with feedbacks: inner products are sequentially produced and computed. Parallel multiplication algorithms often use combinational circuits and do not contain feedback structures. Multiplication of two bits produces an output which is twice that of the original bit. It is usually needed to truncate thepartial product bits to the requiredprecision to reduce area cost. Fixed-width

Multipliers, a subset of truncated multipliers, compute only n most significant bits (MSBs) of the 2n bit product for n×n multiplication and use extra correctio n/compensation circuits to reduce truncation errors.

In previous related papers, to reduce the truncation error by adding error compensation circuits. So that the output will be précised.

In this approach jointly considers the tree reduction, truncation, and rounding of the PP bits during the design of fast parallel truncated multipliers so that the final truncated product satisfies the precision requirement.

In our approach truncation error is not more than 1ulp (unit of least position), so there is no need of error compensation circuits, and the final output will be précised.

II. REDUCTION SCHEMES OF PARALLEL MULTIPLIERS

PP (partial product) generation produces partial product bits from the multiplicand and multiplier. PP reduction is used to compress the partial product bits to two. Finally the partial products bits are summed by using carry propagate addition. Two famous reduction methods are available,

1. Dadda tree
2. Wallace tree

Dadda reduction performs the compression operation whenever it required. Wallace tree reduction always

compresses the partial product bits. In the proposed method, uses RA reduction method. So that the final bit will be reduced.

In the proposed truncated multiplier design, introduces column-by-column reduction. Here two reduction schemes are used, to minimize

the half adders in each column because the full adder has high compression rate when compared to HA.

A. Scheme1 and Scheme2

Fig. 1 shows the reduction procedure of Scheme 1, reduction starting from the least significant column. Column height is h, including the carry bits from least significant columns, are also shown on the top row where the columns that need HAs are highlighted by square boxes. Fig. 2 shows the technology schematic of scheme 1 using Mentor Graphics.

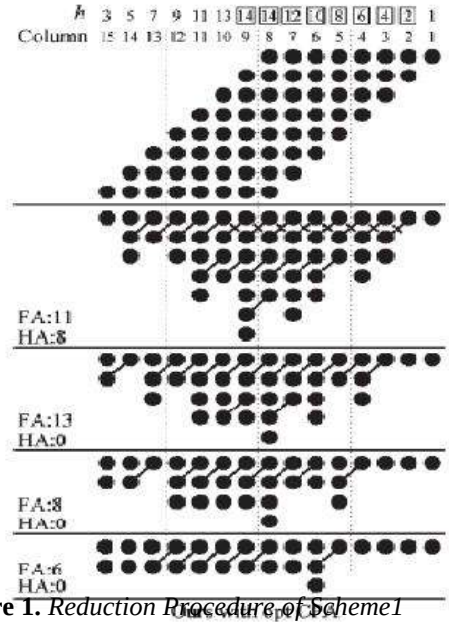

Figure 1. *Reduction Procedure of Scheme1*

These methods mainly discuss about the cost compensation. By comparing the methods of Dadda, Wallace and RA with scheme1 and Scheme2, the reduction of bits are better, so the area can be saved higher than the former methods. From the literature survey it is clear that various researchers are working in these areas to optimize the same. Compression ratio also takes up its major concern here, were it plays a crucial role when output precision is concerned. Fig. 3 shows the reduction procedures by scheme 2 to each column of partial product bits, reduction starting from the least significant column.

Scheme 1 having minimum CPA (carry propagate addition) bit width as twice reduction efficiency when compared to the Wallace method which produces the same result as that of RA method.

Fig. 2 Shows reduction procedure of scheme2. Scheme 1 is only used to determine whether an HA is needed and how many FAs are required in the per-column reduction that does not exceed the maximum number of Carry Save Additions in reduction levels.

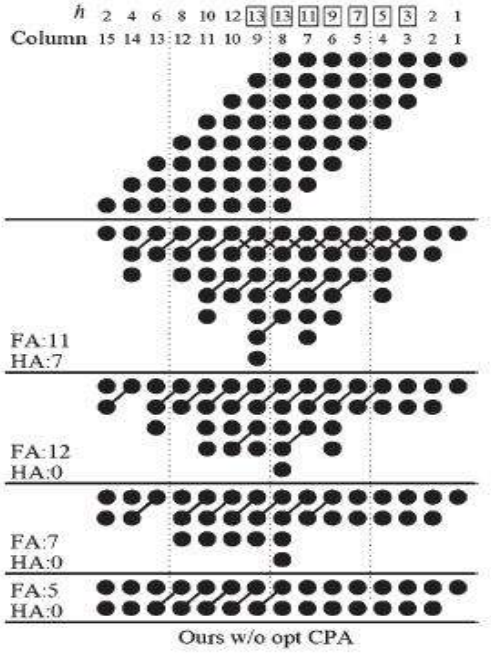

Figure 2.*Reduction Procedure of Scheme2*

The scheme1, scheme2 and proposed multiplier architecture has been simulated and synthesized using XILINX ISE Design Suite 13.2. From the synthesized results, the scheme 1 and scheme 2 has 1056 and 822 number of gates. The proposed multiplier has only 582 gates.Area utilization by the proposed method is less when compared to scheme 1 and scheme 2.

III. PROPOSED TRUNCATED MULTIPLIER

The objective of a good multiplier is to provide a physically compact, good speed and low power consuming chip. To save significant power consumption of a VLSI design. In a truncated multiplier, several of the least significant columns of bits in the partial product matrix are not formed. Figure 5 Show 8x8 truncated multiplication.(a) deletion, reduction and truncation. (b) Deletion, reduction, truncation, and final addition.

In the first step deletion operation is performed, that removes all the avoidable partial product bits which are shown by the light gray dots (fig 3). In this deletion operation, delete as many partial product bits as possible.

Deletion error E_D should be in the range $-1/2$ ulp $\leq E_D \leq 0$. Hereafter, the injection correction bias constant of 1/4 ulp.

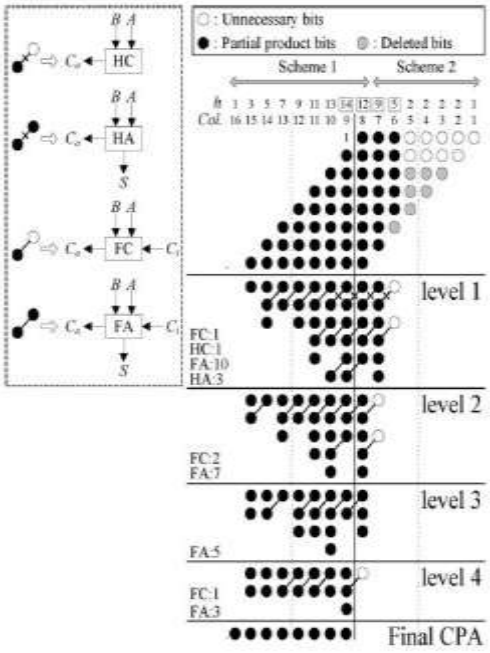

Figure 3.*Proposed Truncated Multiplier*

The deletion error after the bias adjustment $-1/4$ ulp $\leq E_D \leq 1/4$ ulp. In Fig. 5, the deletion of partial product bitsstarts from column 3 by skipping the first two of partial product bits. After the deletion of partial product bits, perform column-by-column reduction of scheme 2. After the reduction, perform the truncation, which will further remove the first row of (n -1) bits from column 1 to column (n-1). It will produce the truncation error which is in the range of $-1/2$ ulp $\leq E_T \leq 0$. Hence introduction of another bias constant of ¼ ulp in truncation part. So the adjusted truncation error is $-1/4$ ulp $\leq E_T \leq 1/4$ ulp.

B. Rounding and Final Addition

All the operations (deletion, reduction, and truncation) are done, finally the PP bits are added by using CPA (carry propagate addition) to generate final product of P bits. Before the final CPA, add a bias constant of ½ ulp for rounding. Rounding error is in the form of - 1/2 ulp $\leq E_R \leq 1/2$ ulp. The faithfully truncated multiplier has the total error in the form of $-\text{ulp} < E = (E_D + E_T + E_R) \leq \text{ulp}$.

C. Proposed Algorithm

In proposed architecture we can multiply 8x8 bits, and the bits are reduced in step by step manner. Deletion is the first operation performed in Stage 1 to remove the PP bits, as long as the magnitude of the total deletion error is no more than 2^{-P-1}.Then number of stages to reduce the final bit width without increasing the error.

In normal truncated multiplier design, the architecture produces the output with some truncation error. But in the proposed design of truncated multiplier the truncation error is not more than 1 ulp, so the precision of the final result is improved. Fig. 3 shows proposed truncated multiplier. This reduces the area and power consumption of the multiplier. It also reduces the delay of the multiplier in many cases, because the carry propagate adder producing the product can be shorter.

IV. IMPLIMENTATION OF FUTURE ENHANCEMENT

Truncated multiplier can be effectively implemented in FIR filter structure. Conventional FIR filer performs ordinary multiplication of co-efficient and input without considers the length.
Thus the structure can be made effective by replacing the existing multiplier with the proposed fixed width truncated multiplier for visible area reduction. Fig. 4 shows the architecture of FIR Filter.

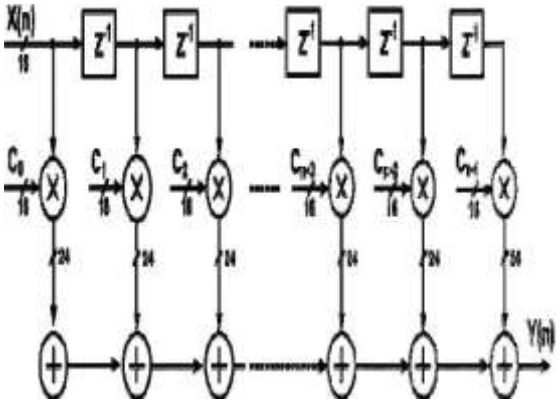

Figure 4.*Fir Filter*

V. EXPERIMENTAL RESULTS

By using the Synthesis tool is
Modelsim. The proposed system is implement-ed by using FPGA-Spartan 3E.This methods are mainly applicable in DSP systems**.**

A. Power Analysis

The scheme1, scheme2 and proposed multiplier architecture has been simulated and synthesized using XILINX ISE Design Suite 13.2. From the synthesized results, it is found that the scheme 1 consumes 185mW, scheme 2 consumes 176mW. The proposed multiplier consumes low power of 88mW when compared to scheme 1 and scheme 2.

B. Area Analysis

Table 1.*Area Analysis of the Scheme 1, 2 & Proposed*

Parameter	Scheme 1	Scheme 2	Proposed
No. of Gate counts	1056	822	582

The table 1 shows that the proposed method reduces the power and area than the previous methods. When compared to previous methods the precision is improved.

VI. SIMULATION RESULTS

Figure 5. *Scheme1 Results*

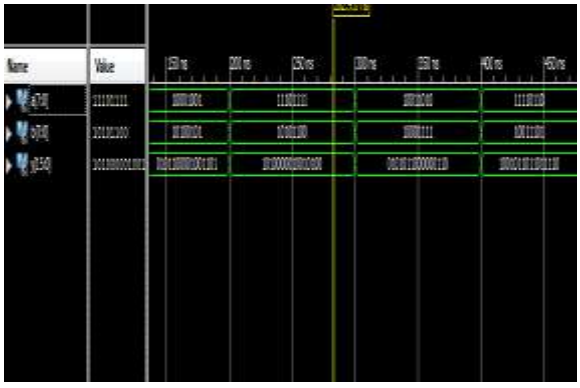

Figure 6. *Scheme2 Results*

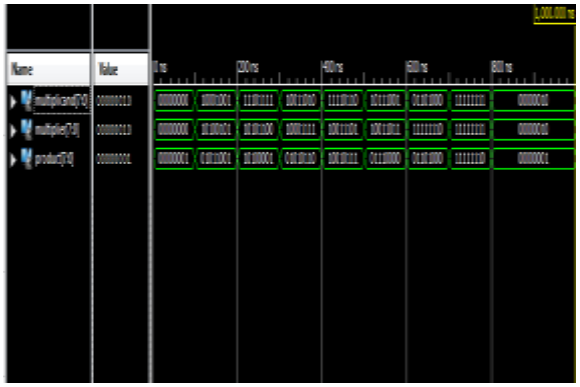

Figure 7.*Proposed Fixed Width Multiplier*

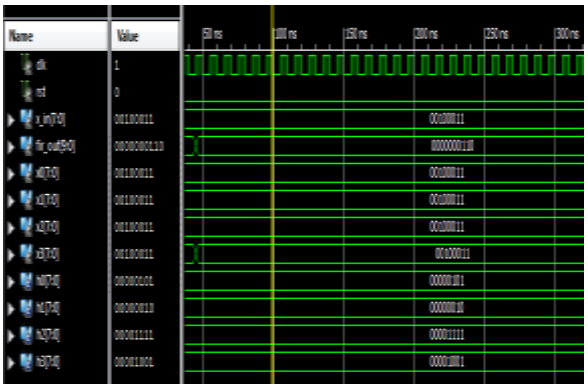

Figure 8.*Fir with Proposed Multiplier*

CONCLUSION

There are many works proposed to reduce the truncation error by adding error compensation circuits so as to produce a précised output. In this approach jointly considers the tree reduction, truncation, and rounding of the PP bits during the design of fast parallel truncated multipliers, so that the final truncated product satisfies the precision requirement.
In this approach truncation error is not more than 1ulp, so there is no need of error compensation circuits, and the final output will be précised. The scheme1, scheme2 and proposed multiplier architecture has been simulated and synthesized using XILINX ISE Design Suite 8.1.
From the synthesized results, it is found that the scheme 1 consumes 185mW, scheme 2 consumes 176mW. The proposed multiplier consumes low power of 88mW when compared to
scheme 1 and scheme 2. The scheme 1and scheme 2 has 1056 and 822 number of gates. The proposed multiplier has only 582 gates. Area utilization by the proposed method is less when compared to scheme 1 and scheme 2.

REFERENCES

[1] J. M. Jou, S. R. Kuang, and R. D. Chen, "Design of low-error fixed- width multipliers for DSP applications," IEEE Trans. Circuits Syst. II, s Analog Digit. Signal Process., vol. 46, no. 6, pp. 836–842, Jun. 1999.

[2] L.-D. Van and C.-C. Yang, "Generalized low-error area-efficient fixed width multipliers," IEEE Trans. Circuits Syst. I, Reg. Papers, vol. 52, no. 8, pp. 1608–1619,Aug. 2005.

[3] M. J. Schulte and E. E. Swartzlander, Jr., "Truncated multiplication with correction constant," in VLSI Signal Processing VI. Piscataway, NJ:IEEE Press, 1993, pp. 388–396.

[4] E. J. King and E. E. Swartzlander, Jr., "Data-dependent truncation scheme for parallel multipliers," in Proc. 31st Asilomar Conf. Signals, Syst. Comput., 1997, pp. 1178– 1182.

[5] M. J. Schulte, J. G. Hansen, and J. E. Stine, "Reduced power dissipation through truncated multiplication," in Proc. IEEE Alessandro Volta Memorial Int. Workshop Low Power Des., 1999, pp. 61–69.

[6] T.-B. Juang and S.-F. Hsiao, "Low-error carry-free fixed-width multipliers with low-cost compensation circuits," IEEE Trans. Circuits Syst. I, Reg. Papers, vol. 52, no. 6, pp. 299–303, Jun. 2005.

[7] A.G.M. Strollo, N. Petra, and D. De Caro, "Dual-tree error compensation for high-performance fixed-width multipliers," IEEE Trans. Circuits Syst. II, Exp. Briefs, vol.52, no. 8, pp. 501–507, Aug. 2005.

[8] E. G. Walters and M. J. Schulte, "Efficient function approximation using truncated multipliers and squarers," in Proc. 17th IEEE Symp. ARITH, 2005, pp. 232–239.

[9] C. S. Wallace, "A suggestion for a fast multiplier," IEEE Trans. Electron. Comput., vol. EC-13, no. 1, pp. 14–17, Feb. 1964.

THE EFFECT OF SUPPLY CHAIN MANAGEMENT PRACTICES AND COMPETITIVE ADVANTAGE IN THE PERFORMANCE OF KERALA PSU'S: A STRUCTURAL EQUATION MODELING APPROACH

[1]Arun A,[2]Asok kumar N
[1][2]College Of Engineering Trivandrum
[1]Aruntkm11@gmail.com,[2]Asok_akn@yahoo.com

Abstract: **Supply chain management (SCM) has become a potentially valuable way of acquiring competitive advantage and improving organizational performance. Supply chain management practices (SCMP) are defined as the set of activities undertaken by an organization to promote effective management of its supply chain. The importance of SCM in the achievement of organizational performance has been highlighted in many studies. The purpose of this study is to propose supply chain management practices (SCMP) and Organizational Performance (OP) model for Kerala PSU's. This paper develops a framework showing the effect of SCMP and competitive advantage on organizational performance. Data for the study were collected from PSU's in Kerala by developing a questionnaire and conducting survey among top level managers in the marketing and purchase department of Kerala public sector units(PSU's). And the relationships proposed in the framework were tested using structural equation modeling (SEM) approach using the software WARPpls.**

Keywords: **Competitive advantage, SCMP, SEM, Organizational performance, WARPpls**

I. INTRODUCTION

The goal of Supply Chain Management (SCM) is to integrate both information and material flows flawlessly across the supply chain as an effective competitive weapon. The Global Supply Chain Forum consists of top executives of leading firms from a wide variety of industries, such as communications and technology, consumer packaged goods, fashion apparel, commodity merchandising, automotive manufacturing, household plumbing and accessories, and consumer electronics. Member companies represent all possible locations across a supply chain: original suppliers, manufacturers of industrial products (business to business), manufacturers of consumer products, distributors,

and retailers. Therefore, the view presented by the Global Supply Chain Forum represents combined knowledge and experiences from leading firms in the corresponding industry.[17-19] Organizations began to realize that it is not enough to improve efficiencies within an organization, but their whole supply chain has to be made competitive. The understanding and practicing of supply chain management (SCM) has become an essential prerequisite for staying competitive in the global race and for enhancing profitably [1–4].

Council of logistics management defines SCM as the systematic, strategic coordination of the traditional business functions and tactics across these businesses functions within a particular organization and across businesses within the supply chain for the purposes of improving the long-term performance of the individual organizations and the supply chain as a whole. SCM has been defined to explicitly recognize the strategic nature of coordination between trading partners and to explain the dual purpose of SCM: to improve the performance of an individual organization, and to improve the performance of the whole supply chain.[1,6].

The purpose of this study is therefore to empirically test a framework identifying the relationships among Supply chain management practices, competitive advantage and organizational performance. The Supply chain management practices are defined as the set of activities undertaken by an

organization to promote effective management of its supply chain. The Supply chain management practices are proposed to be a multi-dimensional concept, including the downstream and upstream sides of the supply chain. Operational measures for the constructs are developed and tested empirically, using data collected from respondents to a survey questionnaire. Structural equation modeling is used to test the hypothesized relationships.[14-16]

The remainder of this paper is organized as follows. Section 2 presents the literature review, provides the definitions and theory underlying each dimension of Supply chain management practices, discusses the concepts of competitive advantage and organizational performance, and develops the hypothesized relationships. The research methodology and analysis of results are then presented.

II. LITERATURE REVIEW

The practice of SCM is also known by other terms such as relationship marketing and global account management [8]. The review of literature revealed that SCMP has been studied and used in many organizations. Different constructs which affect organizational performance are SCMP and competitive advantage. These are discussed below,

2.1 Supply chain management practices

SCM practices have been defined as a set of activities undertaken in an organization to promote effective management of its supply chain. Donlon describes the latest evolution of SCM practices, which include supplier partnership, outsourcing, cycle time compression, continuous process flow, and information technology sharing. Tan et al. use purchasing, quality, and customer relations to represent SCM practices, in their empirical study. Alvarado and Kotzab include in their list of SCM practices concentration on core competencies, use of inter-organizational systems such as EDI, and elimination of excess inventory levels by postponing customization toward the end of the supply chain.[22] Tan et al. identify six aspects of SCM practice through factor analysis: supply chain integration, information sharing, supply chain characteristics, customer service management, geographical proximity and JIT capability. Chen and Paulraj use supplier base reduction, long-term relationship, communication, cross-functional teams and supplier involvement to measure buyer–supplier relationships. Min and Mentzer identify the concept SCM as including agreed vision and goals, information sharing, risk and award sharing, cooperation, process integration, long-term relationship and agreed supply chain leadership. Thus the literature portrays SCM practices from a variety of different perspectives with a common goal of ultimately improving organizational performance. In reviewing and consolidating the literature, seven distinctive dimensions, including supplier selection, strategic supplier partnership, demand management, Outsourcing management, customer relationship, level of information sharing, quality of information sharing are selected for measuring SCM practice.[20]

2.2 Competitive advantage

A competitive advantage is an advantage gained over competitors by offering customers greater value, either through lower prices or by providing additional benefits and service that justify similar or possibly higher prices. Competitive advantage is the extent to which an organization is able to create a defensible position over its competitors.[21] It comprises capabilities that allow an organization to differentiate itself from its competitors and is an outcome of critical management decisions.[5] The empirical literature has been quite consistent in identifying price/cost, quality, delivery, and flexibility as important competitive capabilities[1]. Suhong Li identifies Price, quality, delivery Dependability, Product innovation, time to market.[1] Che Yao Chen et al identify inventory, Quality and Delivery rate.[5] Based on the above, the dimensions of the competitive advantage constructs used in this study are Price, Quality, Time to market, Product innovation.

2.3 Organizational performance

Organizational performance refers to how well an organization achieves its market-oriented goals as well as its financial goals. The short-term objectives of SCM are primarily to increase productivity and reduce inventory and cycle time, while long-term objectives are to increase market share and profits for all members of the supply chain. Any organizational initiative, including supply chain management, should ultimately lead to enhanced organizational performance.[5] A number of prior studies have measured organizational performance using both financial and market criteria, including return on investment (ROI), market share, profit margin on sales, the growth of ROI, the growth of sales, the growth of market share, and overall competitive position.[7] In line with the above literature, the same items is adopted to measure organizational performance in this study.

III. RESEARCH FRAMEWORK

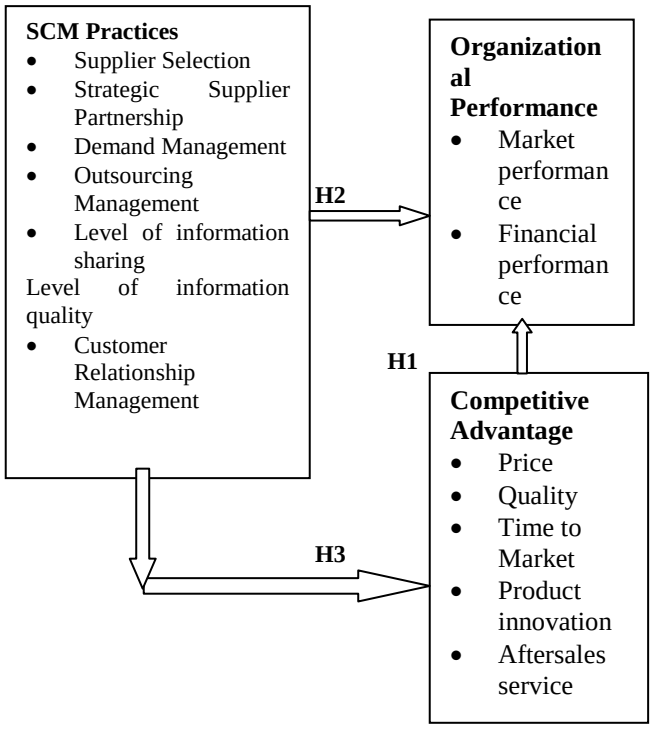

FIG 1 Research framework

Fig. 1 represents the SCM framework developed in this research. The framework proposes that SCM will have an impact on organizational performance both directly and indirectly through competitive advantage [1,2]. Using literature support, the expected relationships among SCM, Competitive advantage and organizational performance are developed, and hypotheses relating these variables are developed

3.1 Research hypotheses

SCM practice is expected to increase an organization's market share, return on investment [1], and improve overall competitive position [2]. For example Customer relation practices have also been shown to lead to significant improvement in organizational performance [1]. The higher level of information sharing is associated with the lower total cost, the higher-order fulfillment rate and the shorter-order cycle time [5]. Based on the above it is hypothesized that:

H1: The higher the level of SCMP, the higher the level of organizational performance.

For example, strategic supplier partnership can improve supplier performance, reduce time to market [1], and increase the level of customer responsiveness and satisfaction [2]. Information sharing leads to high levels of supply chain integration by enabling organizations to make dependable delivery and introduce products to the market quickly. Information sharing and information quality contribute positively to customer satisfaction and partnership quality [1,2,5]. Postponement strategy not only increases the flexibility in the supply chain, but also balances global efficiency and customer responsiveness [1]. The above arguments lead to.

H2: Firms with high level of CRM will have high levels of competitive advantage.

An organization offering high quality products can charge premium prices and thus increase its profit margin on sales and return on investment. An organization having a short time-to-market and rapid product innovation can be the first in the market thus enjoying a higher market share and sales volume.[1] Therefore, a positive relationship between competitive advantage and organizational performance can be proposed.

H3: The higher the level of competitive advantage, the higher the level of organizational performance.

1. Methodology

The purpose of this study is to determine the relationship between the strategic development of supply chain management practice (SCMP), competitive advantage and organizational performance. Surveys were used to collect data. Three measures were used in this study; SCMP, organizational performance, and competitive advantage.

4.1 Procedures

Data for this study were collected using a 20-item survey administered to top management executives from a variety of industries. The survey was administered from April 2014 to July 2014. Survey was conducted among top level managers of Kerala PSU's. The survey included a cover page that further described the purpose of the study. Participation was strictly voluntary; all respondents' anonymity was maintained.

The initial survey was pilot tested with a group of academicians with the purpose of collecting feedback on the instrument to identify confusing and/or misleading items, identify items and/or scale overlap, ensure item clarity and brevity, and identify the time required to complete the survey. Comments and observations were used to create the final survey.

The methodology adopted for this study is given as follows: (1) collection of literature to identify different factors affecting organizational performance. (2)

Develop a framework to show how these factors will affect organizational performance. (3) Developing questionnaire and collecting responses from the targeted group. (4)

Statistical analysis of data using SPSS. (5) Framework testing using SEM.

The questionnaire for this survey is prepared with the help of instruments established through previous researches. The questionnaire consists of a total of 20 questions distributed among individual profile, competitive advantage, CRM, organizational performance. The questionnaire employed a five point interval scale for the measurement. The individual profile of the employees comprised of designation, department, experience etc. Competitive advantage consists of price, quality, time to market, product innovation, after sales service etc. [1,2,3]. CRM consists of customer satisfaction, customer expectation, and relationship with customer etc. [2].

4.2 Participants

The population chosen for the study was drawn from among the top level managers from different PSU's situated in Kerala especially from the marketing and purchase department. The sampling method used for this study is convenient sampling.

The questionnaire was distributed to top level managers of different manufacturing industries in person. The internal consistency of the collected data is carried out using Statistical Solution for Software Solution (IBMSPSS Statistics Version.21). From the analysis, Cronbach's alpha (measure of internal consistency) was found to be 0.832 in organizational performance, 0.712 in SCMP, and 0.821 in Competitive advantage respectively(Table I) Thus it indicates a good level of internal consistency for the collected data.

Table I Cronbach's values for reliability tests on various constructs

Constructs	Cronbach's Alpha
SCMP	0.712
CA	0.821
OP	0.832

2. RESULTS

The purpose of this thesis is to determine if the supply chain management practices (CRM) were positively related to competitive advantage and organizational performance. This chapter summarizes the findings of analysis conducted on data collected using the Survey. The three hypotheses were evaluated using Structural equation modeling.

Structural Equations

In the case of measurement model there are 28 factors to be measured. Each of the factors is manifested by different variables. That is the latent variables are measured using indicator variables. In the path diagram supply chain management practices (SCMP) is measured by 28 indicator variablesSCMP1,SCMP2,… SCMP28 . Similarly the latent construct Competitive Advantage (CA) is measured by 8 indicator variables. Organizational performance (OP) by 6 indicators.

In confirmatory factor analysis the basis is that the latent construct are the causes of the manifest (indicator) variables. By drawing the arrowhead from latent construct to the indicator variable we are actually restricting the model. The parameter depicting the relationship between Supply chain management practices and SCMP1 is denoted by λ_{11} that is 1 the subscript of SCMP1 and Supply chain management practices considered as the first variable.

Before writing the equations, for simplicity all the latent factors can be represented under single variable say X. Therefore in the equations Supply chain management practices will be represented by X_1, Competitive Advantage by X_2 , Organizational performance by X3. Now the equations are as follows:

$SCMP_1 = \lambda_{11}X_1 + 0*X_2 + 0*X_3 + e1$

$SCMP_2 = \lambda_{21}X_1 + 0*X_2 + 0*X_3 + e2$

……

$SCMP_{28} = \lambda_{41}X_1 + 0*X_2 + 0*X_3 + e28$

$CA_{29} = 0*X_1 + \lambda_{52}X_2 + 0*X_3 + e29$

……

$CA_{36} = 0*X_1 + \lambda_{92}X_2 + 0*X_3 + e36$

$OP_{37} = 0*X_1 + 0*X_2 + \lambda_{103}X_3 + e37$

……

$OP_{41} = 0*X_1 + 0*X_2 + \lambda_{143}X_3 + e41$

In the measurement model we have taken all the latent variables without designating which of them are endogenous latent variables and exogenous latent variables. In path analysis or structural model we have to specify which of them are endogenous and exogenous. Here γ is used to find the relationship between exogenous and endogenous latent variables. In this model Supply chain management practices and Competitive advantage are exogenous latent constructs. Organizational Performance is the endogenous latent construct.

For the simplicity of writing equation, certain variables are represented by letter:

Supply chain management practices as S, Competitive advantage as A, and Organizational Performance as O

So the equation can be written as,

$O = \mu_{OC} * S + \mu_{OA} * A + e$

The theoretical framework illustrated in Fig. I has three hypothesized relationships among the variables SCMP, Competitive Advantage, and Organizational Performance. Fig. 4 displays the WARPpls model with results. Based on the result, we can say that competitive advantage significantly related to organizational performance (β=0.21,P=0.05). This significant association is a reflection of that the variables SCMP and CA vary in concert with one another that is the two variables are strongly and positively correlated.[9] .And SCMP and OP are also significantly related (β=0.29, P=0.02). For a strong relation the P value

should be less than 0.05($P<0.05$) and β(Path coefficient) value should be higher. Here both holds good. SEM model drawn in the WARPpls software shown below with its values (fig 4).

And the model fit indices values shown in table 5 say that the model is fit.

● ● ●

Multi-Source Piezoelectric Energy Harvester

[1]Vinitha K J, [2]Nisthul G
[1] PG Student, Saintgits College of Engineering, [2] Asst. Professor, Saintgits College of Engineering
[1]vinithavinek@gmail.com, [2] nisthulg@saintgits.org

Abstract— **Energy harvester gained a great amount of attention due to the recent advances in wireless technology allowing sensors to be flexible placed in remote locations and operate at very low power for low powered electronic devices; especially when being placed in a remote area, micro scale energy harvesting is preferable. Piezoelectric energy harvesting is a promising technology for extracting the power from environmental vibrations. It generates the electrical power of few orders of amplitudes which is sufficient to drive several autonomous electrical devices. Such vibration-based energy harvester enhances the power output by increase the effective area of force or pressure. When the application area reduces, the performance of the generator drastically reduces. In this line, present work first studies the various factors affecting the amount of power harvested. Simplest model to be started is with a single source piezoelectric energy harvester. To enhance the power harvesting capability of such simplest system over a wide bandwidth range, a multi-source energy harvester system is explained in the present work. Multi-source energy harvester is achieved by increased area by developing a piezoelectric stack with increased number of parallel cantilever beam. Its capability to work over a range of frequency and number of stack for required power output is mathematically predicted. The system uses an appropriate interface circuit, SECE interface which can enhance the power output of the harvester. The continuous beam models based on Euler theory is considered in this thesis which is solved using Finite Element Method. Results are validated with ANSYS solutions. As a next step, the multi-source harvesting problem is considered to know the modeling issues and amount of power harvested. In shock absorber motion of motorbike while driving through the road the effective vibration is utilize to harvest power. Results are satisfactory when compared to operate a piezoelectric stack.**

Keywords - **Energy Harvesting, Multi-Source Piezoelectric Energy Harvesting, SECE interface, Piezoelement stack**

I. INTRODUCTION

Energy harvester gained a great amount of attention due to the recent advances in wireless technology allowing sensors to be flexible placed in remote locations and operate at very low power for low powered electronic devices [6]; especially when being placed in a remote area, micro scale energy harvesting is preferable. Energy harvesting is also described as capture and storage or direct use of ambient energy for human purposes [21]. Piezoelectric crystals can be uses its property to transfer ambient motion (usually vibration) into electrical energy that may be stored and used to power other devices. The phenomenon of the generation of voltage under mechanical stress is known as piezoelectric effect. The output power generated will be effective at the instances that obtain mechanical resonance for the time varying inputs from its generator [3]. By implementing power harvesting devices, portable systems can be developed that do not depend on traditional methods for providing power, such as the battery, which has a limited operating life.

Most piezoelectric electricity sources produce power on the order of milliwatts, too small for system application. Davion et al. [4] pointed that energy source such as solar, vibration, thermal and other potential energy sources, and described the mathematical model of each energy source [27]. This method is that changes the solar cells array from series to parallel or series-parallel mixed way to find out a best array that output the maximum power [24]. This method also can be used in other energy source. Vehicles driving along the highway or city street generate vibration as the vehicle tread encounters the texture of the pavement and the vehicle suspension undulates from variations in height along the roadway [1]. The kinetic energy contained in these movements of vehicle goes unused on a system level; although these processes are part of the physics in creating a comfortable and functional ride in a vehicle and maintaining traction [12]. This energy can effectively and efficiently convert to electrical energy by using the application of piezoelectric effect.

The study aims to develop of a complete, integrated multi-source piezoelectric energy harvest (M-PEH) electromechanical system, which can harvest energy from high frequency ambient source by enhancing the power output using multi-

source technique. The ambient low frequency vibration is up-converted to a high resonant frequency one by the periodic impacts between the driving beam and the generating beams. To enhance the power harvesting capability of such simplest system over a wide bandwidth range, increase the available area effect of piezoelectric element. It is done by using multi-source stack.

In this paper, the generation of energy harvesting is take advantage of a piezoelectric cantilever based harvester. For piezoelectric energy harvesting, a composite cantilever beam is the most common way for accumulating vibration energy from host structure. In this study, stack will act as a number of cantilever beams arranged in parallel where piezoelement are mounting over each stack. In order to attain more power piezoelement are arranged in series and parallel connection. Multi-source piezoelectric energy harvester is connected to SECE interface circuit which reduces impedance mismatch with respect to other interface circuit and capacitors in this circuit act as temporary storage unit. Solidwork model of the stack is generated and evaluated using FEA and validated by ANSYS.

Paper follows by overview of piezoelement

II. OVERVIEW OF PIEZOELECTRIC ELEMENT

Piezoelectricity, also called the piezoelectric effect, is the ability of certain materials to generate an alternating current, voltage when subjected to mechanical stress or vibration, or to vibrate when subjected to an AC voltage, or both. The generation of electric field is proportional to the stress. The most common piezoelectric material is quartz. Certain ceramics, Rochelle salts, and various other solids also exhibit this effect.

Vibration-to-electricity conversion is a potential source for self-sustaining wireless sensor network in many environment. Low level vibrations occur in many environments including: large commercial building, industrial environments, automobiles, aircraft, ships, trains, and household appliances. Low level vibration source could generate about 300-800μW/cm³ in such environment. A stress is the function of a piezoelectric device, such as compression from outside forces, impact force. The first application of stress will generate voltage and current (power) within the material, but the stress must be relaxed in order for the material to generate power again. The amplitude and frequency of the signal is directly proportional to the mechanical deformation of the piezoelectric material. The resulting deformation causes a change in the surface charge density of the material so that a voltage appears between the electrode surfaces.

The electrical charges developed by piezo element decay with a time constant that is determined by the dielectric constant and the internal resistance of the element, as well as the input impedance of the interface electronics to which the film is connected. Practically speaking, the lowest frequency measurable with piezo element is in the order of 0.001Hz.

For best performance, the piezoelectric energy harvester should be excited mostly around its resonance frequency, deviation from the resonance frequency significantly reduces the output voltage.

Table 1: List of vibration source with their maximum accelerations and corresponding frequency

Vibration Source	Peak Acceleration (m/s^2)	Frequency of Peak (Hz)
Base of a 5 HP 3-axis machine tool	10	70
Door frame just after door closes	3	125
Kitchen blender casing	6.4	120
HVAC vents in office building	0.2-1.5	60
Wooden deck with people walking	1.3	385
Washing machine	0.5	109
Motor bike shock absorber	5	25

The design model should consider the resonant frequency of the piezoelectric element. Select the piezoelement with respect to the frequency available so that it can attain a resonant frequency enable large amount of power output.

Piezoelectric vibration energy harvesters have advantages of high energy density, non-electromagnetic interface and easy integration with MEMS. To enhance the power harvesting capability of such simplest system over a wide bandwidth range, increase the available area effect of piezoelectric element. It is done by using multi-source stack.

An effective source of piezoelectric harvester is vehicle suspensions which produces a large broadband frequency.

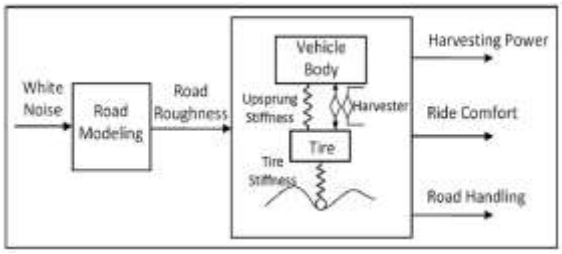

Fig. 2.1: Integrated road-vehicle harvesting model

Fig. 2.1 Explains the possibility of harvesting from vehicle. Harvester from road, pavement already excited, so principle of enhancing can make advantage from the methods. To enhance the power harvesting capability of such simplest system over a wide bandwidth range, increase the available area effect of piezoelectric element. It is done by using multi-source stack.

III. MULTI-SOURCE PIEZOELECTRIC ENERGY HARVESTER

Piezoelement theory: Piezoelectric materials are materials that convert mechanical energy from vibrations, force and pressure into electricity. At present, polycrystalline ceramic is the most common piezoelectric material. Typically, the constitutive equations for a piezoelectric material are given by following equation.

$$\delta = \frac{\sigma}{V} + dE \qquad (3.1)$$

$$D = \varepsilon E + d\sigma \qquad (3.2)$$

where δ is mechanical strain, σ is the mechanical stress, *Y* is the modules of elasticity (Young's Modules), *d* is the piezoelectric strain coefficient, *E* is the electric field, *D* is the electrical displacement (charge density), ε is the dielectric constant of the piezoelectric material. . The open circuit which means that the electrical displacement (D) is zero is defined as:

$$V_{OC} = \frac{-dt}{\varepsilon}\sigma \qquad (3.3)$$

where t is thickness of the piezoelectric material. Power harvested by a piezoelectric is given by:

$$E = \frac{\sigma_y{}^2 k^2}{2Y} \qquad (3.4)$$

Maximum energy available is 17.7mJ/cm³. Piezoelectric material has high energy density, high conversion efficiency and other excellent advantageous, this method has been widely used in ambient energy harvesting.

PZT is best for the application purpose. It is investigated the energy storage characteristics of a power harvesting system consisting of a PZT, full-bridge rectifier and a capacitor. Their work discussed the effect of various parameters on the efficiency of the storage circuit. Following their analytic investigation a prototype was developed and stated to have an efficiency of over 35%, more than three times greater than a solar cell.

To improve the robustness and efficiency of an energy harvester, a few studies have been carried out and the harvesters with wider bandwidth have been proposed or built. Three major ways are used to achieve a wider bandwidth for the piezoelectric harvesters which are (1) nonlinear stiffness, (2) bi-stable vibration and (3) multiple harvesters. While this approach has enjoyed great success in many aspects, there are two shortcomings. The first one is the low power area density and the second is the pronounced power reduction at off-resonance. The former is hard to improve due to limitations in the area of devices and the latter requires sophisticated techniques for frequency tuning by developing adjustable stiffness structures or the use of nonlinear techniques. This has motivated a prototype based on the use of multiple piezoelectric oscillators, since such a design allows multi-source deployment of structures to give increased power area density in a confined space. In addition, the overall bandwidth of an array structure can be enlarged by suitably adjusting the resonance of each oscillator.

A properly designed interface circuit plays a key role in the optimization of piezo elements. The applications of piezo element span from toys to military sensors and interfacing to electronics is highly application dependent. In many cases, piezo element can be directly connected to electronic circuits without special interface considerations. However, for those cases where an interface circuit is required, the following 3 steps are recommended:

1. Consider the frequency range and signal amplitude requirements over the desired dynamic range.
2. Choose a proper load resistance to assure the low end operating frequency and to minimize signal loss due to the loading effect.
3. Select a buffer circuit if the signal level is small. If a high value load resistance is needed, a low leakage high impedance buffer amplifier is recommended.

Energy harvesting applications makes use of a single piezoelectric harvester or cantilever beam, which is called single source piezoelectric energy

harvesting (S-PEH). In reality, S-PEH has some inherent limitations, for example, low power density and narrow operating frequency.

In this paper, new technique called multi-source interface circuit is used. Multi-source said that the cantilever attached with each other in a stack. The equivalent electrical impedance of a nonlinear full-bridge rectifier is difficult to compute in practice, and it cannot be considered a constant because of its intermittent conduction. While cases of serial and parallel connection of multiple piezoelectric elements have been investigated, we still lack a scalable and practical energy harvesting interface for M-PEH.

To optimize the performance of energy harvesting on bridge systems, vibration-based energy harvesting is studied for various bridges under different conditions.

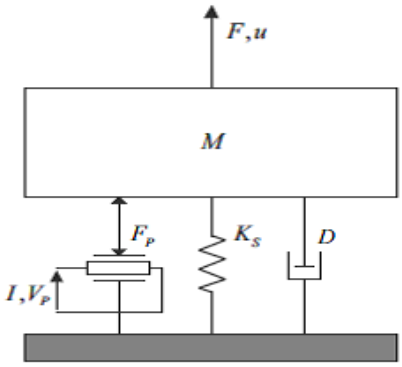

Fig. 3.2: Equivalent model of the cantilever-type piezoelectric energy harvester.

A type of interface simple, low-cost, nonlinear process to improve the efficiency of energy extraction, which is called the Synchronized Switch Harvesting on Inductor (SSHI) technique. Based on SSHI technique, some improved interfaces have been developed to enhance its performance, e.g. Double Synchronized Switch Harvesting (DSSH), Self-Power SSHI(SP-SSHI), SSHI with Magnetic Rectifier (SSHI-MR), Velocity Control SSHI (V-SSHI). Unfortunately, the standard interface and the SSHI interface both encounter the problem of impedance mismatching between the transducer and the load. Therefore, a technique called Synchronous Electric Charge Extraction (SECE), which adds a temporary storage unit to implement load decoupling, has been developed for these interfaces. These techniques can accelerate the charging process and improve the efficiency of energy extraction. However, they all require extra energy to support their active components in fact. While the energy generated from the piezoelectric element is usually low. In short, these above techniques have the same voltage threshold and power consumption due to the use of active components. Several interesting solutions that use mechanical switches instead of these active components in the circuit have been proposed, most of which utilize the motion of the piezoelectric cantilever beam to close mechanical contact and activate the switch control.

Scalable SECE Interface for M-PEH

The scalable standard interface for M-PEH is derived from the full-wave rectifier bridge circuit, where half of the full-wave rectifier bridge has been replaced by the middle point filtering capacitance pair (C_{f1}, C_{f2}), and the other half has been replaced by pairs of rectifying diodes (D_{n1}, D_{n2}), which corresponds with the number of piezoelectric elements. To obtain the rectified voltage, one output port of each piezoelectric element connects to the middle point of its rectifying diode-pair, and another output port of each piezoelectric element connects with the middle point of the filtering capacitance-pair. Assume that the rectifying diodes are ideal. When the absolute value of the i-th piezoelectric voltage V_p is less than the rectified voltage V_{DC1} (resp. V_{DC2}), the i-th rectifying diode-pair is blocked and the i-th piezoelectric element is in open circuit, causing the piezoelectric voltage V_p to vary with thedisplacement. Conversely, when the absolute value of the piezoelectric voltage V_p equals the rectified voltage V_{DC1} (resp. V_{DC2}),the rectifying diode D_{n1} (resp. D_{n2}) conducts and the current flows from the i-th piezoelectric element to the filtering capacitance C_{f1} (resp. C_{f2}). Multiple piezoelectric elements conducting at the same time can enhance the total charging current. The energy extraction process of the i-th piezoelectric element terminates when its piezoelectric voltage V_p drops to below the rectified voltage V_{DC1} (resp. V_{DC2}), and the current I_p cancels simultaneously.

Owing to the direct connection between the piezoelectric element and the storage unit, the harvested power of the other interfaces such as scalable standard interface and scalable series-SSHI interface for M-PEH is seriously influenced by the problem of impedance mismatching. But, the fact of impedance mismatching is almost unavoidable even though it has a match initial value. To overcome this difficulty, the scalable SECE interface for M-PEH, which adds an inductor L_i and a switch S_i to each piezoelectric element, has been proposed. Unlike the scalable series-SSHI inter-face, the inductor L_i of the scalable SECE interface is installed between the i^{th} rectifying diode-pair and the filtering capacitance pair, which acts as a temporary storage unit to

implement the technique of load decoupling.

The SECE technique divides the energy extraction process into two stages. First, when the local extreme displacement of the i[th] piezoelectric harvester occurs, the switch S_i is closed for a very short period and the energy in the i[th] piezoelectric element is transferred to the inductor L_i. Then, the switch S_i opens and the energy stored in the inductor L_i is transferred to the storage capacitance C_{f1} (resp. C_{f2}). Figure 3.7 displays the schematic of the scalable SECE interface for M-PEH.

The governing differential equation of this SDOF system in its linear range is given by (3.1) in which F is the equivalent external excitation force on the mass, and F_p is the restoring force due to the piezoelectric element.

$$M\ddot{u} + D\dot{u} + K_s + F_p = F \tag{3.5}$$

The expressions of the harvested power of these scalable M-PEH interfaces are derived as follows. According to the principle of the SECE technique, the harvested power of the

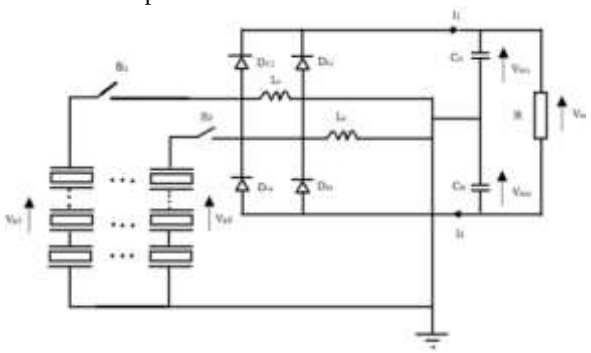

Fig. 3.3: Schematic of the scalable SECE interface for M-PEH.

scalable SECE interface for M-PEH is a function of each peak piezoelectric voltage V_{PMi}, and has no relation theoretically with the load resistance R. Therefore, the expression of the harvested power of the scalable SECE interface for M-PEH can be described by

$$p^{SECE} = \frac{1}{T}\sum_{i=1}^{N}\int_0^T V_{Pi} I_{Pi} dt = \frac{1}{T}\sum_{i=1}^{N} C_{Pi} V_{PMi}^2 \tag{3.6}$$

$$V_{PMi} = 2\frac{\alpha_i}{C_{Pi}} u_{Mi} \tag{3.7}$$

$$p^{SECE} = \sum_{i=1}^{N} \frac{2\omega\alpha_i^2 u_{Mi}^2}{\pi C_{Pi}} \tag{3.8}$$

where, I_{Pi} is the current of the i[th] piezoelectric element and correspond to the displacement

IV. MATHEMATICAL FORMULATIONS

An accurate model of a piezoelectric energy harvester plays a very important role in the study, design and application of the energy harvesting system. The modeling of piezoelectric materials has been studied thoroughly in the last century. The direct and inverse piezoelectric effects can be accurately described through the equations with a piezoelectric stain coefficient or piezoelectric stress coefficient. However, a more accurate model of a piezoelectric composite beam which is the typical formation of a piezoelectric energy harvester is in urgent demand for the study of energy harvesting.

Voltage and power output of single piezoelement very low compared to that required, in order to enhance both voltage and power output a stack is designed in cantilever beam model and piezoelement are arranging series and parallel connections.

Considering the low natural frequency of bridge structures, a cantilever with a single piezoelectric layer is used for the energy harvester in the present study to reduce the stiffness of the cantilever beam and therefore the fundamental natural frequency of the harvester. Apply Newton's second law of motion to the differential element in the *y* direction to obtain

$$\sum \mathrm{F_y} = \mathrm{ma_y} \Rightarrow \mathrm{V} + \frac{\partial \mathrm{V}}{\partial \mathrm{x}}\mathrm{dx} - \mathrm{V} - \mathrm{q(x,t)dx} = (\rho \mathrm{Ax})\frac{\partial^2 \mathrm{v}}{\partial \mathrm{t}^2}$$

where ρ is the material density and *A* is the cross-sectional area of the element. The quantity *A* represents mass per unit length in the *x* direction.
The consistent mass matrix for a two-dimensional beam element is given by

$$[\mathrm{m}^{(e)}] = \rho \mathrm{A}\int_0^{\mathrm{L}} [\mathrm{N}]^{\mathrm{T}}[\mathrm{N}]\mathrm{dx} \tag{4.2}$$

Substitution for the interpolation functions and performing the required integrations gives the mass matrix as

$$[m^{(e)}] = \frac{\rho AL}{420}\begin{bmatrix} 156 & 22L & 54 & -13L \\ 22L & 4L^2 & 13L & -3L^2 \\ 54 & 12L & 156 & -22L \\ -13L & -3L^2 & -22L & 4L^2 \end{bmatrix} \tag{4.3}$$

and it is to be noted that we have assumed constant cross-sectional area in this development.

V. RESULTS and Discussions

Single cantilever model in solid works is shown below. Calculation conducted for ABS material which is (i) Good impact resistance with toughness and rigidity (ii) Metal coating have excellent adhesion to ABS (iii) Formed by conventional thermoplastic methods (iv) A light weight plastic

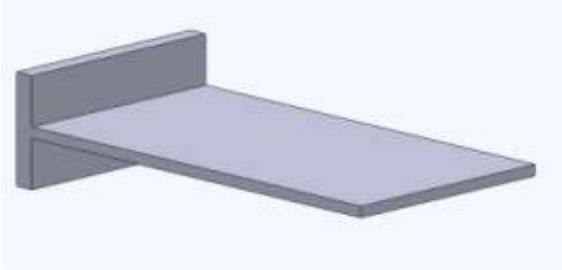

Fig. 5.1: Cantilever beam

Selected material is Acrylonitrile Butadiene Styrene (ABS)

Specifications of single cantilever beam,

Length, l = 90mm
Breadth, b = 58mm
Height, h =2mm

The table 5.3 shows the properties of the Acrylonitrile Butadiene Styrene (ABS) material

Table 5.1: Properties of ABS

Property	Value
Density, ρ	1.42g/cm³
Tensile Strength	40-50N/mm²
Young's Modulus, E	2.00GPa
Poisson's Ratio	0.42

By applying the equation

$$\frac{\rho AL}{420}\begin{bmatrix} 156 & -22L \\ -22L & 4L^2 \end{bmatrix}\begin{Bmatrix} \ddot{v} \\ \ddot{\theta} \end{Bmatrix} + \frac{EI}{L^3}\begin{bmatrix} 156 & -22L \\ -22L & 4L^2 \end{bmatrix} = \begin{Bmatrix} 0 \\ 0 \end{Bmatrix}$$

$$\omega_1 = 4.3\text{Hz}\,;\,\omega_2 = 29.58\text{Hz}$$

Analysis in ANSYS

Compared with the traditional analytical modeling, finite element analysis (FEA) is a more tractable approach to predicting he dynamic response of a harvester. The finite element analysis (FEA) simulation was performed using ANSYS.14.5. The finite elements in ANSYS that can be used to model the piezoelectric devices include 2NODE 188 and 3NODE 189 elements the specific descriptions of these elements can be found in the ANSYS theory manual

Table 5.2: ANSYS Analysed Result

SET	FREQUENCY
1	1.629
2	4.6672
3	10.398
4	14.117
5	23.915
6	30.231
7	34.295
8	36.731
9	45.473
10	57.583

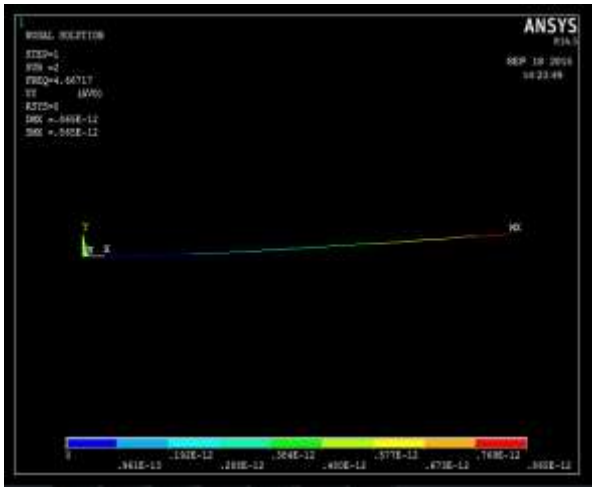

Figure 5.2: Deflection for frequency 4.667Hz

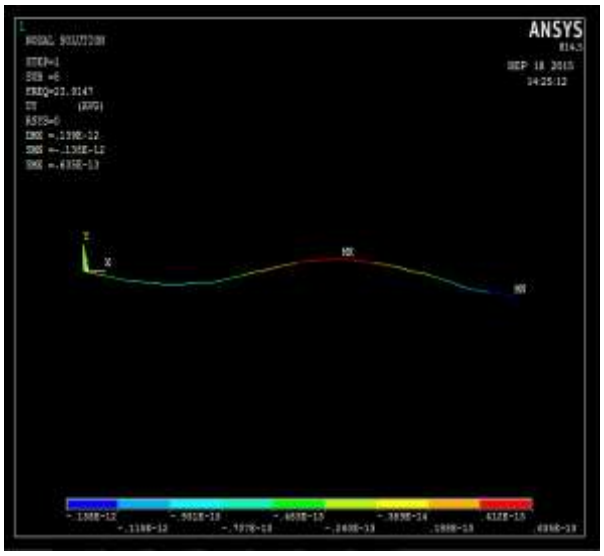

Fig. 5.3: Deflection for frequency 23.914Hz

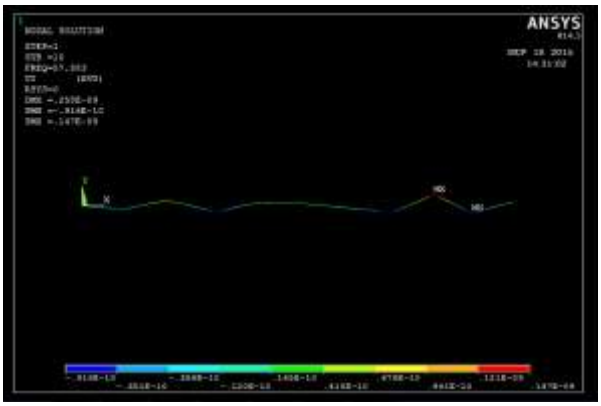

Fig. 5.4: Deflection for frequency 57.583Hz

VI. SOLIDWORKS MODEL OF THE PIEZOELEMENT STACK

Cantilever beams stack into case and piezoelements are mounting over it. Each stack contains six piezoelement. By considering the performance, features, durability, conformance and aesthetic aspects find an optimized position for the placing the multi-layer piezoelectric energy harvester.

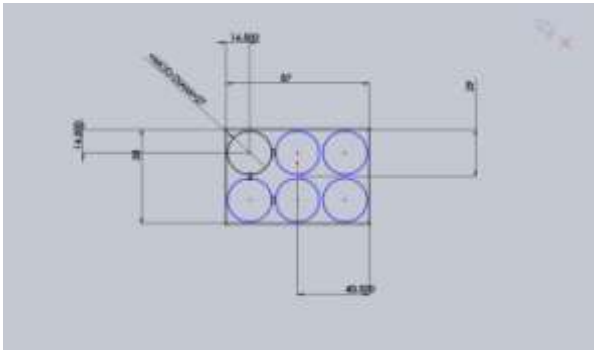

Fig/ 3.8: Single stack of cantilever beam

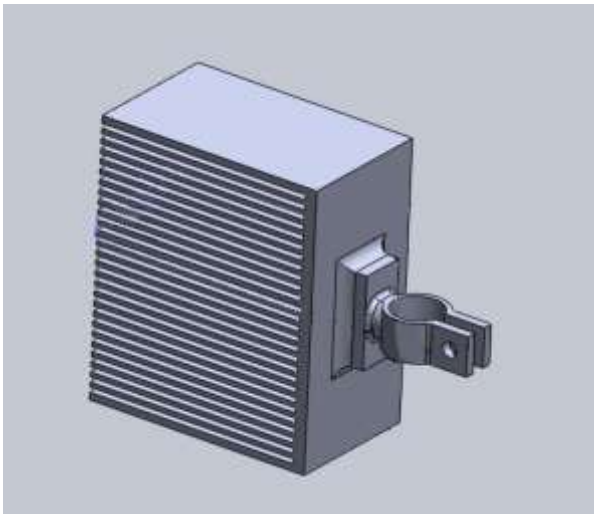

Fig. 3.9: Piezoelement stack

CONCLUSIONS

Harvesting energy from the ambient environment is generally considered to be the best way to power small electronic devices, especially for those installed in irreplaceable and inaccessible locations. Converting mechanical energy to electrical energy using piezoelectric materials seems to be the most promising solution for powering these devices.

In this project, an integrated piezoelectric energy harvester is designed to scavenge enhanced energy. A single piezoelement is not sufficient for the generation of the application. Thus the design of a multi-source piezoelement stack of cantilever beams and combination of series and parallel connections of piezoelements are mounted for obtaining the required voltage and power. Acrylonitrile Butadiene Styrene (ABS) is used for modeling the cantilever beam stack. Synchronous Electric Charge Extraction (SECE) interface is used for enhancing the power output of the piezoelement stack which offers reduction in impedance mismatching. Piezoelectric stack was modeled in SOLIDWORKS.

Analyzed the modal analysis using FEA analysis and validated it with ANSYS software. An experiment was conducted based on single stack of PEH. Analysis gave a sufficient value of power output which can multiply by increasing the number of stacks.

Further work can be carried out by considering integrated circuit of the interface circuit. Study can be conducted based on low frequency input utilization for energy harvesting.

REFERENCES

[1] Bandivadekar A, Bodek K, Cheah L, et al., “On the road in 2035: reducing transportation’s petroleum consumption and GHG emissions”, Cambridge, MA: MIT Laboratory for Energy and the Environment, 2008, Report no. LFEE 2008-05 RP, pp. 126-158

[2] Bell LE, “Cooling, heating, generating power, and recovering waste heat with thermoelectric systems”, Journal of science, 2008 Science 321(5895): pp. 1457–1461

[3] David V. Hutton, “Fundamentals of Finite Element Analysis”, The McGraw−Hill Companies, 2004, pp. 407-410

[4] Davion Hill et al., “Assessment of Piezoelectric Materials For Roadway Energy Harvesting” California Energy

Commission, Publication Number: CEC-500-2013-007, Jan 2014, pp. 3-12

[5] Erturk A et al., "A Distributed Parameter Electromechanical Model for Cantilevered Piezoelectric Energy Harvester", Journal of Vibration and Acoustics, August 2014, Vol. 130/041002, pp. 1-15

[6] Evan Murani et al., "Piezoelectric Energy Harvester- An Overview", Proceedings of the 2012 Mechanical Engineering Conference on Sustainable Research and Innovation, May 2012, Vol. 4, pp. 117-121

[7] Francisco J. Maldonado, Stephen Oonk, Tasso Politopoulos, "Enhancing Vibration Analysis by Embedded Sensor Data Validation Technologies", 2012 IEEE, vol. 978-1-4673-0700-0/12, pp. 1-6

[8] Henry A. et. al, "Estimation of Electric Charge output for Piezoelectric Energy Harvesting" ,Journal of Sensors and actuators, 2006, Vol 2/44, pp. 23-29

[9] Henry A. Sodano and Daniel J. Inman, "Comparison of Piezoelectric Energy Harvesting Devices for Recharging Batteries" Journal of Intelligent Material Systems and Structures, 2005, Vol. 16(10), 799-807,pp.1-7

[10] Huakang Xia et al., "Design and Analysis of a Scalable Harvesting Interface for Multi-Source Piezoelectric Energy Harvesting", Journal of Sensors And Actuators, July 2014, Vol. A21B, pp. 33-40

[11] Kai Kang et al., "Multi-Source Energy Harvesting for Wireless Sensor Nodes", pp.1-64

[12] Kowalski D et al., "Dynamic testing of shock absorbers under non-sinusoidal conditions", Proc Instn Mech Engrs Automobile Engineering,Vol. 216 Part D: J pp.373-384

[13] Li L U et al., "Fractal-Inspired Multi-Frequency Structures for Piezoelectric Harvesting of Ambient Kinetic Energy", Sensors and Actuators A: Physical, 2010, Vol. 2/36, pp.85-94

[14] Lin H C et, al., "Analysis of an Array of Piezoelectric Energy Harvesters Connected in Series", Journal of Acoustics, 2007, Vol. 13/56, pp. 1-13

[15] Liu Y P et al., "Self-Powered Electronics for Piezoelectric Energy Harvesting Devices", Small-Scale Energy Harvesting, 2012, pp. 327-337

[16] Michael Goldfarb et al., "On the efficiency of Electric Power Generation with Piezoelectric Ceramic", Vol. 121, September 1999, pp. 566-571

[17] Michael W. Shafer, Ephrahim Garcia, "The Power and Efficiency Limits of Piezoelectric Energy Harvesting", Journal of Vibration and Acoustics, 2014, Vol. 136 / 021007-1, 1-11

[18] Morgan Electro Ceramics, Technical Publication TP-238 Piezoelectricity, pp. 1-8

[19] Nechibvute A. et al., "Modelling of a PZT Beam for Voltage Generation", J. Sci. & Technol., Vol 19 (2): 259 – 271, 2011

[20] Pearson Luhanga et al., "Piezoelectric Energy Harvesting Using Synchronized Switching Techniques", International Journal of Engineering and Technology, 2012, vol 2/6, pp. 936-945

[21] Philipp Becker et al., "High efficiency piezoelectric energy harvester with synchronized switching interface circuit", Sensors and Actuators, 2013, Vol. 202, pp. 155-161

[22] Piezo Film Sensors Technical Manual, Measurement Specialties Inc, 2010, pp. b23-b45

[23] Rami Reddy A et al., "Design optimization and experimental analysis of Piezoelectric Energy harvester", Journal of Electrical and Electronics Engineering, Vol. 9, January 2014, pp. 18-27

[24] Shadrach Joseph Roundy, "Energy Scavenging for Wireless Sensor Nodes with a Focus on Vibration to Electricity Conversion", Journal of Electrical andelectronics, 2001, pp.175-184

[25] U K Singh et al., "Piezoelectric Power Scavenging of Mechanical Vibration Energy", Australian Mining Technology Conference, 2007, pp.:111-118

[26] Wen Y et al., "A Magnetoelectric Energy Harvester and Management Circuit for Wireless Sensor Network," Sensors and Actuators A: Physical, 157(2010) 100-106.

[27] William P., "Modeling of Low Frequency Multi-Source Energy Harvesting Systems", journal of mechatronics, 2013, Vol 23, pp.68-73

[28] Xin chang Liu, Yoan Civet and Yves Perriard, "Equivalent Piezoelectric Actuator Circuits and Comparison, IEEE,

2014, Vol.: 978-1-4799-5736, pp. 222-226

[29] Yang J, "Develop thermoelectric technology for automotive waste heat recovery" DOE 2009 vehicle technologies annual merit review and peer evaluation meeting, Arlington, 2009, Vol. A21, pp. 18–22

[30] Ye Zhang et al., "Piezoelectric Based Energy Harvesting on Low Frequency Vibrations of Civil Infrastructures", University of Houston , 2014, Vol 27, pp. 12-26

[31] Yuan-Ping Liu and Dejan Vasic, "Self-Powered Electronics for Piezoelectric Energy Harvesting Devices", Journal of Smart Electronics, 2009, Vol. 451/4871, pp. 324-362

[32] Zhang Y, Huang K and Yu F et al., "Experimental verification of energy-regenerative feasibility for an automotive electrical suspension system", IEEE International Conference on Vehicular Electronics and Safety, 2007, ICVES, 13–15, pp. 1–5

● ● ●

Dynamics of Pipe Conveying Fluids

[1]Shibin Pinto, [2]AjuZacharia Mani
[1]M.Tech scholar, Saintgits College of Engineering, [2] Assistant Professor, Saintgits College of Engineering
[1]shibinpinto1@gmail.com, [2]aju.zacharia@saintgits.org

Abstract: **Flow induced vibrations and instabilities are present in the fluid conveying pipes.The effect of flow velocity on the vibration frequency of the fluid conveying pipe with simply-supported boundary condition is analyzed. Finite Element Analysis methodology is used to determine the critical fluid velocity that induces the threshold of pipe instability. The equation of motion governing the lateral vibrations of the pipe is employed to develop the stiffness and inertia matrices corresponding to the terms of the equations of motion. Finite Element Model is developed for vibration analysis of a pipe carrying fluid and developed. The effect of flow velocity on the vibration frequency of the pipe conveying fluids has been investigated.**

Keywords: **Natural Frequency; Finite Element; Critical Flow Velocity; Pipe Instabilities**

I. INTRODUCTION

Dynamics of pipe conveying fluidshave many practical applications. They are encountered, for example, in the form of exhaust pipes, refinery, air-conditioning ducts, pipes carrying fluids in chemical and power plants, in offshore platformsrisersand tubes in heat exchangers and power plants. The fluid inside the pipe dynamically interacts with the pipe motion that causes the pipe to vibrate.

Studies regarding fluid-conveying pipes have been discussed in a number of papers. A survey by Paidoussis [1] regarding the subject indicates that more than 200 papers have been written in the open literature. The early contributions to the literature are by Ashley and Haviland [2], Feodosyev [3], Housner [4], Benjamin T. B. [5], and Naguleswaran S. and Williams C. J. H. [6]. They all studied flexural vibration of a pipe conveying a fluid. Crandall [7] and Dimarogonas A. D. and Haddad S. [8] developed the equations of motion of fluid conveying pipes using Euler-Bernoulli beam theory kinematics. Paidoussis and his coworkers [9-14] studied dynamics of pipes conveying fluid using the Euler-Bernoulli beam theory and the Timoshenko beam theory. Semler, et al. [14] derived a set of nonlinear geometrical equations of motion of fluid conveying pipes. The linear vibration of the system has been understood for some time Linear models are found. However, when the fluid flow velocity approaches a critical value, it gets in serious error [15] or the pipe performs large-amplitude vibration of in-plane force components (which are a function of the vibration shape) have a marked effect.

Recently some effort has been devoted to assessing non-linear dynamic behavior mainly by using numericaland analytical methods [16]. However, numerical work on the non-linear vibration of pipes conveying fluid is quite limited.

Subsequently,Housner[3] derived the equations of motion of a fluid conveying pipe more completely and developed an equation relating the fundamental bending frequency of a simply supported pipe to the velocity of the internalfluid flow. He also stated that at certain critical velocity, a statically unstable condition could exist. Long [17] presented an alternate solution to Housner's[3] equation of motion for the simply supported end conditions and fixed-free end conditions. He compared the analysis with experimental results to confirm the mathematical model. His experimental results were rather inconclusive since the maximum fluid velocity available for the test was low and change in bending frequency was very small. Other efforts to treat this subject were made by Benjamin, Niordson [18] and Ta Li. Other solutions to the equations of motion show that type of instability depends on the end conditions of the pipe carrying fluid. If the flow velocity exceeds the critical velocity pipes supported at both ends bow out and buckle. Cantilever pipes fall into flow induced vibrations and vibrate at a large amplitude when flow velocity exceeds critical velocity.

The present work implements numerical solutions method, more specifically the Finite Element Analysis (FEA) to obtain solutions for simply supported boundary conditions and fluid flow characteristics. The governing dynamic equation describing the structural vibrations due to

internal fluid flow has been formed. The governing equation of motion is partial differential equation that is fourth order in spatial variable and second order in time. A finite element model is created to solve the equation of motion. For simply supported boundary condition, based on the user defined parameters natural frequency for free vibration is calculated for first three mode. The effects of flow velocity on the vibration frequency of the pipe conveyingfluids are investigated.

II. MATHEMATICAL MODELLING

A. Equation of Motion

Consider a pipe of length L, modulus of elasticity E, and its transverse area moment I. A fluid flows through the pipe at pressure p and density ρ at a constant velocity v through the internal pipe cross-section of area A. As the fluid flows through the detecting pipe it is accelerated, because of the changing curvature of the pipe and the lateral vibration of the pipeline. The vertical component of fluid pressure applied to the fluid element and the pressure force F per unit length is applied on the fluid element by the tube walls oppose these accelerations.

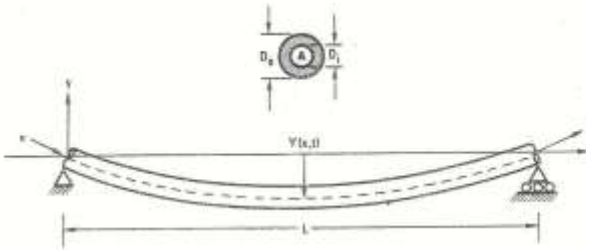

Fig. 1 Simply-supported pipe carrying fluid

The equation of motion is

$$EI\frac{\partial^4 w}{\partial x^4}+MU^2\frac{\partial^2 w}{\partial x^2}+2MU\frac{\partial^2 w}{\partial x\partial t}+(M+m)\frac{\partial^2 w}{\partial t^2} \quad (1)$$

EI is pipe flexural rigidity, M is the fluid mass per unit length, flowing with a steady flow velocity U, m is the pipe mass per unit length, and w is the lateral deflection of the pipe; x is the axial coordinate and t is time. The first term in the equation (1) represents the force due to bending of the pipe conveying fluids, the second term represents the force that conform fluid to the Curvature of Pipe, the third term is the force required to rotate the fluid element as each point in the span rotates with angular velocity. Which result inCoriolis Effect or the coriolis force. The fourth term result of Inertia of the pipe and the fluid flowing through it.

B. Finite Elment Model

By using the Galerkin technique, the finite element equations are formulated and the different matrices for element length l are used here. The equation of motion for the coupled fluid structure is

$$[\mathrm{M}]\{\ddot{w}\}+[\mathrm{C}]\{\dot{w}\}+[\mathrm{K_1}\text{-}\mathrm{K_2}]\{w\}=0 \quad (2)$$

These assembled matrices are solved for the natural frequency and onset of instability of a cantilever and simply supported pipe carrying fluid has been analyzed.

C. Results And Discussions

In the paper, free vibration equation of the fluid conveying pipe has been derived and the corresponding finite element codes are formulated and the analysis has been done using MATLAB. In order to analyze the effect of flow velocity on the frequency we assume a 3.2 m long aluminum pipe, with a 2.54 cm diameter and 1.67mm thick wall. The flowing liquid is water. The other parameters are ρA=.384kg/m,E=68.9×10^9 Pa,I=8.64×10^{-9} m^4 , m=.342kg/m.

Figure 2 shows the imaginary components of dimensionless frequency β , function of dimensionless flow velocity v_n for the first three modes of the simply supported aluminum pipe conveying fluid. When v_n =0, β is an imaginary number and equal to the natural frequency of a simply supported pipe.The imaginary component of β decreases as the flow velocity increases. *Im* (β) are equal to zero for the first mode, When flow velocity increases to π. Thiscorresponds to the divergence instability of the aluminum. The divergence instability of the second mode takes place when the dimensionless flow velocity reaches about 2π. For the divergence instability, the critical flow velocity is independent of frequency because it is a static behavior. Beyond the velocity, the combination of the first and second modes occurs, and the frequency becomes conjugate complex. This implies that the pipe undergoes a coupled mode flutter.

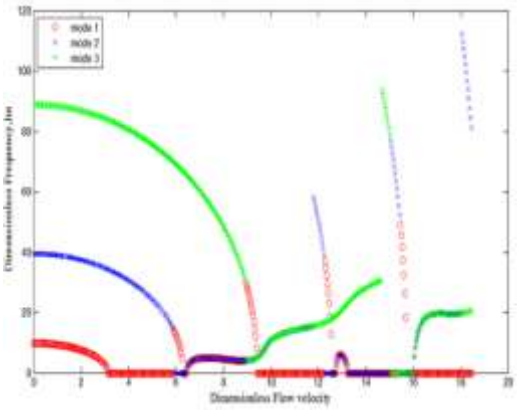

Fig. 2Imaginary component of dimensionless frequency as function of dimensionless flow velocity for the first three modes of a simply supported pipe conveying fluids

Figure 3 shows the real component of the dimensionless frequency β as function of dimensionless flow velocity v_n for the first three mode of simply supported pipe conveying fluid. The real component gives the damping characteristics of the pipe.

When v_n =0, the real component of the dimensionless frequency β remains zero. This implies that the fluid flow in the nanotube does not contribute to damping of the SWCNT. As the flow velocity increases to π the$Im(\beta)$ and $Re\,\beta$) are zero for the first mode. As the flow velocity increases further the frequency of the first mode purely real. Further increasing the flow velocity the real part of the first mode is coupled with the second mode and this indicates the onset of coupled mode flutter

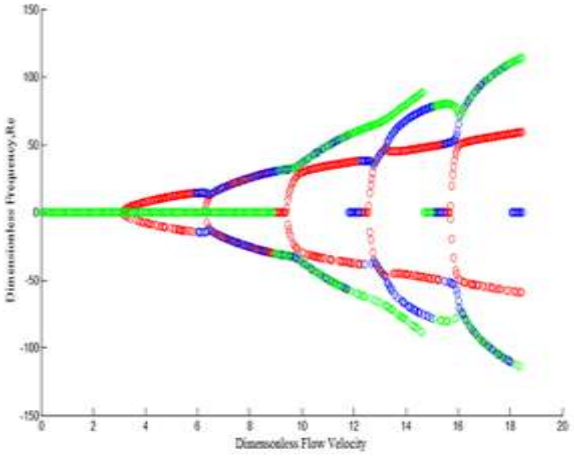

Fig. 3 Real component of dimensionless frequency as function of dimensionless flow velocity for the first three modes of a simply supported pipe conveying fluids

CONCLUSIONS

The flow of fluids in a pipe has many dynamical effects and correspondingly for a simply supported case the analysis has been done and it is found that

- Increasing the flow velocity the natural frequency of the pipe decreases and at critical velocity the natural frequency gets to zero and pipe instability occurs
- For flow velocity less than the first divergence flow velocity, the real part β of is zero; i.e., the fluid flow does not contribute to damping. As the flow velocity increases, the imaginary part of β in decreases with flow.
- The pipe loses stability first by divergence. It is the same as that of a pipe subjected to an axial compression of magnitude v^2. Because the divergence is a static phenomenon, the critical flow velocity for divergence is independent of β

REFERENCES

[1] Paidoussis, M. P. andLi, G. X., "Pipes Conveying Fluid: A Model Dynamical Problem," Journal of Fluids and Structures, 7, 137-204, 1993.

[2] Ashley, H. and Haviland, G., "Bending Vibrations of a Pipe Line ContainingFlowing Fluid," Journal of Applied Mechanics, 17, 229-232, 1950.

[3] Feodosyev, V. I., "On the Vibrations and Stability of a Pipe Conveying aFluid," (in Russian) Engineer Book, 10, 169-170, 1951.

[4] Housner, G. W., "Bending Vibrations of a Pipe Line Containing FlowingFluid," Journal of Applied Mechanics, 19, 205—208, 1952.

[5] Benjamin, T. B., "Dynamics of a System Articulated Pipes Conveying Fluid:Theory," Proceedings of the Royal Society of London, Series A, 261, 457-486, 1961.

[6] Naguleswaran, S. and Williams, C. J. H., "Lateral Vibration of a PipeConveying a Fluid," Journal of Mechanical Engineering Science, 10, 228-238, 1968.

[7] Crandal, S. H., Karnopp, D. C., Kurtz, Jr., E. F., and Pridmore—Brown, D.C., Dynamics of Mechanical and Electromechanical Systems, McGraw-Hill,New York, 1968 (see pp. 390—395).

[8] Dimarogonas, A. D. and Haddad, S., Vibration for Engineers, Prentice-Hall,Englewood Cliffs, NJ, 1992 (see p. 446).

[9] Paidoussis, M. P., “Dynamics of Flexible Slender Cylinders in Axial Flow,”Journal of Fluid Mechanics, 26, 717—736, 1966.
[10] Paidoussis, M. P., “Dynamics of Tubular Cantilevers Conveying Fluid,” Journal of Mechanical Engineering Science, 12, 85—103, 1970.
[11] Paidoussis, M. P. and Issid, T. D., “Dynamic Stability of Pipes Conveying Fluid,” Journal of Sound and Vibration, 33, 267—294, 1974.
[12] Paidoussis, M. P. and Laithier, T. D., “Dynamics of Timoshenko Beam Conveying Fluid,” Journal of Mechanical Engineering Science, 18, 210—220, 1976.
[13] Paidoussis, M. P., Luu, T. P., and Laithier, B. E., “Dynamics of Finite- Length Tubular Beams Conveying Fluid,” Journal of Sound and Vibration, 106, 311—331, 1986.
[14] Semler, C., Li, G. X., and Paidoussis, M. P., “The Non-Linear Equations of Motion of Pipes Conveying Fluid,” Journal of Sound and Vibration, 169, 577—599, 1994.
[15] Dodds, H. L. and Runyan, H. Effect of high-velocity fluidflow in the bending vibrations and static divergence of asimply supported pipe. National Aeronautics and SpaceAdministration Report NASA TN D-2870, June 1965.
[16] Edelstein, W. S., Chen, S. S. and Jendrzeczyk, J. A. A finiteelement computation of flow-induced oscillations in a cantilevered tube. J. Sound and Vibr., 1986, 107, 121–129.
[17] Long.R.H "Experimental and Theoretical Study of Transverse Vibration of a tubeContaining Flowing Fluid". J.Appl.Mech. 22,65-68(1955).
[18] Niordson,F.I.N "Vibrations of a Cylinderical Tube Containing Flowing Fluid".Trans. Roy. Inst.Technol.Stockholm 73(1953).

Development of Finite Element Code for 3D Four Noded Isoparametric Membrane Shell Elements

[1]Prasanth P Nair, [2]George T. S
[1] [2]Dept. of Mech Engg.
[1] [2]Saintgits College of Engineering
[1] [2]Kottayam, Kerala, India
[1]Prasanth1991atm@gmail.com, [2]George.ts@saintgits.org

Abstract: **The paper presents the development of code for finite element analysis of shell structures. It consists of linear analysis of shell structures. A four noded quadrilateral element is formulated general curved elastic geometric surface. The element is formulated using degenerated shell theory. The described isoparametric element is of constant thickness and assumes a constant plane stress criterion. An important aspect of the work is to implement these elements on the computer using ANSYS and MATLAB software. A finite element analysis program that calculates deflections was also developed in order to verify the accuracy of these elements. Mass matrix formulation and 3D plotting of shell elements are done in MATLAB. The results obtained for a test problem was compared with those from a commercial finite element analysis program.**

Keywords: **Degneration, Shell formulation, FE Analysis, Matlab coding, Isoparametric 4 node shell element.**

I. INTRODUCTION

A shell is a type of structural element which is characterized by its geometry, being a three-dimensional solid whose thickness is very small when compared with other dimensions, and in structural terms, by the stress resultants calculated in the middle plane displaying components which are both coplanar and normal to the surface. There are different types of shell elements such flat shell elements, curved shell elements, axisymmetric shell elements and, Mindlin type degenerated solid elements. Based on thickness shell elements are again classified into two types. They are thick and thin shell elements. The formulation of thin shell elements are based on discrete krichoff theory and thick shell elements are based on mindlin theory. Isoparametric elements are useful for modelling structures with irregular boundaries [1]. The word isoparametric indicates that the same functions are used to define the shape and displacements of the element. It is often difficult to model the geometry of a structure with just the regular shaped triangular or rectangular elements [2]. Isoparametric elements are useful for modelling structures; since the isoparametric elements can have curved sides. Such elements are formulated using higher order interpolation functions. The first developed arbitary shell structure was triangular flat shell elements by Green et.al in 1961 [3]. Shells with cylindrical shapes or regular curved surfaces can be modeled using rectangular or quadrilateral flat shell elements. Zienkiewicz (1971) recommended modelling curved surface by a series of flat shell elements, rather than using the more complex curved shell elements. He suggested developing a built up element by combining membrane and plate bending elements to develop a flat shell elements [4]. Bathe and Ho (1981) studied two approaches for the development of shell elements [5]. The first approach is to use the higher order isoparametric elements, which are formulated on the basis of three dimensional stress conditions and using the higher order shape functions and integration scheme. The second approach is to use lower order shell elements, which are developed by superimposing previously available membrane and plate bending elements and hence obtaining the membrane and bending properties of the shell element. Fernando and Eugenio presented a formulation for analysis of thin elastic membranes using a rotation-free shell element within an explicit time integration strategy [6].

The focus of this thesis is to develop curved shell elements for the finite element

analysis of thin shell structures. The curved shell elements are developed by combining membrane elements with plate bending elements. An important aspect of the work is to implement these elements on the computer using an object oriented approach and the MATLAB software. MATLAB was chosen as the programming language for this work; since MATLAB is an object oriented programming Language.

A finite element analysis program that calculates deflections was also developed in order to verify the accuracy of these elements [7]. This program was written in Matlab using the object oriented approach. The results obtained for a series of test problems were compared with those from a commercial finite element analysis program.

II. SHELL THEORY

A. DEGENERATION

The idea of the degeneration concept is to eliminate nodes from a solid element by imposing on it kinematic constraints and assumptions, that represent shell-like behaviour. In principle a shell structure is a special type of solid structure and one may be tempted to model the structure by solid elements as shown in Figure 1**.**

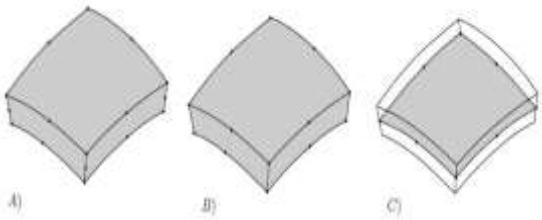

Fig. 1: Degeneration Process of A) 20-Node Solid Element to B) 16-Node Solid Element to C) 8-Node Shell Element.

A four nodes element is obtained by degenerating the eight nodes solid element as shown in Figure 2 and 3 [8].

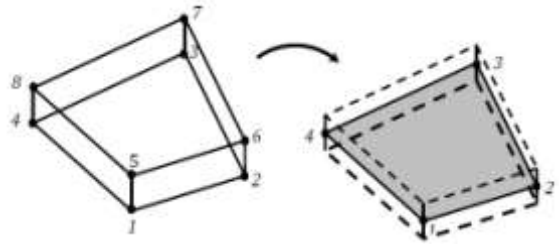

Fig. 2: Four Nodes Shell Element Degenerated from Eight Nodes Solid Element

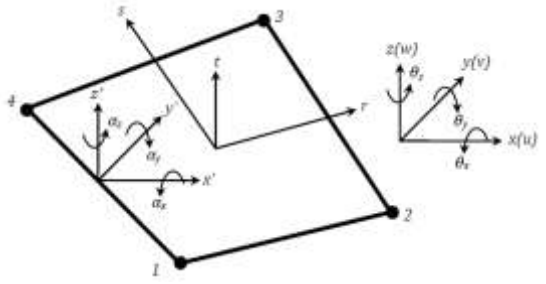

Fig. 3: Four Nodes Shell Element

A point in a shell structure can be expressed by a vector sum of two vectors. The first vector is a position vector from the origin of the coordinate system to a point on the surface of the shell element. The second vector is a position vector from this reference to a point under consideration.

A generic point on a shell may now be described in terms of the position vectors of the nodes and the shape functions [9].

$$x_i(r,s,t)=\sum_{k=1}^{n} N^k(r,s)x_i^k+\sum_{k=1}^{n} N^k(r,s)H^k(t)V_{3i}^k \quad (i=1,2,3) \qquad (1)$$

where x_i^k is the position vector of node k in the reference surface; V_{3i} is the unit vector at the node k and n is the number of nodes per element. Two shape functions are used to describe a position in the element. N^k is the two dimensional shape function in the r-s plane, and H^k is the one dimensional shape function along the t- axis, where (r, s, t) describes a point in the natural coordinate system.

The displacement field in the can be written as

$$u_i(r,s,t)=\sum_{k=1}^{n} N^k(r,s)u_i^k+\sum_{k=1}^{n} N^k(r,s)H^k(t)\left(-V_{2i}^k\theta_1^k+V_{1i}^k\theta_2^k\right) \qquad (2)$$

In which u_i is the displacement along the x_i axis, u_i^k is the nodal displacement at the node k, and the unit vectors V_{1i}^k and V_{2i}^k lie along the reference surface.

B. STRAIN-DISPLACEMENT RELATION

Six strain components are computed from equation by taking the derivative with respect to the x_i be written in matrix form as

$$\{\varepsilon\}=[B]\{d\} \qquad (3)$$

Where

$$\{\varepsilon\}=\{\varepsilon_{11}\ \ \varepsilon_{22}\ \ \varepsilon_{33}\ \ \gamma_{12}\ \ \gamma_{23}\ \ \gamma_{13}\}^T$$
$$[B]=[B^1\ \ B^2\ \ .\ \ .\ \ .\ \ B^n]$$

And

$$\{d\} = \{d^1 \quad d^2 \quad . \quad . \quad . \quad d^n\}^T \tag{4}$$

The detailed expansion of $\left[B^k\right]$ is

$$\left[B^k\right] = \begin{bmatrix} \frac{\partial N^k}{\partial x_1} & 0 & 0 & -g_1^k V_{21}^k & g_1^k V_{11}^k \\ 0 & \frac{\partial N^k}{\partial x_2} & 0 & -g_2^k V_{22}^k & g_2^k V_{12}^k \\ 0 & 0 & \frac{\partial N^k}{\partial x_3} & -g_3^k V_{23}^k & g_3^k V_{13}^k \\ \frac{\partial N^k}{\partial x_2} & \frac{\partial N^k}{\partial x_1} & 0 & -g_2^k V_{21}^k - g_1^k V_{22}^k & g_2^k V_{11}^k + g_1^k V_{12}^k \\ 0 & \frac{\partial N^k}{\partial x_3} & \frac{\partial N^k}{\partial x_2} & -g_3^k V_{22}^k - g_2^k V_{23}^k & g_3^k V_{12}^k + g_2^k V_{13}^k \\ \frac{\partial N^k}{\partial x_3} & 0 & \frac{\partial N^k}{\partial x_1} & -g_3^k V_{21}^k - g_1^k V_{23}^k & g_3^k V_{11}^k + g_1^k V_{13}^k \end{bmatrix} \tag{5}$$

In which

$$g_i^k = \frac{\partial N^k}{\partial x_i} H^k + N^k \frac{\partial H^k}{\partial x_i} \tag{6}$$

The strain components are computed as

$$\varepsilon_{11} = \frac{\partial u_1}{\partial x_1} \tag{7}$$

$$\frac{\partial u_1}{\partial x_1} = \sum_{k=1}^{n} \frac{\partial N^k}{\partial x_1} u_1^k + \sum_{k=1}^{n} \frac{\partial N^k}{\partial x_1} H^k \left(-V_{21}^k \theta_1^k + V_{11}^k \theta_2^k\right) + \sum_{k=1}^{n} \frac{\partial H^k}{\partial x_1} N^k \left(-V_{21}^k \theta_1^k + V_{11}^k \theta_2^k\right)$$

$$\frac{\partial u_1}{\partial x_1} = \sum_{k=1}^{n} \frac{\partial N^k}{\partial x_1} u_1^k + g_1^k \left(-V_{21}^k \theta_1^k + V_{11}^k \theta_2^k\right) \tag{8}$$

Thus, the strain component becomes

$$\varepsilon_{11} = \sum_{k=1}^{n} \frac{\partial N^k}{\partial x_1} u_1^k + g_1^k \left(-V_{21}^k \theta_1^k + V_{11}^k \theta_2^k\right) \tag{9}$$

Shear strains are derived using the equation

$$\gamma_{12} = \frac{\partial u_1}{\partial x_2} + \frac{\partial u_2}{\partial x_1} \tag{10}$$

Therefore shear strain component along and axis is given by

$$\gamma_{12} = \sum_{k=1}^{n} \frac{\partial N^k}{\partial x_2} u_1^k + \sum_{k=1}^{n} \frac{\partial N^k}{\partial x_1} u_2^k + \left(-g_2^k V_{21}^k - g_1^k V_{22}^k\right)\theta_1^k + \left(g_2^k V_{11}^k + g_1^k V_{12}^k\right)\theta_2^k$$

C. JACOBIAN MATRIX

In order to compute the derivatives such as $\frac{\partial N^k}{\partial x_i}$ and $\frac{\partial H^k}{\partial x_i}$, the jacobian matrix is required and is defined as

$$[J] = \begin{bmatrix} \frac{\partial x_1}{\partial r} & \frac{\partial x_2}{\partial r} & \frac{\partial x_3}{\partial r} \\ \frac{\partial x_1}{\partial s} & \frac{\partial x_2}{\partial s} & \frac{\partial x_3}{\partial s} \\ \frac{\partial x_1}{\partial t} & \frac{\partial x_2}{\partial t} & \frac{\partial x_3}{\partial t} \end{bmatrix} \tag{11}$$

Where,

$$\frac{\partial x_1}{\partial r} = \sum_{k=1}^{n} \frac{\partial N^k}{\partial r} x_1^k + \sum_{k=1}^{n} \frac{\partial N^k}{\partial r} H^k V_{3x}^k$$

$$\frac{\partial x_1}{\partial s} = \sum_{k=1}^{n} \frac{\partial N^k}{\partial s} x_1^k + \sum_{k=1}^{n} \frac{\partial N^k}{\partial s} H^k V_{3x}^k$$

$$\frac{\partial x_1}{\partial t} = \sum_{k=1}^{n} \frac{\partial H^k}{\partial t} N^k V_{3x}^k \tag{12}$$

D. CONSTITUTIVE MATRIX

Stresses and strains can be expressed as

$$\{\sigma\} = \left[D\right]\{\varepsilon\} \tag{13}$$

Where $\{\sigma\}$ and $\{\varepsilon\}$ are the stresses and strains components in the local axes which are set along the reference plane made of vectors V_1 and V_2 as shown in the figure. The constitutive matrix $\left[D\right]$ is given for an isotropic material.

$$\left[D\right] = \begin{bmatrix} \frac{E}{(1-\upsilon^2)} & \frac{E\upsilon}{(1-\upsilon^2)} & 0 & 0 & 0 & 0 \\ \frac{E\upsilon}{(1-\upsilon^2)} & \frac{E}{(1-\upsilon^2)} & 0 & 0 & 0 & 0 \\ 0 & 0 & 0 & 0 & 0 & 0 \\ 0 & 0 & 0 & \frac{E}{2(1+\upsilon)} & 0 & 0 \\ 0 & 0 & 0 & 0 & \frac{\kappa E}{2(1+\upsilon)} & 0 \\ 0 & 0 & 0 & 0 & 0 & \frac{\kappa E}{2(1+\upsilon)} \end{bmatrix} \tag{14}$$

In which E and υ are the elastic and Poisson's ratio respectively. This matrix includes the transverse shear deformation. The fifth and sixth rows are for the transverse shear deformation. κ is the shear correction factor which is chosen as 5/6 for an isotropic material.

The material property matrix $[D]$ is transformed into a matrix in terms of the stresses and strains of the global axes. The transformed material property matrix is

$$[D] = [T_\varepsilon]^T [D'] [T_\varepsilon] \tag{15}$$

Where the transformed matrix $[T_\varepsilon]$ is

$$[T_\varepsilon] = \begin{bmatrix} l_{1x}^2 & l_{1y}^2 & l_{1z}^2 & l_{1x}l_{1y} & l_{1y}l_{1z} & l_{1x}l_{1z} \\ l_{2x}^2 & l_{2y}^2 & l_{2z}^2 & l_{2x}l_{2y} & l_{2y}l_{2z} & l_{2x}l_{2z} \\ l_{3x}^2 & l_{3y}^2 & l_{3z}^2 & l_{3x}l_{3y} & l_{3y}l_{3z} & l_{3x}l_{3z} \\ 2l_{1x}l_{2x} & 2l_{1y}l_{2y} & 2l_{1z}l_{2z} & l_{1x}l_{2y}+l_{2x}l_{1y} & l_{1y}l_{2z}+l_{2y}l_{1z} & l_{1x}l_{2z}+l_{2x}l_{1z} \\ 2l_{2x}l_{3x} & 2l_{2y}l_{3y} & 2l_{2z}l_{3z} & l_{2x}l_{3y}+l_{3x}l_{2y} & l_{2y}l_{3z}+l_{3y}l_{2z} & l_{2x}l_{3z}+l_{3x}l_{2z} \\ 2l_{3x}l_{1x} & 2l_{3y}l_{1y} & 2l_{3z}l_{1z} & l_{3x}l_{1y}+l_{1x}l_{3y} & l_{3y}l_{1z}+l_{1y}l_{3z} & l_{3x}l_{1z}+l_{1x}l_{3z} \end{bmatrix} \tag{16}$$

Here l_{ij} are the directions cosines of the unit vector V_i with respect to the x_j - axis.

E. ELEMENT STIFFNESS MATRIX

The element stiffness matrix is computed from

$$[K] = \int [B]^T [D] [B] d\Omega \tag{17}$$

The rotational degrees of freedom are expressed in terms of the local vectors and they should be expressed in terms of the global axes so that they can be assembled properly. Such a transformation is obtained from

$$\{d^k\}_{global} = [T_{rot}] \{d^k\} \tag{18}$$

For a four node shell element, the transformation matrix for rotational degrees of freedom becomes

$$[\overline{T_{rot}}] = \begin{bmatrix} [T_{rot}] & 0 & 0 & 0 \\ 0 & [T_{rot}] & 0 & 0 \\ 0 & 0 & [T_{rot}] & 0 \\ 0 & 0 & 0 & [T_{rot}] \end{bmatrix} \tag{19}$$

The local nodal degrees of freedom vector in equation include for the proper coordinate transformation as shown below

$$\{d^k\} = \{u_1 \quad u_2 \quad u_3 \quad \theta_1 \quad \theta_2 \quad \theta_3\} \tag{20}$$

As a result, the element stiffness matrix should be explained to incorporate the degrees of freedom at each node, as shown in equation. Then, the transformed element stiffness matrix is

$$[\overline{K}] = [\overline{T_{rot}}]^T [K] [\overline{T_{rot}}] \tag{21}$$

F. MASS MATRIX

The consistent mass matrix (me) for the shell element is given by

$$T_e = \frac{1}{2}\{u\}^T \int_{-1}^{+1}\int_{-1}^{+1}\int_{-1}^{+1} \rho [N^k + H^k]^T [N^k + H^k] |J| d\xi\, d\eta\, d\zeta \{u\}$$
$$m_e = \int_{-1}^{+1}\int_{-1}^{+1}\int_{-1}^{+1} \rho [N^k + H^k]^T [N^k + H^k] |J| d\xi\, d\eta\, d\zeta \{u\} \tag{22}$$

III. TEST EXAMPLES AND VEIFICATION OF RESULTS

A. IMPLEMENTATION OF THE CURVED SHELL ELEMENT IN MATLAB

The pinched-cylinder problem has been widely used to test shell elements. The physical problem is presented in Figure. 4 [10].

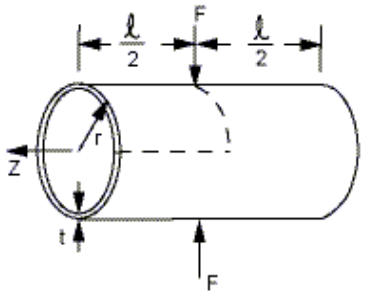

Fig. 4: Problem Sketch – Pinched Cylinder

The thin circular cylindrical shell is subjected to equal and opposite point loads and the ends are restrained by rigid diaphragms as shown in Figure 5.4. A thin-walled cylinder is pinched by a force F at the middle of the cylinder length. The specifications of the pinched cylinder is given as Elastic modulus, E = 10.35*106 psi, Poisson's ratio, υ = 0.3125, Length of the cylinder, l = 10.35 in, Radius, r = 4.953 in, Thickness, t = 0.094 in, Point load, F = 100 lb. A one-eighth symmetry model is used. One-fourth of the load is applied due to symmetry. The finite element is discretized into 64 elements which have 81 nodes. Each element has 4 nodes with 6 degree of freedom per node, 3 translational and 3 rotational degrees of freedom. Due to symmetry conditions only one

octant of the cylinder needs to be considered.

1) Results in Matlab

3D plotting of the shell element is not predefined. A code has to be written so that nodes, coordinates, connectivity etc. is taken and finally plotted as a clean picture. To write a code for plotting, it has to rely on logic. The 3D plotting of the curved shell is obtained as shown in the Figure 5.

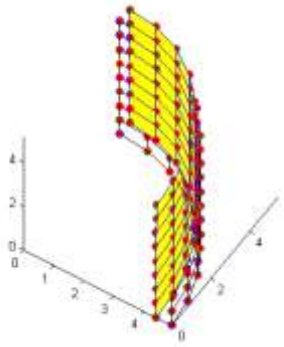

Fig. 5: 3D Plotting of the Curved Shell Elements

The maximum displacement is obtained at node 73 as 0.1086 which is shown in the Figure 6.

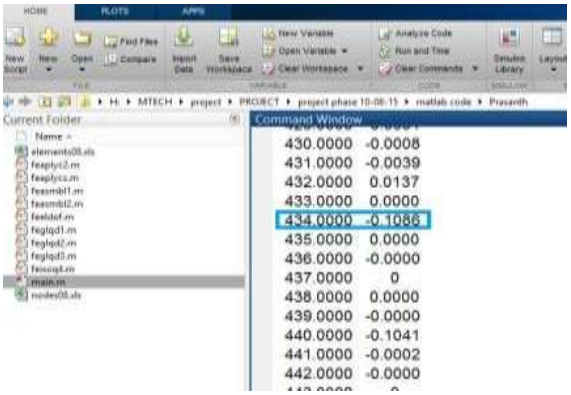

Fig. 6: Maximum Value of Displacement

2) Results in Ansys

Figure 7 shows a typical mesh used in this solution (for 1/8th of the cylinder). This figure 5.6 also shows that 6 nodal degrees of freedom have been specified at the symmetry lines and otherwise 5 nodal degrees of freedom have been employed. This allocation of nodal point degrees of freedom is efficient because then symmetry conditions can be easily imposed. In the finite element model, the load is applied at the 18th node in downward direction (y-axis).

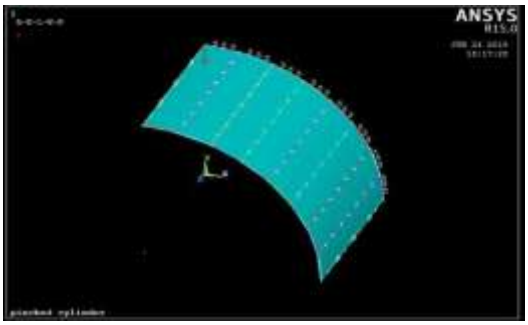

Fig. 7: Meshed Finite Element Model

The deformed shape obtained is shown in the Figure 8. The value of the maximum displacement is found at node 73 is 0.10996 in.

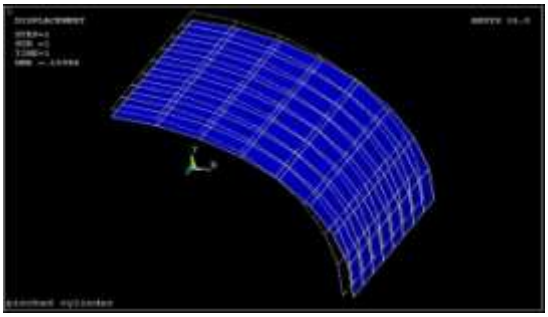

Fig. 8: Deformed and Un-Deformed Shape

The results from the analysis obtained from the program and from ANSYS are shown in Table. The results shown are the displacements at nodes 73 and 50. From Table 1, it is seen that the results given by the program are identical to those given by ANSYS. Similar results were obtained for the other nodes.

Table 1: Comparison of Displacement at Different Nodes

Node	Displacement	Using MATLAB (in)	Using Ansys (in)	Percentage deviation (%)
73	ux	0	0	0
	uy	0.1086	0.10996	1.25
	uz	0	0	0
50	ux	0.0195	0.0196	0.51
	uy	0.0552	0.05585	1.17
	uz	0.0001	0.0001	0

B. IMPLEMENTATION OF MASS MATRIX IN SHELL ELEMENT USING MATLAB

A cantilever is fixed at one end and other end is free.it has the length of 20 cm, thickness of 1 cm, and height of 4 cm. The material has the elastic modulus of 210 GPa and Poisson's ratio 0.3 and density of 7800 kg/m3. The cantilever is modeled using 50 four node shell elements. The cantilever is divided into 50 elements and each element consists of 4 nodes. Cantilever is fixed at one end i.e., Restraints are provided in the x and y directions at the left end of the cantilever.

The 3D plotting of the cantilever is obtained as shown in the Figure 9 in MATLAB.

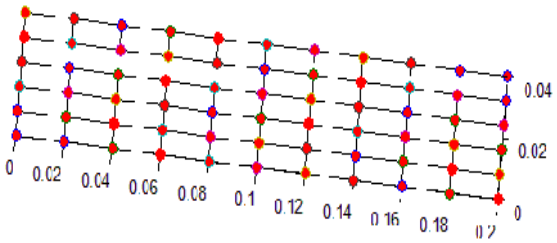

Fig. 9: 3D Plotting of Cantilever

The first ten modes of the frequency is obtained as shown in Table 2

	Frequency (Hz)
1	211.2408
2	799.8836
3	1342.4
4	1921.9

The cantilever beam was modelled in the ANSYS software is shown in the Figure 10.

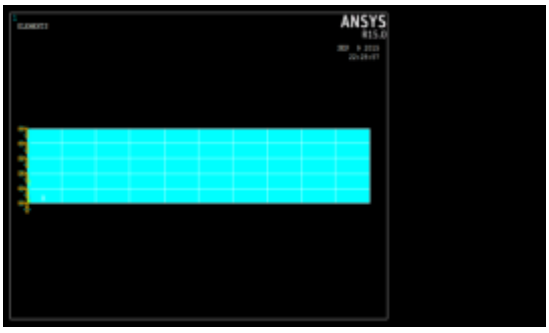

Fig. 10: Meshed Model of Cantilever Beam

The results obtained for the first ten modes is given in the Figure 11

Fig. 11: Frequency Modes of the Cantilever Beam

The results from the analysis obtained from the program and from ANSYS are shown in Table. The results shown are the first ten modes of frequencies. From Table 3, it is seen that the results given by the program are nearly identical to those given by ANSYS. Similar results were obtained for the remaining.

Table 3: Comparison of Results

Modes	Using MATLAB (Hz)	Using Ansys (Hz)	Percentage deviation (%)
1	211.2408	211.41	0.08
2	799.8836	803.12	0.40
3	1342.4	1339.5	0.21
4	1921.9	1901.4	1.06

CONCLUSIONS

This thesis presented the development of curved shell element using the object oriented programming concept in MATLAB as an alternative to the traditional procedural programming approach. A finite element analysis program was developed to verify the accuracy of the results.

A series of test example problems were analyzed using the developed program. The results from these analyses were compared with those obtained from the commercial finite element analysis program ANSYS in order to verify the accuracy of the developed program.

The results obtained from the analysis of the example problems using the curved shell element was found to be very accurate when compared to those obtained from the MATLAB. The difference in displacements computed by the two programs was around 1 %. The results obtained from the analysis of cantilever problem using shell element for mass matrix verification

was found to be accurate with a difference of around 1 % when compared with those obtained from the MATLAB.

REFERENCES

[1] Andrzej Ambroziak and Pawel Klosowski, "A Four Node 3D Isoparametric Membrane Element", *Journal of Structural Mechanics*, 2006, pp. 35-47.

[2] Boisse.P, Daniel.L and Gelin J.C, "A Simple Isoparametric Three-Node Shell Finite Element", *Journal of computers and structures"*, 1992, vol. 44, pp. 1263-1272.

[3] Green B. E., Strome D. R., and Weikel R. C., "Application of the stiffness method to the analysis of shell structures", *Procedures on Aviation Conference, American Society of Mechanical Engineers*, Los Angeles, 1961.

[4] Zienkiewicz O. C., "The Finite Element Method in Engineering Science", 2nd ed., McGraw-Hill, 1971.

[5] Bathe, K. J., and Ho, L. W., "A Simple and Effective Element for Analysis of General Shell Structures", *Journal of Computers and Structures*, 1981, vol. 13, pp. 673-681.

[6] Eugenio Onate, Fernando G. Flores, "Wrinkling and folding analysis of elastic membranes using an enhanced rotation-free thin shell triangular element", *Journal of Finite Elements in Analysis and Desig*, 2011, pp. 982- 990.

[7] Bathe K. J., Chapellet D., "Fundamental Considerations for The Finite Element Analysis of Shell Structures", *Journal of computers and structures*, 1998, vol. 66, pp. 19-36.

[8] Fathelrahman M, et.al, "Degenerated Four Nodes Shell Element with Drilling Degree of Freedom", *IOSR Journal of Engineering*, 2013, vol. 3, pp. 10-20.

[9] Young W Kwon and Hyochoong Bang, "The Finite Element Method Using MATLAB", Second Edition.

[10] Cook R. D., "Concepts and Applications of Finite Element Analysis", John Wiley & Sons, 1974.